INVESTIGATING BIOLOGICAL EFFECTS OF NANOPARTICLES WITH 3-DIMENSIONAL CELL MODELS

CHIA SING LING

(B. Eng. (Hons.), Monash University Malaysia)

A THESIS SUBMITTED

FOR THE DEGREE OF DOCTOR OF PHILOSOPHY

DEPARTMENT OF CHEMICAL AND BIOMOLECULAR ENGINEERING

NATIONAL UNIVERSITY OF SINGAPORE

2016

DECLARATION

I hereby declare that this is my original work and it has been written by me in its entirety. I have duly acknowledged all the sources of information which have been used in this thesis.

This thesis has not been submitted for any in any University or Institution previously.

CHIA SING LING

i

ACKNOWLEDGEMENTS

This thesis would not have been possible without the kind help and support from the great many people.

First of all, a special gratitude I give to my supervisor, Assistant Professor Leong Tai Wei David, whose insightful suggestions, valuable advice, guidance and wealth of knowledge helped me from the start to the completion of this thesis work.

I would like to show my gratitude to my thesis advisory committee members, Assistant Professor Xie Jianping and Assistant Professor Lee Dong-Yup, for their constructive suggestions and ideas.

It is a pleasure to offer my regards and thanks to all my friends in the Leong's laboratory (Dr. Dalton Tay Chor Yong, Dr. Magdiel Inggrid Setyawati, Marcella Giovanni, Dr. Rajaletchumy Veloo Kutty, Dr. Qian Hang, Wang Jinping, Nandita Menon) who assisted and supported me in many aspects throughout my candidature.

I also like to thank the staffs in the Department of Chemical and Biomolecular Engineering, especially Mdm. Siew Woon Chee, Ms. Vanessa Chan, Dr. Yang Liming for their kind assistance during my research.

Last, I would like to express my deepest appreciation to my family, who have been encouraging and supporting me all these years.

TABLE OF CONTENTS

SUMMARY

While nanotechnology development has grown by leaps and bounds, the depth of understanding of the biological effects of engineered nanomaterials (NM) continued to play catch up. Current mechanistic knowledge of engineered NM on cellular physiology is mostly derived from *in vitro* study using 2-dimensional (2D) cell culture model. Conventional 2D cell culture model, also known as monolayer cell culture, is a simplified *in vitro* cell model that can be easily established in standard biological laboratory setup; however, the cells in this model have a very limited anatomical and physiological relevance of the real tissue. As a result of lacking these paramount characteristics of a tissue, 2D cell culture fails to reflect the real context and therefore the tissue's actual biological response to a treatment.

This study aimed to improve the tissue-mimicry of *in vitro* model for nanotoxicity study to more accurately predict the biological interactions and the underlying mechanisms of NM to biological systems. To achieve the objectives of the study, more tissue-like 3-dimensional (3D) cell culture gut and kidney models were used to assess the complex biological phenomena of commercial NM to the specific tissue target.

First, examination of the toxicity of commercial grade ZnO NM and reevaluation of the often reported high toxicity of ZnO NM (based on the high cytotoxicity observed in 2D cell culture model) were conducted in reproducible 3D cell culture model. Through these 3D cell culture models, interesting cells' biological responses toward ZnO NM which could not be observed in a 2D model were identified. The tissue-like construct and realistic

mass transfer gradient in 3D cell model showed the protective effects of tissue to the foreign entity such as ZnO NM. By way of contrast, cells in traditional 2D cell culture model were susceptible to the toxic effects of ZnO NM.

In addition to understand the toxicity response of a representative tissue model, 3D model was also used to understand the effect of the ZnO NM towards a specific tissue function. Here, the transfer and clearance of NM in the tissue was chosen as the main tissue function to investigate. Transwell assay was used to mimic the multilayer tissue construct mimicking a simplified kidney section to determine the role and mechanism of cells in regulating the passage of NM. By using this model, the diffusion path, dosimetry, direct and indirect effect of NM to different cell types and tissue can be estimated.

Collectively, the differential responses between 2D and 3D cell culture model to ZnO NM showed the importance of cell dimensionality, cell's microenvironment, cell's role, and cell-to-cell interactions in governing the cellular response to NM. With these improved *in vitro* models, the understanding of biological interactions and effects of NM might be improved. Last, but not least, the understanding of biological effects of NM will enable the re-development of safer-by-design nanotechnology to benefit the society in a sustainable and safe way.

LIST OF TABLES

LIST OF FIGURES

LIST OF ILLUSTRATIONS

LIST OF ABBREVIATIONS

BSA	bovine serum albumin
CFC	chlorofluorocarbon
CXCL-5	C-X-C motif chemokine 5
DAMPs	danger-associated molecular patterns
DLD-1	human colorectal adenocarcinoma epithelial cell
DLS	dynamic light scattering
DMEM	Dulbecco's Modified Eagle's Medium
DMEM/F12	Dulbecco's Modified Eagle's Medium: Nutrient Mixture F-12
DNA	deoxyribonucleic acid
ECM	extracellular matrix
EDTA	ethylenediaminetetraacetic acid
EDX	energy-dispersive X-ray spectroscopy
EndoGRO	EndoGRO-MV-VEGF Complete Culture medium
FBS	fetal bovine serum
FTIR	Fourier transform infrared
FITC	fluorescein isothiocyanate
GAPDH	Glyceraldehyde 3-phosphase dehydrogenase
HK-2	human proximal tubule epithelial cells

HMVEC	human microvascular endothelial cells
HRP	horseradish peroxidase
ICP-OES	inductively coupled plasma optical emission spectroscopy
IL1B	Interleukin-1 beta
IL18	Interleukin 18
IRF1	Interferon regulatory factor 1
NanoEL	nanomaterials induced endothelial leakiness
NCM460	normal human colon mucosal epithelial cell
NFκB	nuclear factor kappa B
NLRC4	NOD-like receptor family, CARD domain containing 4
NM	nanomaterials
NP	nanoparticles
PAMPs	pathogen-associated microbial patterns
PBS	phosphate buffered saline
PCR	polymerase chain reaction
PDI	polydispersity index
P/S	Penicillin/streptomycin
pγ-H2AX	phosphorylated gamma Histone H2AX

RNA	ribonucleic acid
ROS	reactive oxygen species
SD	standard deviation
SDS	sodium dodecyl sulfate
STM	scanning tunnel microscope
SW480	human colon adenocarcinoma cell
TBP	TATA binding protein
TEM	transmission electron microscopy
TLR	toll-like receptor
UV	ultraviolent
2D	two-dimensional
3D	three-dimensional

Chapter 1: Introduction

1.1   Nanotechnology

Nanomaterials (NM) are actually not something new. For example, the water-repellent surface exhibited by the leaves of the lotus flowers and the vivid color of stained glass in the 1600-year old Roman chalice are the results of nature and man-made nanotechnologies (Checco et al., 2014). However, as NM are imperceptible to the human eye, the use and study about NM did not gain much serious attention back to the time before the invention of scanning tunneling microscope (STM) (Zumdahl and DeCoste, 2012). The creation of STM by Gerd K. Binning and Heinrich Rohrer in the early 1980s catalyzes the development and research of nanotechnology to one of the hottest and popular research topics around the world of the 21st century (Zumdahl and DeCoste, 2012).

One of the advantages of nanotechnology is that we can precisely manipulate materials right down to the atomic scale to alter or tune the properties of these substances. When the size of a material reduced, the fraction of atoms located at the surface and the edges increased significantly. These atoms are less stable than those in the interior due to a lower coordination with other atoms and therefore have fewer bonds. Consequently, these surface atoms have higher affinity to form bonds with other atoms and molecules. This surface effect dominates over the bulk effect and gives NM a highly reactive property (Roduner, 2006). For example, gold in the coarse grain matter is known to be inert and stable; however, the nano form of gold is highly reactive and can be used as a catalyst for hydrogenation process of different chemical substances (Mitsudome and Kaneda, 2013). The change in electronic, optic, and magnetic properties of the substance could be accounted

by the quantum confinement effect that encloses the motion of electrons in small area, in the crystallite (Joshi et al., 2009). Quantum confinement effect is important for the development of high-speed hetero-structured field-effect transistors, quantum well lasers, quantum wires and dots (Sakaki, 1996). Besides varying the size, mere adjustments to the shape and surface chemistry of the NM can also change the properties of the NM.

These altered and unprecedented properties of NM (versus their bulk counterparts) have created many new applications and breakthroughs. In consequence, both government and private sectors have been investing heavily on nanotechnology research to further explore the potential and benefits of NM. The growth of nanotechnology has introduced a new revolution to many other different industries. The global market for NM incorporated products was valued at $ 26 billion in 2014 (Research, 2014). Statistics showed that the market of products incorporating NM is growing exponentially and predicted to rise to US$ 2.95 trillion by 2015 (Plunkett et al., 2015). Industries such as chemicals, semiconductors, electronics, health care, pharmaceutical, and food industry are major contributors to this phenomenal jump. Nevertheless, other sectors are also starting to adopt nanotechnology and growing rapidly (Hailing, 2007). It is expected that nanotechnology will continue its technological dominance in many of the above sectors.

1.2   Nanotoxicity

Nanotechnology brings revolution and exciting advancement to the industries. At the same time, this rapid advancing technology also carries

unknown health risks to the workers and consumers. Reflection on the examples of chlorofluorocarbon (CFC), genetic modified crop, and ultrafine particle; it is inevitably that knowledge and understanding of the new technology should not only be limited to the applications but also their possible biological and environmental effects. The biological and environmental effects of the new substance are particularly crucial for the engineers and researchers to implement adequate prevention measures (if needed) in order to ensure the use of the substance benefits the society in a safe way (Fadeel and Garcia-Bennett, 2010; Yan et al., 2005). With the burgeoning of nanotechnology enabled products, a new field of study known as nanotoxicity has emerged to assess the safety of these products. Nanotoxicity investigates not only the potential toxic effects of NM but also the underlying mechanism of NM interaction with the biological systems is assessed to understand their health implications in detail. From biological assessments of NM conducted on *in vitro* and *in vivo* models, researchers found unexpected interactions and complex reactions between NM and biological system. Furthermore, some preliminary toxicological studies of NM have unraveled that engineered NM exert higher and unexpected toxicity to biological system than the bulk-size counterpart (Gaiser et al., 2009; Setyawati et al., 2013a; Zoroddu et al., 2014). These results raise many concerns regarding the safety of NM. As a result, more research on NM was conducted, the results show that NM are not only more chemically reactive but also more biologically active than the bulk materials (Jiang et al., 2009). NM with a size smaller than 100 nm, which is comparable to the size of a bacteria, virus or biological molecules, can be easily taken up by the mammalian cell of about

4

10-30 µm in size (Rao, 1997). Nevertheless, not only size, other factors such as shape and surface modification also greatly influence the uptake rate and uptake mechanism of NM by cell. For example, polyvinylpyrrolidone-coated iron oxide nanoparticles of 37 nm exhibit higher cellular uptake as compared to NM of 8 nm, 23 nm, and 65 nm (Huang et al. 2010), whereas CeO_2 nanoparticles of 250-500 nm have higher cellular uptake than 20-50, 40-80, and 80-150 nm CeO_2 nanoparticles (Limbach et al. 2005). Besides that, NM have stronger surface adhesion and binding affinity to biomolecules such as proteins than the bulk counterpart (Cedervall et al., 2007; Garnett and Kallinteri, 2006).

Following the principle of life cycle analysis, the end use of the NM justifies the fate of the NM. For the case of NM incorporated in electronic devices and semiconductor, the potential health hazards of the NM are more likely confined within the manufacturing factory. With the proper engineering and administrative control, the occupational exposure to engineered NM and risks of the particular engineered NM to the worker can be minimized to acceptable level (Schulte et al., 2008). On the other hand, NM incorporated in consumable products and nanomedicine are more likely to pose risk to the consumer, who is less aware of the hazard control and not equipped with proper protective equipment. Therefore, it is safer to determine the biological effects of NM especially those will be incorporated in consumable products before they enter market.

Human is potentially exposed to the NM, which incorporated in the consumable products, through various route, namely inhalation, ingestion, and

dermal absorption (Oberdörster et al., 2005). It is also necessary to consider the possibility of unintended bioaccumulation of engineered NM incorporated in non-consumable products such as paints due to wear and degradation over time or improper disposal of NM incorporated products. These NM with size smaller than 100 nm is invisible to the naked eye, they could be easily absorbed unintentionally.

The knowledge of the NM's biological interactions will be useful to implement strategies to tackle the undesired toxicity in order to implement proper uses and safe designs of NM. Moreover, the information of the biological interactions will be useful for utilizing the effects in desired applications such as nanomedicine that targets diseased cells, upregulates certain expression of biomolecules and triggers certain biological events. Nevertheless, the main purpose of nanotoxicology study is to ensure the development of nanotechnology will benefit the society by introducing the advantages of NM and reducing the harm to the biological system and environment.

1.3   The use of zinc oxide (ZnO) nanoparticles

Zinc is one of the essential minerals for the growth of all life forms. Zinc is important for many biological functions, enzymatic reactions, and immune responses in all organisms (Stefanidou et al., 2006). In human, zinc can be found in all tissues and body fluids. Zinc coordination induces the correct folding of "zinc finger-like" structure in certain proteins (Trumbo et al.,

2001). Deficiency of zinc can weaken immune system, impair development, and impede growth of human (Jones and Grainger, 2009).

Human body is unable to produce zinc. As such, it draws zinc from its diet to maintain a good health. Generally, zinc can be obtained from foods such as red meat, seafood, and dairy products. Nevertheless, zinc supplements in various forms are also available in the market in order to prevent and treat zinc deficiency. However, the absorption efficiency of most zinc supplements, which is available in the market, is generally low (Raspopov et al., 2011). The low bioavailability of zinc in the supplement largely reduces the effective dose of zinc. In order to increase the absorption efficiency of zinc, some healthcare industries and researchers are looking into other alternative forms of zinc such as ZnO NM as an improved product (Raspopov et al., 2011).

On the other hand, ZnO NM also attracted the attention from cosmetic and healthcare industries. Compared to some organic ultraviolent (UV) filters, which will break down under UV light, ZnO is more stable and has wider range of UV filtering ability (both UVA and UVB) (Singh and Nanda, 2014). The nano form of ZnO further improved the UV light blocking property of ZnO and it is transparent (Morabito et al., 2011). Therefore, the use of ZnO NM to replace bulk ZnO is gaining popularity in cosmetic products such as sunscreen and lipsticks. In addition to the above applications, ZnO NM also exhibit good anti-bacterial property as compared to the benign bulk ZnO. This enables the use of ZnO NM in packaging, food supplements, deodorant spray, and clothing as anti-microbial agent (Becheri et al., 2008; Lin et al., 2009; Source, 2015). In addition, there are substantial research studies that explore

7

the therapeutic and theranostic potentials of ZnO NM in nanomedicine applications (Rasmussen et al., 2010; Wang et al., 2015). These new applications of ZnO NM in nanomedicine and consumable products might significantly increase the intended and unintended exposure to ZnO NM.

In addition to that, ZnO NM possess unique optoelectronic and electronic properties that suitable for different applications. ZnO NM have large electrochemical coupling but lack of any center of symmetry in wurtzile. These properties provide a strong piezoelectric and pyroelectric property that is suitable for sensors and actuators application. ZnO has a wide band-gap of 3.37 eV at room temperature with a large exciton energy of 60 meV that can be used for short wavelength optoelectronic applications (Wang et al., 2007b). The high electron mobility of ZnO NM is also suitable for semiconductor industry. The ability of controlling the growth mechanisms of ZnO nanocrystal, which affect the shape and form of the nanostructures, further enhance the applications of ZnO NM.

In 2012, the annual production of ZnO NM in European Union has reached 1600 tons (Sun et al., 2014). ZnO NM is the third highly produced metal oxide NM after TiO_2 and SiO_2 NM (Piccinno et al., 2012). *In vitro* assays showed that ZnO NM are more cytotoxic as compared to other engineered NM such as TiO_2 and SiO_2 NM (Danielsen et al., 2015; Zhi-Peng et al., 2006). However, bulk ZnO is known as a benign chemical so the unexpected high toxicity of nano ZnO is also drawing researchers' attention to look at the specific biological interactions of ZnO NM (Huang et al., 2010; Lin et al., 2009).

8

In view of the potential exposure of ZnO NM to human being, the biological effects and safety of ZnO NM should be explored systematically. A more detailed overview of the nanotoxicity assessment will be presented in **Chapter 2**. **Chapter 3** outlined the research gaps, aims and hypothesis of this study. **Chapter 4**, **5** and **6** describes the different models and improvements of nanotoxicity model to link the gaps. Lastly, **Chapter 7** summarizes the overall findings of this study followed by other potential application of the models used in **Chapter 4**, **5** and **6**.

Chapter 2: Literature Review

2.1 Studies about the toxicity of ZnO nanomaterials

ZnO NM have been shown to induce significant toxicity to both mammalian cell and rodent models (Lam et al., 1985; Setyawati et al., 2013c; Wang et al., 2008). However, whether this toxicity is translatable to human body or not is still questionable.

Many attempts have been made to reveal the underlying toxic mechanism of ZnO NM (Vandebriel and De Jong, 2012). One of the popular debates of toxicity of ZnO NM is the dissolution of ZnO NM to Zn^{2+} ion, in turn, the influx of Zn^{2+} affects the zinc homeostasis in the cell (Song et al., 2010; Xia et al., 2008). Besides the dissolution of ZnO NM to Zn^{2+} in culture medium, the acidity endosomes and lysosomes can also increase the dissolution of ZnO NM to Zn^{2+} in cell (Xia et al., 2008). High concentration of intracellular Zn^{2+} can further trigger release of Zn^{2+} sequestration in mitochondria to interferes the zinc homeostasis (Kao et al., 2012).

Another observation associated with ZnO NM treatment is elevated intracellular reactive oxygen species (ROS). ROS are oxygen based chemically reactive molecules and free radicals. These molecules are generally produced as byproduct during mitochondrial electron transport of aerobic respiration (Fernández-Checa et al., 1998). However, cells can also produce ROS when encounter exogenous substances such as cytokines, xenobiotics, and bacteria (Ray et al., 2012). Normally, the cells kept the production of ROS in balance with the removal of ROS by way of activating their antioxidant mechanism. When the production of ROS exceeds the cell's antioxidative capacity to remove them or the influx of ROS from external sources occur, it

11

results in oxidative stressed cell (Romano et al., 2010). Studies showed that ZnO NM induce elevation of intracellular ROS and disturb this oxidative balance (Lin et al., 2009; Sawai et al., 1998). Undesired downstream events including DNA damage (Ng et al., 2011), lipid peroxidation (Lin et al., 2009), cellular dysfunction (Huang et al., 2010), disruption of mitochondria integrity (Moos et al., 2010), and inflammatory response (Andrea et al., 2007) were found to be associated with high oxidative stress induced by ZnO NM.

Although extensive research has shown that exposure to ZnO NM result in high intracellular oxidative stress, the exact underlying mechanism still remains unclear. Several molecular and cellular mechanisms of ZnO NM induced ROS were proposed. UV irradiation on ZnO NM leads to formation of ROS such as superoxide anion, hydroxyl radical, and singlet oxygen by redox reaction (Li et al. 2012). Nevertheless, the presence of functional groups, discontinuous crystal plane or defects on the surface might also contribute to ROS generation (Saliani et al. 2016). Another hypothesis is disruption of mitochondrial respiration by ZnO NM to produce more radical byproduct (AshaRani et al. 2008). It is possible that the underlying mechanism of ZnO NM inducing ROS is the combination of more than one of these proposed mechanisms.

All these endeavour and assembled knowledge to identify the toxicity mechanism of ZnO NM showed the complexity of ZnO NM's toxicity.

2.2   Focus of nanotoxicity study

In general, nanotoxicity assessment will focus on specific exposure route of selected NM. The reason is due to the unique applications, chemical properties and physical properties of each NM contribute to their own biological interactions that require individual assessment (Love et al., 2012; Seunarine et al., 2006). Even for the NM with the same chemical form, the generalization and prediction of the biological effects of the NM are also a huge challenge. Taking example of ZnO NM, there are rod-like, spherical, nanowire, and porous forms of nano ZnO (Zhi-Peng et al., 2006). Each form of NM has its distinct uptake pattern, affinity to biomolecules, cell processing and toxicological outcomes when they encounter the biological system (Jones and Grainger, 2009).

One of the major studied exposure routes of NM is inhalation (Ahmed et al., 2013; Ke et al., 2012; Li et al., 2003). Lung as a major organ, which contact with the airborne particles via inhalation, is an obvious interest of study to determine the effect of small and airborne NM to respiratory system.

Hepatotoxicity study gained its high popularity as *in vivo* studies showed that liver has a high distribution of NM via the administration route of intravenous injection (Liu et al., 2010; Xie et al., 2010a). Skin, which is the organ that separates and protects the internal structures of the body from damage, is the first organ that contacts with external environments; thus, it is also likely to expose to NM in the air and water. Besides that, the increasing use of ZnO NM in sunscreen and cosmetic product also raised the study of dermal exposure (Filipe et al., 2009; Wu et al., 2009).

Nevertheless, the likelihood of consumers expose to engineered NM *via* other exposure route has significantly increased with the growing of new nano-incorporated consumer products. For example, the use of NM in consumable products such as toothpaste, lipstick, food supplement, and antimicrobial packaging significantly increase the possibility of NM ingestion (Thomas and Mathew, 2013). Compared to inhalation and dermal exposure, the biological interaction study of ZnO NM to human body via ingestion exposure is relatively scarce as the application of ZnO NM in these consumable products is only popular within recent years. Ingested NM will first be in contact with the digestive system. After digestion, these NM will be absorbed into the blood or lymph and get circulated through the body via circulatory system. *In vivo* studies showed that orally administrated NM can be found in kidneys, liver and spleen (Schleh et al., 2012; Wang et al., 2008; Wang et al., 2007a). Studies showed that ZnO NM can induce severe toxicological effects such as swelling of kidney tissue and glomerular segmentation on rat kidney (Esmaeillou et al., 2013; Hong et al., 2013; Vandebriel and De Jong, 2012). Enzyme-linked immunosorbent assays and histopathological examination showed that ZnO NM induced elevation of serum inflammatory markers and renal epithelial desquamation (Faddah et al., 2012).

Nevertheless, for the NM to reach these targeted organs, they must first get in contact with gastrointestinal tract and cross the respective epithelial cell barrier to enter the blood stream (Hagens et al., 2007). However, little is known about the transcellular transport and effects of ZnO NM across gastrointestinal tissue. *In vivo* studies found that positively charged particles

have higher absorption in gastrointestinal tract as compared to negatively charged particles (El-Shabouri, 2002; Hariharan et al., 2006).

It is understood that the fate of the substances is largely depends on the exposure route and the environment that the cell encountered. Therefore, the biological effects of ingested ZnO NM to organs such as intestine and kidneys will provide important information for the engineering assessment of incorporated ZnO NM in consumable products.

2.3   State of art technologies for nanotoxicity assessment

In 2007, the European Union introduced Registration, Evaluation, Authorization and Restriction of Chemicals (REACH) legislation to all chemicals produced and imported into the European Union in order to reorganize and enforce chemical safety regulations. The implementation of REACH spurs the toxicity testing and risk assessment analysis of new chemicals that concerning the potential hazards of chemical to biological system and environment (Williams et al., 2009). Under the REACH legislation, NM as a new group of chemicals are scrutinized and undergone toxicity testing and risk assessment analysis to determine their potential hazards to the consumer health in addition to the environment.

The most common way to conduct this NM risk assessment is through the *in vitro* culture, where a cell type from tissue of interest is cultured in the petri dish and is exposed to the tested NM. This approach is favoured by many as it is known to be simple and could be easily established in the lab.

Moreover, the approach is more convenient and less expensive as compared to the animal model (Arora et al., 2012). Furthermore, *in vitro* model enables detailed examination of specific cellular responses and mechanisms under different test conditions.

Alternatively, NM risk assessment could be done with *in silico* model to simulate the biological system for predicting the possible outcomes induced by the stimulus (van der Burg et al., 2015). However, there are still many challenges for the development of *in silico* model for nanotoxicity assessment, for instances, the limited data and complexity of interrelated variables of NM (shape, size, surface function, charge, and *etc*.) (Cohen et al., 2013). Large amount of data and information from *in vitro* or *in vivo* models is needed in order to establish a reliable model that can simulate behaviour and response of the organism when it is subjected to the stimulus. Both high throughput assays, which can significantly improve the efficiency and reduce time required to obtain the large data sets for nanotoxicity assessment (George et al., 2011), and detailed study to uncover the interactive and synergistic effects of these variables are desired for *in silico* model.

Due to the inherent nature of human body that is built by multiple types of cells that form various complex functional systems, a biological response derived from a single type of cells (such that is derived from the *in vitro* study) might not well represent the biological response complexity arise in the real case situation. As such, though they are widely used, the two aforementioned approaches are normally used as preclinical toxicity tests or

screening prior to moving on the real multicellular organism testing, the *in vivo* model.

Generally, biological effects of a particular cell lines to the NM, such as cytotoxicity, cell proliferation, genotoxicity, inflammatory response, gene expression, and protein expression, can be determined by using *in vitro* model (Hillegass et al., 2010). Animal studies can be used to determine more complex interactions and effects of NM to biological systems (Joris et al., 2013).

After the prescreening step, the verification and complex biological interactions can be determined by animal model and/or clinical trials. In a typical drug testing, stage one to stage three clinical trials are required before the drug is approved to enter the market (Olaf, 2013). The whole process from the different stages of testing to the introduction of drug into market is normally very long and many drugs will be screened out in each step.

Similarly, most of the nanotoxicity assays utilized the *in vivo* model to verify the *in vitro* findings (Soenen et al., 2011; Yong et al., 2013). The diversity of NM and fast growing of nanotechnology makes it a daunting task to test all the NM on the animal model.

2.3.1 2D cell culture models

The most simplistic *in vitro* model is achieved by forcing the cell lines, which derived from human or animal, to attach on culture dish with a monolayer configuration. The treatment of NM is generally applied to this 2D cell culture model by introducing NM into the culture media. This *in vitro*

model was first developed by Wilhelm Roux in 1885 (Barford, 1995). Nowadays, 2D cell culture model is still widely used in life science research including cell biology, drug discovery, and toxicology studies due to the ease of use in laboratory.

Although 2D cell culture model can be used to conduct cellular study easily, 2D cell culture model is not an accurate representation of the cell in real tissue in many aspects (Sun et al., 2006). First, the cells in 2D are forced to adapt to the artificial environment which is very different from the native 3D microenvironment of a tissue (Godugu et al., 2013). In the native 3D cell environment, cells are surrounded by other cells and a complex network of extracellular matrix (ECM) that has structural and biochemical roles in a tissue. Studies have shown that the spatial arrangement of cells within an environment is important for a tissue as it affects how the cells interact with each other and their surroundings (Von Recum and Van Kooten, 1996).

In the 2D cell culture configuration, the membrane receptors will be intensified at the side where the cell is exposed to the culture medium rather than the original orientation observed in the tissue (Zhang et al., 2005). Membrane receptors are important for communication and signalling between cells and external environment (Turturici et al., 2014). The misalignment of membrane receptors might result in an artifact rather than the actual response of cell to the stimulus. The monolayer configuration also depicts the interactions between cells as there is limited contact area and membranes interaction among cells especially when the cells are not confluent on the culture dish (Tay et al., 2011; Tay et al., 2010). This is undesirable for the cell

communications especially for those that require direct cell-cell contact. Moreover, the adhesion of cells on hard substrate impedes the transcytosis of substance from the apical side to the basal side (Kathawala et al., 2013).

Another important parameter that becomes extremely simplified in 2D cell culture model is the tissue-like mass transfer. The monolayer cell configuration does not create a realistic concentration gradient for the mass transfer of molecules; more specifically, the exposure of molecules to cell membrane and membrane receptors was greatly enhanced in 2D cell culture model as the single cell layer and lack of ECM in the system directly exposed the cells to all the molecules in culture medium (Santos et al., 2012).

All these factors can have a profound effect on the downstream cellular events such as cell proliferation, metabolism, and response to a stimulus.

2.3.2 Animal testing

2D *in vitro* model is limited to cellular level, this intrinsic bottleneck constraint the ability of 2D *in vitro* model to reflect the interactions between the testing substances and tissues or organs in a multicellular organism. The current approach to address this issue is to implement preclinical animal study to determine the complex interactions of the tested substances with the biological systems (**Table 2.1**) (Yoon et al., 2012).

Table 2.1: Summary of complex biological interactions that have to be studied in animal model.

Animal model
Chronic toxicity
Skin irritation
Eye irritation
Reproductive toxicity
Metastasis
Developmental toxicity

Animal testing refers to experimentation carried on non-human animals, which usually is mammalian or vertebrate, to assess the biological effects of a substance in order to predict the likely human response to the particular substance. The main assumption of animal testing is that the adverse effects observed in one animal species could also occur in another animal species (Martignoni et al., 2006).

Mice, rats, fishes, guinea pigs, monkey, and rabbits are the commonly used animals in laboratory test. They are used to determine toxicity such as chronic toxicity, skin irritation, eye irritation, skin sensitization, reproductive toxicity, and developmental toxicity of embryo (Fischer and Chan, 2007).

Besides the toxicity assays mentioned above (Ema et al., 2010; Kim et al., 2006), animal model is also widely used in nanotoxicity study to determine the distribution, accumulation and clearance of NM (Sadauskas et al., 2009; Sharma et al., 2012).

2.4   Issues related to current *in vitro* and *in vivo* model

Although *in vitro* and *in vivo* models are widely used for toxicity analysis, the disparity between *in vitro* model and animal model to clinical trials has been raising many concerns (Hutchinson and Kirk, 2011; Perel et al., 2007). Overall, only about 15% of overlap between animal study and human clinical trial was observed. The disparity is even greater in the cancer research, less than 8 % overlap between animal models and clinical trial was observed (Mak et al., 2014). Not to mention the worst success rate in preclinical cancer drug research with a trivial 5 % of candidate compounds, which found by preliminary screening in *in vitro* and *in vivo* models, passing phase III clinical trials for safety and efficacy (Hutchinson and Kirk, 2011). These data showed that there is a disconnection between the actual cellular responses with the current models used in safety assessment. We outlined some of the limitations and disadvantages, which might explain the reason of the disconnection, of the current 2D cell culture and animal model in **Table 2.2**.

Table 2.2: Summary of the disadvantages of 2D cell culture and animal model.

2D cell culture model	Animal model
Inaccurate cell orientation and polarity (Vergani et al., 2004).	Species-species difference (imperfect analogs).
Inhibit exocytosis to the basal side.	Expensive and time-consuming (Khan, 1984).
Receptor intensifies at the apical side (Knight and Przyborski, 2015).	Ethical issues and animal welfare (Ferdowsian and Beck, 2011).
Different metabolism rate (Knight and Przyborski, 2015).	Expertise in animal handling.
Lack of realistic mass transfer gradient (Barrila et al., 2010).	

The rationale of prescreening and preclinical trial is to reduce the test load of clinical trial. The quality of the models is based on the clinical relevance. The statistics and disadvantages of current models showed that they failed to demonstrate the physiological relevance to facilitate the development of nanotoxicity study; therefore, it is apparent that current nanotoxicity testing system was flawed, their suitability to serve as a prescreening model is questionable. It is the time to re-examine the basic premise of the current approaches of toxicity pre-clinical testing. The continual usage of non-reliable model can significantly impede the development of understanding in nanotoxicity. To address this burden, a more effective, reliable, and

appropriate testing model should be used for the early stage safety assessment of nanotoxicity study.

2.5   3D cell culture models

The apparent shortfalls of 2D cell culture especially the inability of 2D cell culture model to recreate tissue-like microenvironment has prompted researchers to look for an alternate platform to study the cellular response to external stimulus. Among the different approaches to improve the current *in vitro* model, 3D cell culture was found to be one of the potential models to bridge the gap between *in vitro* and *in vivo* models.

3D cell culture not only can be used to construct more complex and sophisticated cellular organization but also can address most of the shortcomings of 2D cell culture model. For example, 3D cell culture can more accurately replicate the microenvironment of a real tissue as compared to 2D cell culture model (Kim, 2005), resulting in a more realistic oxygen/nutrient/growth factor gradient from the environment to the cells. Cells cultured in 3D format can form the correct apical–basal polarity of cells and have the suitable cell-cell interactions (Mazzoleni et al., 2009), unlike the cell-to-cell contact that only exist at the periphery in 2D format. These factors play important role in the cellular response to an external stimulus such as NM. The potential of 3D cell culture model is beginning to be realized. As the results, there is an increasing trend that researchers are adopting more sophisticated 3D cell culture model in their studies (Godugu et al., 2013).

More and more studies showed that cells cultured in 3D were found to have a more *in vivo* like morphology (Chang and Hughes-Fulford, 2009; Myungjin Lee et al., 2013; Yamada and Cukierman, 2007). Direct applications of 3D cell culture in tissue engineering and cancer studies are popular (Loessner et al., 2010; Ohmori et al., 1998; Volkmer et al., 2008; Weigelt et al., 2010).

One of the foundation studies about the development of 3D cell culture model is the work done by Professor Mina Bissell, Lawerence Berkeley National Laboratories. In her studies, the importance of ECM and cell polarity on the biochemical features of a tissue was demonstrated. The culture of mammary epithelial cells in 3D format with suitable basement membrane was able to form the *in vivo*-like mammary epithelial acinus, secrete milk protein, and display tissue-specific metabolic pattern (Ashkenas et al., 1996; Bissell et al., 2003).

Besides that, the cells in 2D generally are highly active in metabolism; the cells proliferate until confluent without structural change, whereas the growth and metabolism of the cells in 3D spheroid were controlled by the intrinsic nutrient/oxygen/growth factor gradient as the tissue (Petersen et al., 1992; Tibbitt and Anseth, 2012; Wu et al., 2011).

Although cells cultured in 3D are significantly differ with the cells cultured in 2D, most of the common cell-based toxicity assays can still be conducted in 3D cell culture. **Table 2.3** summarized some of these important cell-based assays and applications in 2D and 3D cell culture models to these assays.

Table 2.3: Summary of different toxicity assessments in 2D and 3D cell culture model.

Toxicity assessment and assays	2D cell culture	3D cell culture
Cell viability	✓	✓
Cell metabolism	✓	✓
Cellular uptake	✓	✓
Gene expression	✓	✓
Protein expression	✓	✓
Inflammatory response	✓	✓
Cell migration	✓	✓
Live cell imaging	✓	✓
Enzyme functionality test	✓	✓
Transcellular transport	✗	✓
Spatial expression of biomarker (genes, proteins and etc.)	✗	✓
Developmental toxicity	✗	✓

Collectively, there are more assays that can be done in 3D cell culture model. Moreover, some of the toxicity assessments are actually more suitable to be conducted on cells cultured in 3D format than in 2D. Here, we outlined some of these assays and highlighted the reason in **Table 2.4**.

Table 2.4: Summary of the reason of why 3D cell culture is more suitable for a particular cell-based assay as compared to 2D cell culture.

Assay	Reason	Ref
Metastasis	• More tumor-like microenvironment: cell aggregates encapsulated in ECM. • Cells need to release matrix-metalloproteinase to digest ECM for metastasis.	(Chia et al., 2015; Poincloux et al., 2011; Sundqvist et al., 2013; Wang et al., 2011)
Chronic effects of a stimulus	• Cell cultured in 2D are still insufficient for long term culture. • Cell in 3D format can be cultured and maintained for weeks and months without subculture.	(Poincloux et al., 2011; Sundqvist et al., 2013; Wang et al., 2011; Yan et al., 2005)
Cross-talk between different cell types	• Better cell-to-cell interactions. More *in vivo*-like cell polarity and orientation.	(Yamada and Cukierman, 2007; Yan et al., 2005)
Morphogenesis change	• Branching or duct formation can only be induced in 3D microenvironment.	(Brinkmann et al., 1995; Yamada and Cukierman, 2007)

Compared to other alternatives such as organ culture, 3D cell culture model also has more advantages. For instances, organ culture requires specimen of interest which in most cases is difficult to obtain (Kim, 2005). 3D cell culture model, which can be constructed by using human cell lines, also provides a better and more species relevant model for real time and fixed imaging to study specific interactions and responses than organ culture and animal model (Rangarajan et al., 2004; Yamada and Cukierman, 2007).

3D cell culture offers a wide range of freedom in the design (Haycock, 2011). Some of commonly found models such as cell spheroids, multilayer

culture (Ishiwata et al., 2014), microfluidic cell culture (Li et al., 2012), and 3D cell printing. The detailed description and suitable tissue type of the commonly used 3D cell culture model was outlined in **Table 2.5**.

Table 2.5: Summary of different 3D cell culture models.

3D Model	Description	Suitable for	Ref
Cell spheroids	Spheroid aggregates formed by cells by culture the cells in the environment that prevent cells to attached on the culture surface.	• Cancer study. • Tissue with thick multilayer configuration.	(Justice et al., 2009; Kelm et al., 2003)
Multilayer culture	3D construct with multilayer of cells (same or different cell types) in a construct.	• Tissue composed of different layers of cells.	(Netzlaff et al., 2005)
Microfluidic 3D cell culture	3D tissues culture incorporated with microfluidic system. Perfusion of liquid through the tissue construct. The cell and substances can also migrate between fibers of scaffolds.	• Tissue exposed to flow. • System with systemic substances transfer.	(Domansky et al., 2010; Yang et al., 2015)
3D tissue printing	Cell-laden medium was used as ink to fabricate 3D tissue construct.	• Complex 3D constructs.	(Moon et al., 2010)
Magnetic levitation	Cells were incubated with magnetic particles to uptake the particles. Cells were then levitated and subjected to magnetic field in order to form the desired shape.	• Special structure such as ring • Co-culture	(Haisler et al., 2013; Timm et al., 2013)
Cell aggregates embedded in structural support	Cells were encapsulated in structural supports such as hydrogel and solid scaffold to form different structure of microtissue.	• Complex 3D construct can be created by micropatterning the structural supports.	(Nichol et al., 2010)

Overall, the characteristics and features of 2D cell model, 3D cell model, and animal model can be summarized in **Table 2.6**.

Table 2.6: Summary of the features of 2D cell model, 3D cell model, and animal model.

Features	2D cell model	3D cell model	Animal model
Costs of apparatus	Cheap plastic ware and glassware.	Relatively expensive but the costs can be reduced by large scale production.	Expensive.
Equipment and set up	Easy to set up. General cell culture equipment (centrifuge, incubator, and cell culture hood).	Easy to set up. Besides general cell culture equipment, specific equipment such as shaker might be required.	Need animal shelter, operation theatre, and other equipment to maintain and perform experiment.
Sample availability	Abundant for transformed cell lines, cell can be stored and preserved easily.	Abundant for transformed cell lines, cell can be stored and preserved easily.	Sample number is limited by the lab space, sample cannot be stored or preserved for long period.
Sample replication	Fast replication. Experiment can be performed few hours after subculture.	Cell replication is fast but time is needed for cell to assemble and sort to form the desired tissue construct.	Slow replication.
Sequencing	All cells are genetically similar, cheaper and easier for sequencing.	Heterogeneous cell. Subtype can be developed in the same system.	Complex biological system.

Based on Table 2.6, 3D cell culture model is more complex as compared to 2D cell culture model. The disadvantages of 3D cell culture

29

model includes higher costs and more time-consuming in preparation than conventional 2D cell culture model. However, it is still cheaper and more convenient model in handling and downstream assays preparations as compared to the complicated animal model. There is also additional advantages of using any cell type in combination or singly to ask questions that could never be answered with a mouse model.

Chapter 3: Aims of the Study

3.1   Objectives

Research gaps for the current study of nanotoxicity of ZnO NM are summarized as follows:

- The toxicity and underlying mechanism of ZnO NM are still unclear, different mechanisms have been proposed. It is debatable whether the observed toxicity will also occur in the human body as the reliability of the models (2D cell culture models and animal models) used for these studies are questionable due to the intrinsic limitations for replicating the biological responses of human body to ZnO NM.

- New applications of ZnO NM in consumable product significantly increase the likelihood of consumer exposure to NM especially *via* ingestion and inhalation. However, the biological effects of ZnO NM to organs involved in detoxification and digestion process, for example, kidney and intestine, have yet to be explored.

The main aim of this study was to improve the *in vitro* model for nanotoxicity study to more accurately estimate the biological interactions and the underlying mechanism of NM to human being. The specific objectives of this study are as follows:

- Propose alternative model(s) (3D cell culture model) for different tissues such as intestinal and kidney tissues, which might expose to ingested ZnO NM, to estimate the biological effects of ZnO NM to these tissues.

- Demonstrate the effect of different parameters such as cell dimensionality and cell-cell contact on the biological response of the cell towards ZnO NM.

- Evaluate the degree of toxicity of ZnO NM towards a multilayered tissue mimicry *via* 3D cell spheroid models.

- Estimate the transcellular transport and biological effects of ZnO NM to kidney tissue by using 3D cell model.

- Improve the biological safety of ZnO NM by surface modification and compare the toxicity of the unmodified and modified ZnO NM in both 2D and 3D cell culture models.

3.2   Research Scope

This thesis was designed to focus on establishing different 3D cell culture models to mimic different tissues. The cell lines used in this thesis are limited to human cell lines because the focus of study is on the effects of NM to human. Not to mention that, rodents and other animals, which are generally used for animal studies, might not process NM in the same way as human does due to species to species variation. Hence, cell lines from other source of organism (animals) were not considered in this thesis. Animal study and clinical trial were not conducted in this thesis because it is not the main focus of this study. Nevertheless, comparison between the 3D model and the published animal and clinical trials will be discussed to make this thesis well-rounded. In addition to cytotoxicity, which is the ultimate parameter of toxicity, other toxicity parameters such as inflammatory response, oxidative

balance, gene expression, and genotoxicity will also be studied in order to assess the possible biological interactions of NM.

3.3   Significance

The results of this study may have significant impact on both providing insight about the advantages of using 3D cell culture model as a better *in vitro* model for nanotoxicity study and improving the understanding about the biological interactions of NM. The use of different 3D cell culture techniques in this study should present the versatility of 3D cell cultures in modelling different *in vivo*-like microenvironment to improve the exploration of biological interactions of NM. The results of this study shed light on the novel characteristics offered by 3D cell culture that can be useful to overcoming the limitations of current *in vitro* and *in vivo* model for nanotoxicity assessments.

3.4   Hypothesis

The hypothesis of this study is that the toxicity of NM depends on the cell dimensionality. We hypothesized that 3D cell culture model, which can better replicate the characteristics and microenvironment of tissue, can more accurately predict the nano-bio interactions and demonstrate the potential toxicity mechanisms of NM.

More specifically, the hypotheses are listed as follows:

- The cells cultured in 3D format can more accurately replicate the characteristics of cells in tissue as compared to cells in 2D format.

- The presence of cell layer and ECM in 3D cell culture model can act as a barrier to limit the mass transfer of NM to the inner layers of cells; as a result, the overall toxicity of ZnO NM in 3D cell culture model might be lower than the 2D cell culture model.

- Although lower mass transfer of NM across the 3D tissue construct than 2D monolayer culture can significantly reduce the toxicity of NM, other characteristics of cells cultured in 3D format such as better cell communication might also contribute to lower toxicity of NM.

To achieve the objectives and verify the hypothesis of this study, **Chapter 4** compared the cellular responses of intestinal cell in 2D and 3D cell culture model (cell spheroid) in order to determine the effects of cell dimensionality to the biological responses of cell to ZnO NM. A different 3D cell culture model (bilayer tissue construct) was used in **Chapter 5** to study the transcellular transport and biological effects of ZnO NM to kidney tissue construct. Moreover, the 3D cell model was also used to demonstrate the effects of cell communication to the biological response of cell to ZnO NM. The overall finding in **Chapter 4** and **5** provided an outline of the different characteristics of the studied 3D cell culture models, **Chapter 6** utilized the suitable 3D cell culture model to compare the toxicity of unmodified and modified ZnO NM to determine the efficacy of surface modification in an attempt to make a toxic nanoparticle type, safer.

Chapter 4: 3-Dimensional Spheroid Intestinal Model

4.1   Introduction

Foods are broken down in digestive system for the generation of energy and absorption of nutrients. As mentioned in **Section 1.3**, there is increasing use of ZnO NM as food supplement, toothpastes, and food packaging, the likelihood of exposure to ZnO NM via ingestion will also increase. To address this concern, we utilize a reproducible 3D model to mimic the intestinal tissue to study the ZnO NM induced toxic effects and the underlying mechanisms.

As mentioned in Section 2.5, there are different 3D cell culture models to mimic the characteristics of native tissue. Among the different models, cell spheroid was chosen to mimic the intestinal tissue for further analysis in this study. The reason of using cell spheroid is due to the cell spheroid naturally mimics several aspects of a solid tissue and has inherent diffusion coefficient for mass transfer of substances such as oxygen, nutrients and wastes (Glicklis et al., 2004). The intestinal tissue is composed of multilayer of cells. Compared to bilayer tissue model, cell spheroid is suitable to study and measure the degree of detrimental effects of NM to the intestinal tissue (Achilli et al. 2012). Besides that, cells in spheroid exhibit strong cell-cell adhesion as the cells found in intestinal tissue. Lastly, even though the intestinal epithelium at the cellular level is a layered tissue but at the sub-tissue level, it is undulating in topography to increase the surface area for increased absorption *in vivo*. Therefore, the spheroid culture with the curvature is a better mimic than the flat bilayer model.

To complete the analysis, we chose one normal colorectal epithelial cell line and one cancerous colorectal epithelial cell line for this study. These two cell lines are commonly used colonic epithelial cell lines in research such as drug screening and biomarker discovery (Ahmed et al., 2013; Ke et al., 2012; Li et al., 2003). SW480, human colon adenocarcinoma cell line, exhibits cancer stem cell like characteristics (Ke et al., 2012).

The use of normal and cancerous cell line allows us to make comparisons between the cellular response of cancerous and normal cell lines to NM.

4.2   Literature review

Cell spheroid is the simple 3D cell culture model that could be formed by using different techniques such as forced-floating, hanging-drop, agitation-based method or cell embedded in structural supports. Each method has their advantages and disadvantages, the comparisons of these four methods were summarized in **Table 4.1**.

Table 4.1: Summary of the advantages and disadvantages of different techniques to generate 3D cell spheroid.

Technique	Methodology	Advantages	Disadvantages
Hanging drop	Culturing a small aliquot of cell suspension upside down, cells will accumulate at the tip of the drop and form spheroid.	- Easy and reproducible. - Homogenous spheroids.	- Only small amount of culture medium was used so care is needed during addition and removal of medium. - Culture medium need to be changed more frequently.
Forced-floating	Culturing cell suspension on modified surface that prevent cell attachment on the surface and promote cell aggregation.	- Easy and reproducible. - Easy to change medium and treat the cell spheroid. - Suitable for high-throughput study.	- Variation in cell size and shape if the seeding density was not optimized. - Small irregular size aggregates when low seeding.
Agitation-/rotation-based	Culturing cell in a suspension which is kept in motion.	- Easy for large scale production. - Motion assists nutrient transport. - Spheroid can be formed in short time with the aim of centrifugation.	- Specialized equipment is needed (Nickerson et al., 2007). - No control over size and shape of aggregate especially when culturing multiple spheroids in a single flask. - Shear force generated during agitation may impose problems to the sensitive cell.

Technique	Methodology	Advantages	Disadvantages
Cell embedded in structural support (matrix or scaffold)	Encapsulating cells in pre-formed ECM or scaffold (natural derived or synthetic).	- Improved cell-to-ECM interaction.	- Batch to batch variation. - Difficulty for live imaging. - Additional matrix digestion step for retrieving cell spheroid. - Variation in size and shape.(Du et al., 2008)

The first three methods utilized the natural tendency of adherent cells to form spheroid. As the cells were impeded from attach to substrate, they aggregate together to form spheroid that has the lowest state of energy (Haycock, 2011).The last methods utilized external aid (matrix) to assist the formation of cells spheroid.

Cell-cell contact and native ECM are important parameters that control the cellular response and tissue specific functions. Among the four different methods, hanging drop and forced floating methods offer the advantage of forming cell spheroids with native cell-cell contact and ECM as no preformed matrix and minimum shear force are involved in the process. Compared to hanging drop method, forced-floating method allows imaging of cell spheroids during formation. Another advantage of using forced-floating method is that the cells spheroids can be easily transferred.

4.3   Materials and methods

4.3.1   Materials

4.3.1.1   Cell lines

Normal human colon mucosal epithelial cell (NCM460) and human colon adenocarcinoma cell (SW480) were purchased from Incell, USA and American Type Cell Culture, USA respectively.

4.3.1.2   Chemicals

ZnO NM, bromophenol blue, β-mercaptoethanol, bovine serum albumin (BSA), glycine, sodium diphosphate (Na_2HPO_4), paraformaldehyde,

potassium diphosphate (KH_2PO_4), potassium chloride (KCl), protease and phosphatases inhibitors cocktail, Tween 20, Tris, Triton X-100, and 3,4,5-dimethylthiazol-yl-2,5-diphenyl tetrazolium (MTT) were purchased from Sigma Aldrich, USA. Dulbecco's Modified Eagle's Medium (DMEM), fetal bovine serum (FBS), Hoechst 33342, Annexin V/propidium iodide kit, and CellROX Orange Reagent were purchased from Thermo Scientific, USA. Penicillin/streptomycin (P/S) and trypsin-EDTA were purchased from PAA Laboratories Inc., USA. Agarose was purchased from First Base, Singapore. SsoAdvanced^{TM} SYBR$^{®}$ Green Supermix was purchased from Bio-rad, USA. Immobilon Western Chemiluminescent HRP substrate was purchased from Merck Millipore, USA. Hydrochloric acid (HCl) and sodium dodecyl sulfate (SDS) were purchased from Fisher Scientific, USA. O.C.T. Tissue Freezing medium was purchased from Leica Microsystem, USA. NucleoSpin$^{®}$ RNA kit was purchased from Macherey-Nagel, USA. iScript cDNA Synthesis Kit and SsoAdvanced^{TM} SYBR$^{®}$ Green Supermix were purchased from Bio-rad, USA. Sodium chloride (NaCl) was purchased from Merck KGaA, Singapore. Glycerol was purchased from QReC Chemical, Singapore. Dimethyl sulfoxide (DMSO) was purchased from Alfa Aesar, UK.

4.3.1.3 Primers

The sequences of primers used in quantitative polymerase chain reaction (PCR) are summarized in **Table 4.2**.

Table 4.2: Summary of the primers sequence used in quantitative PCR.

Gene name	Forward primer 5' to 3'	Reverse primer 5' to 3'
Glyceraldehyde 3-phosphase dehydrogenase (GAPDH)	TTC GCT CTC TGC TCC TCC T	TGA CTC CGA CCT TCA CCT TC
Interleukin-1 beta (IL1B)	TTC GAC ACA TGG GAT AAC GAG G	TTT TTG CTG TGA GTC CCG GAG
Toll-like receptor 6 (TLR6)	TTC TCC GAC GGA AAT GAA TTT GC	CAG CGG TAG GTC TTT TGG AAC
NOD-like receptor family, CARD domain containing 4 (NLRC4)	TCA GAA GGA GAC TTG GAC GAT	GGA GGC CAT TCA GGG TCA G
Interleukin 18 (IL18)	TCT TCA TTG ACC AAG GAA ATC GG	TCC GGG GTG CAT TAT CTC TAC

4.3.1.4 Antibodies

Rabbit anti- phospho-Histone H2A.X (catalogue no. ab11174) was purchased from Cell Signaling Technology, USA. Mouse anti-TATA binding protein (TBP; catalogue no. ab51841) was purchased from Abcam, UK. Rabbit anti-nuclear factor kappa B (NF-κB; catalogue no. sc-109) p65, horseradish peroxidase (HRP) conjugated goat anti-rabbit (catalogue no. sc-2004) and goat anti-mouse (catalogue no. sc-2969) antibodies were obtained from Santa Cruz Biotech, USA. Alexa Fluor 488 chicken anti-rabbit (catalogue no. A-21441) was purchased from Life Technologies, USA.

4.3.1.5 Buffers

The buffers used in this study were prepared with the following composition:

- Phosphate buffered saline (PBS)

137 mM NaCl, 2.7 mM KCl, 10 mM Na_2HPO_4, 2 mM KH_2PO_4; pH 7.4

- Laemmli's sample buffer

  60 mM Tris-HCl, 2 % SDS, 10 % glycerol, 5 % β-mercaptoethanol, 0.01 % bromophenol blue

- Running buffer for immunoblotting

  25 mM Tris, 192 mM glycine, 0.1 % SDS

- Transfer buffer for immunoblotting

  25 mM Tris, 192 mM glycine, 10 % methanol, 0.05 % SDS

- Tris buffered saline with Tween 20

  20 mM Tris-HCl, 137 mM NaCl, 0.05 % Tween 20

4.3.2 Methods

4.3.2.1 2D cell culture

Both the cell lines were grown in DMEM supplemented with 10% FBS and 1% P/S in a standard cell culture condition of 37 °C with 5 % CO_2. For treatment conducted in 24-well plate, SW480 cells and NCM460 cells were seeded in density of 1.2×10^5 cells and 1.8×10^5 cells per well respectively. For PCR and immunoblotting of phosphorylated Histone (pγ-H2AX) assays conducted in 6-well plate, 3.6×10^5 SW480 cells per well and 5.4×10^5 NCM460 cells per well were seeded. Prior to the treatment, the cells were allowed to attach and grow for one day.

4.3.2.2   3D cell culture

Micro-well agarose (2 %) hydrogel was casted by using 3D Petri Dish$^{\circledR}$ (Sigma-Aldrich, Singapore). Each agarose hydrogel can fit into 24 well-plate format with 96 small wells. The solidified hydrogel was sterilized by ultraviolent visible (UV) and equilibrated with DMEM for one day prior to use. The DMEM was removed before cell seeding. Fifty microliter of dispersed SW480 (1.2×10^5 cells) and NCM460 cell suspension (1.8×10^5 cells) in supplemented DMEM were seeded onto each micro-patterned agarose hydrogel. Five minutes after the settling of cells, supplemented DMEM (500 μl) was added into the culture plate. Cells were allowed to aggregate into 3D cell spheroid within the hydrogel for one day. For treatment, the formed cell spheroids were flushed out from the micro-patterned agarose hydrogel to a 24-well plate with a layer of flat agarose hydrogel. For the assays required higher cell number, cell spheroids from three micro-patterned agarose hydrogel were combined and transferred into a 6-well plate with a layer of flat agarose hydrogel. **Scheme 4.1** summarized the procedures of 3D cell culture used to form cell spheroids.
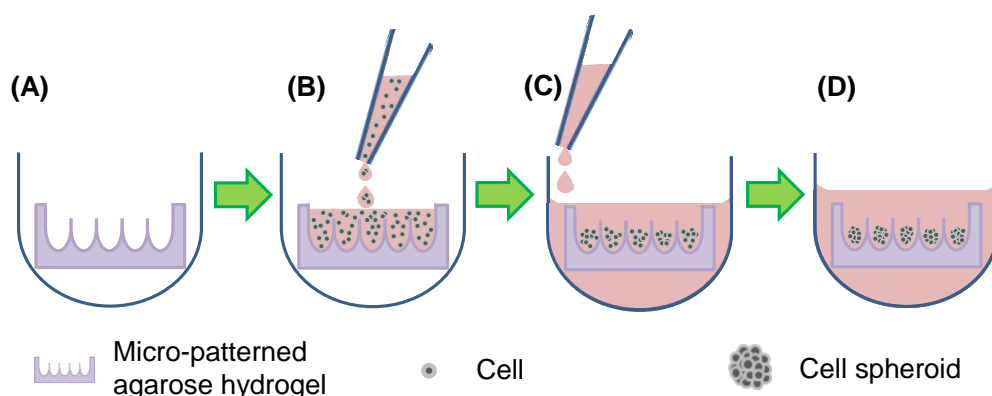
Scheme 4.1: Summary of the procedures to fabricate uniformly sized 3D cell spheroids with micro-patterned agarose hydrogel. (A) micro-patterned

agarose hydrogel was casted and sterilized before seeding cells. (B) mono-dispersed colorectal cells in complete DMEM were seeded into the hydrogel. (C) Complete DMEM was added into the culture plate after the cells have settled in the hydrogel. (D) Cells were incubated in 37 °C to self-assemble to cell spheroid.

4.3.2.3 Characterization of ZnO NM

The primary size (smallest dimension of an individual nanoparticle) and morphology of ZnO NM were determined by transmission Electron Microscopy (TEM; JEM 2010, JEOL, Japan). The preparation of sample is as follows: ZnO NM (50 μg ml^{-1}) in ethanol was dropped on carbon-coated copper grid and dried at room temperature. The measurement of primary size was derived from scoring 50 randomly selected NM with the aid of ImageJ software (Abramoff et al., 2004).

The hydrodynamic size and surface charge of ZnO NM were determined by Dynamic Light Scattering (DLS; Malvern co., UK). Dispersed ZnO NMs (500 μM) were sonicated by probe sonicator (Microson^{TM} XL 2000, Qsonica, USA) before measurement was taken. For the hydrodynamic size and charge measurement in complete DMEM, ZnO NM (500 μM) were first dispersed in supplemented DMEM and sonicated. The NM solution was then centrifuged (21,000 g; 30 minutes) and washed with ultrapure water for three times to remove unbound proteins. The collected ZnO NM were re-suspended in ultrapure water and sonicated before analysis.

4.3.2.4 Preparation of treatment solution

ZnO NM (4.176 mM) were used as received without any chemical modification. The properties of ZnO NM, which provided by the supplier, was

summarized in Table 4.3. The treatment solutions of ZnO NM were prepared by diluting the stock solution in supplemented DMEM to the final working concentrations (31.5, 125, 500, 1000 μM). The working solutions were sonicated for one minute before introduce to the cells. For all the experiments, cells that are not treated with ZnO NM served as the negative control.

Table 4.3: Summary of the properties of commercial ZnO NM provided by supplier.

Properties	Value
Concentration	20 wt. %
Particle size	< 100 nm (DLS)
Average particle size	≤ 40 nm
pH	7.5 ± 1.5
Density	1.7 ± 0.1 g ml^{-1} at 25 °C

4.3.2.5 Quantification of oxidative stress in 2D and 3D cell model

Thirty minutes before the end of the treatment timepoint, one microliter of CellROX Orange Reagent (2.5 mM) was added into the treatment solution in each well. After 30 minutes incubation, cells were washed with PBS thrice and trypsinized with trypsin-EDTA for 5 minutes. The trypsinized cells were neutralized with supplemented DMEM and centrifuged (2500 g, 5 minutes) to separate the supernatant. The cells pellets were dispersed with PBS for quantification of intracellular ROS using Tali® Image cytometer.

4.3.2.6 Isolation of RNA and quantitative PCR for 2D and 3D cell models

Cells were treated on 6-well plate. ZnO NM treated cells were trypsinized and collected after treatment. The cells were washed with PBS before centrifuged at 2500 g for 5 minutes to remove supernatant. RNA in the treated cells was isolated by using NucleoSpin® RNA kit according to the manufacturer's instructions. Isolated RNA was converted to first strand cDNA by iScript cDNA Synthesis Kit according to the manufacturer's instruction. Quantitative PCR was performed with SsoAdvanced™ SYBR® Green Supermix in CFX96™ Real-Time PCR Detection System (Bio-rad, USA).

4.3.2.7 Extraction of protein and immunoblotting of pγ-H2AX

Cells were treated with ZnO NM on 6-well plate for 12 hours. At the end of the treatment, the treated were washed, trypsinized, and centrifuged as the above section. The collected cells were lysed by standard Laemmli sample buffer supplemented with 1 % of protease and phosphatase inhibitors cocktail. Cell lysate was sonicated by using probe sonicator for 30 seconds and centrifuged at 21000 g to remove cell debris. The proteins in the supernatant were separated in a 15 % SDS-polyacrylamide gel and electro-transferred onto a nitrocellulose membrane. After transfer, the membrane was blocked with 5 % skim milk for one hour and incubated with primary antibodies according to the supplier's instructions (working dilution of rabbit anti- phospho-Histone H2A.X and mouse anti TBP is 1 : 1000 and 1 : 2000 respectively). The membrane was then washed and incubated with HRP conjugated secondary antibody according to supplier's instruction (working dilution of HRP conjugated goat anti-rabbit and goat anti-mouse antibodies is 1 : 5000). The

protein bands on membrane were visualized by using Chemiluminescence Imaging System (Syngene, UK) after added with Immobilon Western Chemiluminescent HRP substrate.

4.3.2.8   Annexin V/propidium iodide assay

Cells were treated with ZnO NM on 24-well plate for 24 hours. All the floating (non-viable) and attaching (viable) cells were collected, washed, trypsinized, and centrifuged at 2500 g for 5 minutes. Annexin V binding buffer and Annexin V-Alexa Fluor$^®$ 488 conjugate mixture were added to the cell pellet at the ratio of 20 : 1 for 20 minutes incubation. After the incubation, the cell suspension was centrifuged to separate supernatant. Fresh Annexin V buffer and propidium iodide in the ratio of 100 : 1 was added into the cell pellet for 5 minutes incubation. The apoptotic and necrotic cells were assayed by Tali$^®$ Image cytometer.

4.3.2.9   Imaging and quantification of cell spheroid diameter

Bright field images of the 2D cells and 3D cell spheroids were captured by inverted microscope Olympus-CX41 (Olympus, Japan). The average diameter of the cell spheroids were measured from 10 randomly selected spheroids with the aid of ImageJ software (Abramoff et al., 2004).

4.3.2.10   Immunofluorescence labelling of nuclear factor kappa B (NF- κB)

The ZnO NM treated SW480 cell spheroid were collected, washed with PBS, and fixed with paraformaldehyde (4 %) for 1 hour. The fixed cell spheroids were labelled with bromophenol blue (1 mg ml^{-1}) for 30 minutes before embedded in O.C.T. Tissue Freezing medium. The freeze sample was

cryosectioned with a thickness of 10 μm and transfer onto polysine slides. The sections were permeabilized by Triton X-100 (0.2 % in PBS) for 15 minutes and blocked with 2 % BSA for 1 hour. The sections were incubated with 1 : 250 of rabbit polyclonal antibody to NF-κB p65 antibody overnight at 4 °C. After that, the sections were washed with PBS thrice, and incubated with 1 : 400 of Alexa Fluor® 488 chicken anti-rabbit antibody for 1 hour. The fluorescence images of the sections were captured by Olympus FluoView FV1000 laser scanning confocal microscope (Olympus, Japan).

4.3.2.11 Determination of cell metabolism rate

2D and 3D cell spheroids were exposed to MTT (0.5 mg ml^{-1} dissolved in culture medium, 0.5 ml) in dark at 37 °C for 3 hours. The precipitated formazan crystal was dissolved by DMSO (0.5 ml) and shake gently with orbital shaker for 30 minutes. The absorbance of the solution at 570 nm was quantified by microplate spectrophotometer (Epoch, Bio-Tek, USA).

4.3.2.12 Statistical analysis

Data reported are means ± standard deviation (SD). Statistical analysis was ascertained with paired sample Student's *t*-test comparison. Comparison was considered as statistically significant with *p*-value of < 0.05.

4.4 Results and discussions

4.4.1 Formation of reproducible 3D cell culture model - colorectal cell spheroid

In order to achieve the objectives of this study to form an inexpensive and reproducible 3D cell culture model, forced-floating method with the assistant of micro-patterned agarose hydrogel was used. With the aid of micro-patterned agarose hydrogel, colorectal cells such as NCM460 and SW480 can self-assemble to uniformly sized cell spheroids (**Figure 4.1**).
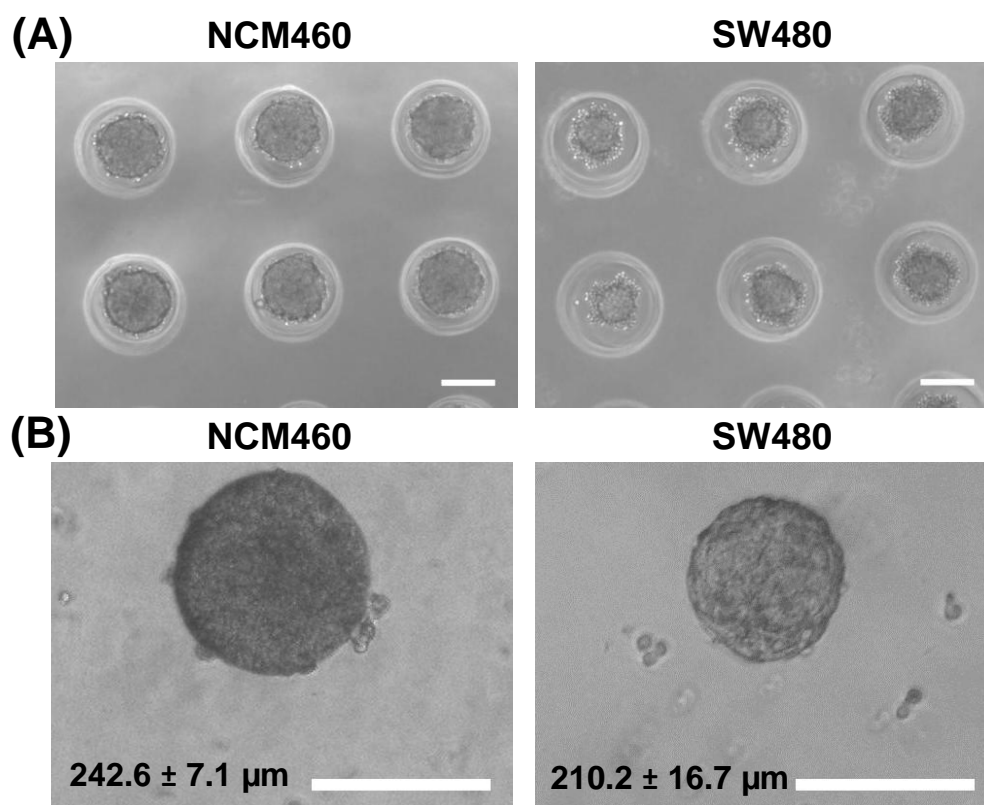
Figure 4.1: Uniformly sized 3D colorectal cell spheroids for nanotoxicity study. (A) Both NCM460 and SW480 cells can self-assemble to form cell spheroids in micro-patterned agarose hydrogel. (B) The cell spheroids can be transferred to flat surface for treatment. Scale bar used is 200 µm.

These uniformly sized cell spheroids can be transferred to flat agarose hydrogel for the ease of treatment. The shape of the cell spheroids was

51

maintained even after leaving the confines of the micro-patterned agarose hydrogel. This suggests that the cells in this configuration have strong cell-cell interactions to hold them in the spheroid shape.

The size of the cell spheroids was optimized to be larger than the minimum thickness of submucosa layer of human sigmoid colon (0.2 mm) by adjusting the seeding density of cell in micro-patterned agarose hydrogel (Castro-Poças et al., 2015). The average diameter of NCM460 and SW480 cell spheroid is 242.6 ± 7.1 µm and 210.2 ± 16.7 µm respectively. This difference might be contributed to the difference in cell size and packaging in tissue.

We found that cells culture in 3D format have different metabolic rate as compared to 2D cells. The lower metabolic rate of cells in 3D formats (**Figure 4.2**) suggests that cell in 3D are not as actively dividing as the cells in 2D format. One of the reasons might be the limited access of nutrients and oxygen across the cell barriers and ECM. The concentration of nutrients and oxygen are inversely proportional to the distance from the surface. Besides that, cancerous SW480 cells were more metabolically active as compared to the normal cells, NCM460.
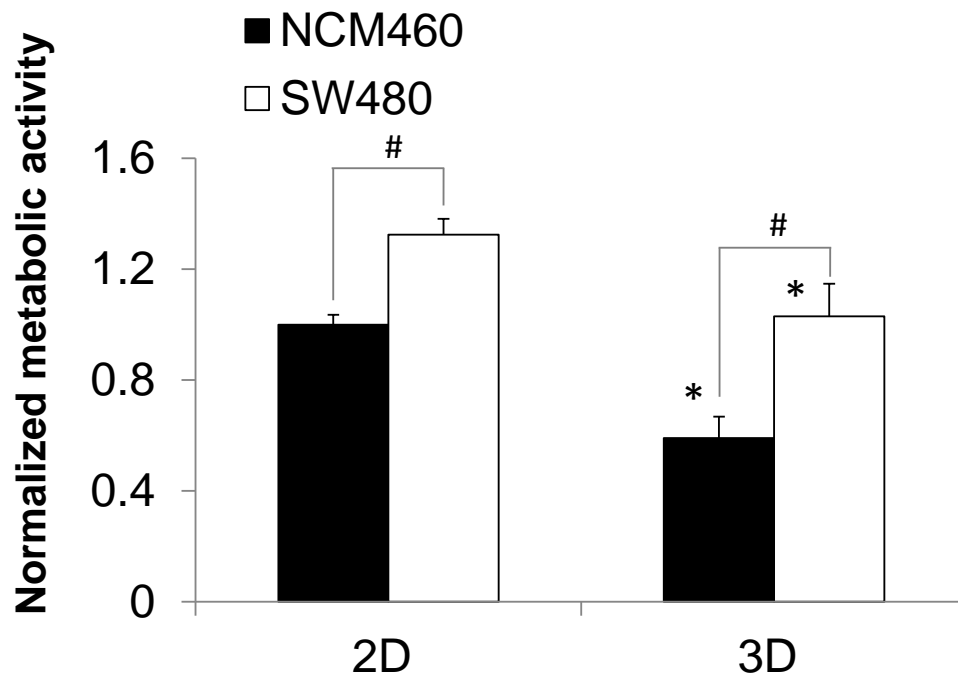
Figure 4.2: Cells cultured in 3D format have lower metabolism as compared to cells cultured in 2D format. Cancerous SW480 cell is more metabolically active as compared to the normal NCM460 cell line in both 2D and 3D cell formats. Data represent means $\pm$ SD, $n = 3$. Student's t-test, $p < 0.05$, *significantly different from the cells in 2D, #significantly different between the two groups.

4.4.2 Characterization of commercial ZnO NM

The physical and chemical properties of NP are critically dependent on several parameters such as the size, polydispersity, and surface charge. As the matter of fact, these parameters are also the important factors that affect the biological interaction between NP and cell (Cong et al., 2011).

As was previously stated, the characterization of NM is important before the start of the nanotoxicity assessment. To accurately address the characteristics of NM in different environment, the commercial ZnO NM, which employed in this study, in both water (the initial dispersant used to keep

the stock) and serum supplemented culture medium (dispersant for cell treatment) were characterized before conducting the subsequent toxicity tests.

Figure 4.3 showed the primary size and the shape of ZnO NM captured by TEM. The commercially available ZnO NM has a primary size (smallest dimension of an individual nanoparticle) of 24.0 ± 6.08 nm, which is similar to the specifications stated by the supplier (average particle < 35 nm). Based on the TEM images, the shape of ZnO NM is irregular, spherical and polygonal NP can be seen in the images. **Table 4.4** summarized the physical properties of ZnO NM in both water and culture medium. The data obtained by DLS showed that ZnO NM formed aggregates when dispersed in water or culture medium. However, the hydrodynamic size of ZnO NM was reduced by 35.9 % when dispersed in serum supplemented culture medium. This reduction of hydrodynamic size could be attributed to stabilizing effect of protein corona on the surface of ZnO NM (Pelaz et al., 2013). The negatively charged proteins in serum were physically absorbed onto the surface of positively charged ZnO NM. As a result, the surface charged of ZnO NM in serum containing culture medium was negative, even though the isoelectric point of ZnO NM is known to be between 9 and 10 (Rasmussen et al., 2010).

(A)

24.02 ± 6.08 nm

(B)
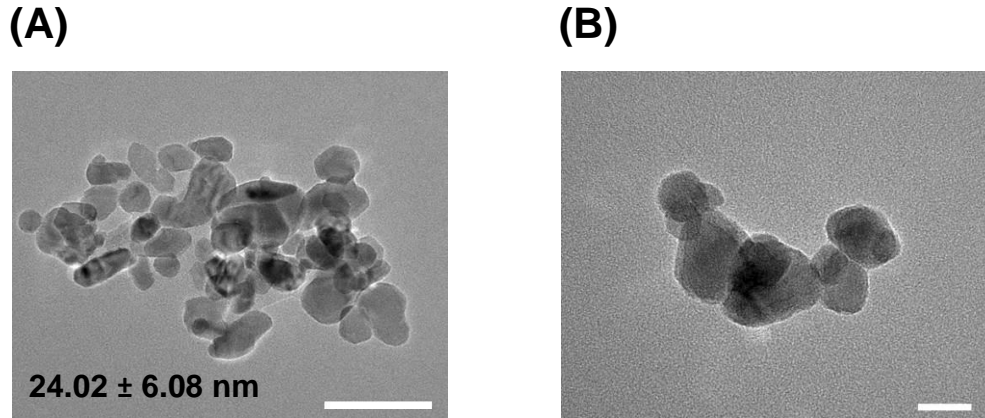
Figure 4.3: The physical characterization of ZnO NM. TEM images showed (A) the size and shape of the ZnO NP, and (B) a close-up image of the ZnO NM. Data represent means ± SD, *n = 50*. Scale bar used in (A) is 100 nm and (B) is 25 nm.

Table 4.4: Summary of the physical properties of ZnO NM in different dispersant.

Dispersant	Hydrodynamic size, nm	PDI*	Zeta potential, mV
Ultrapure water	222.0 ± 12.2	0.29 ± 0.04	+ 15.3 ± 0.7
Complete DMEM (with 10 % FBS)	142.2 ± 1.3	0.18 ± 0.01	- 16.4 ± 1.0

All data are means ± standard deviation of three independent measurements.

*PDI denoted polydispersity index.

4.4.3   Nanotoxicity assessment

Given that ZnO NM-induced oxidative stress is believed to be one of the toxicity mechanism of ZnO NM to 2D cell model (Xia et al., 2009), CellROX Orange reagent was used to detect the intracellular ROS level after 2 hours and 6 hours of ZnO NM treatment. As shown in **Figure 4.4**, ZnO NM induced differential response in different cell lines and cell models. Within 2 hours of the ZnO NM treatment, the levels of intracellular ROS in both 2D

NCM460 and SW480 cells were slightly upregulated; on the other hand, the upregulation of ROS level is prominent in the 2D SW480 cell when the treatment was extended to 6 hours. In contrast, the large increase in highly oxidative stressed cell in non-cancerous NCM460 cell was only observed at the highest concentration of ZnO NM within 6 hours treatment. This result is similar as the reported 2D cellular responses to ZnO NM (Setyawati et al., 2013c).
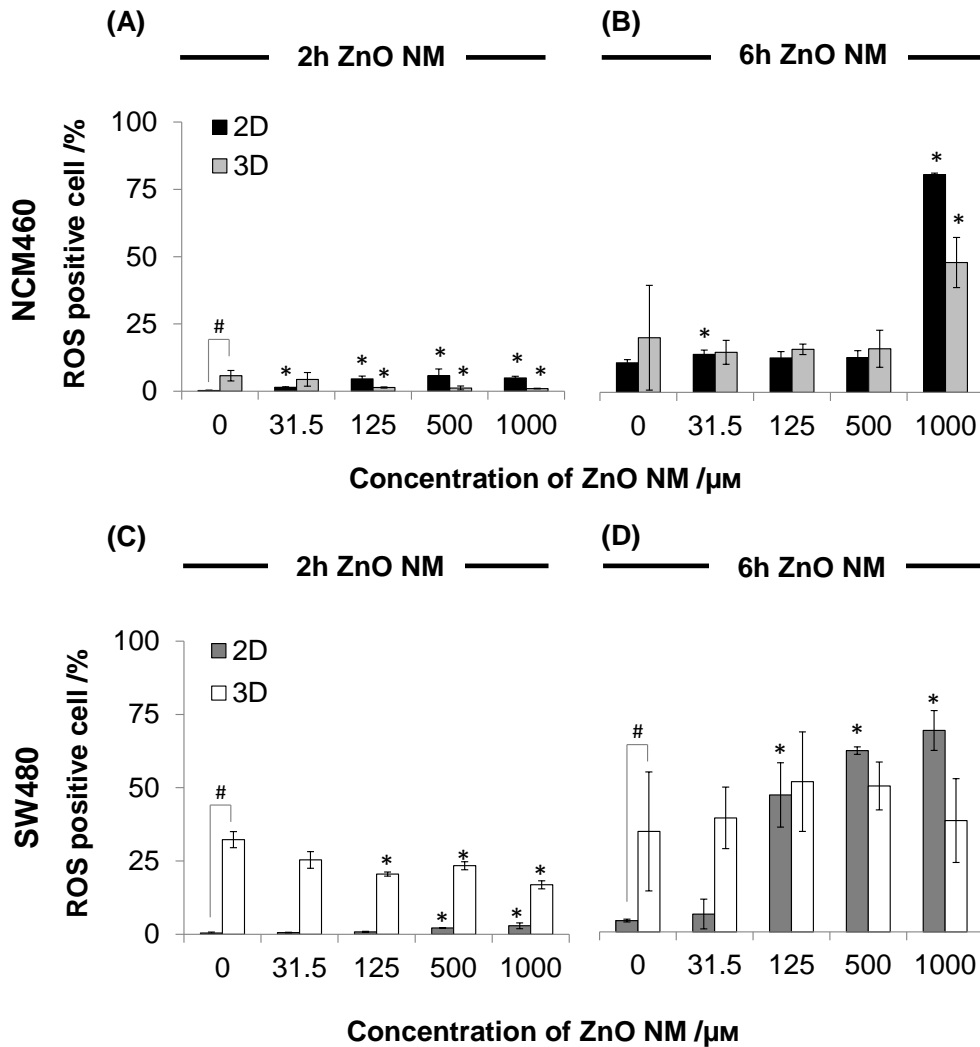
Figure 4.4: ZnO NM induced oxidative stress in 2D cell culture model at early timepoint. ZnO NM induced intracellular oxidative stress in (A) 2D NCM460 cells at early timepoint, (B) 3D NCM460 cell spheroids at the highest concentration after 6 hours treatment, and (C) 2D cancerous SW480 cells with a time- and concentration-dependent manner but not in (D) 3D SW480 cell spheroid model. Data represent means ± SD, $n = 3$. Student's t-test, $p < 0.05$, *significant different from control, #significant different between the two control groups (concentration = 0).

For the cells cultured in 3D spheroid model, differential cellular response to ZnO NM was observed. ZnO NM failed to induce significant ROS upregulation in 3D SW480 cells with high ROS and only induced the oxidative stress in 3D NCM460 cells after 6 hours of 1000 μM ZnO NM treatment. The difference in cellular response between 2D and 3D cell models

implies that cellular microenvironment could affect the cellular response to an external stimulus. Therefore, the different microenvironment of cell between 2D cell culture model and *in vivo* might largely affect the cellular outcomes in toxicity assessment.

Another interesting observation is that the cancerous SW480 cell was found to have significantly higher endogenous ROS level than non-cancerous NCM460 cell when cultured in the 3D cell spheroid model (3D SW480 cell is 5.6 folds higher than NCM460 cell). Studies have revealed that *in vivo* cancerous cells express high level of ROS than the normal cells (Cairns et al., 2011; Trachootham et al., 2009). Although high level of ROS is known to induce detrimental effects such as DNA damage, lipid peroxidation and trigger inflammatory response, low and manageable level of ROS is essential for many biological functions. For instances, increase of cellular oxidation is important for immune defeat in organism (Romano et al., 2010).

Another role of ROS is that they are able to activate AKT8 virus oncogene cellular homolog pathway and inhibit activity of phosphatase to inhibit pro-apoptotic pathway and stimulate cell proliferation (Le Belle et al., 2011). Therefore, it could be deduced that cancerous cell utilizes its high level of endogenous ROS to increase proliferation and decrease programmed cell death. Our result suggests that *in vitro* spheroid environment enables SW480 cells to replicate the important tumorigenic *in vivo* characteristic, which completely dissipates when the same cell was cultured in 2D environment. Once again, this finding supports the involvement of cellular microenvironment in affecting the characteristics and behaviors of cell.

58

4.4.4 ROS-independent inflammatory response in 3D SW480

To determine the expression of inflammatory gene after ZnO NM treatment, real time PCR was conducted. As inflammatory response can be mediated by different pathways, we included the genes involved in early pro-inflammatory signaling, NOD-like receptor family CARD domain containing 4 (NLRC4) and interleukin 1 beta (IL1B); downstream inflammatory process, interleukin-18 (IL-18); and adaptive immune response, Toll-like receptor (TLR6) to examine the inflammatory responses induced by ZnO NM.

The encoded protein of NLRC4 (NLRC4 protein) and IL1B (IL-1β) genes are involved in the early pro-inflammatory signaling. NLRC4 inflammasome complex, which promotes the activation of caspase-1, is assembled after NLRC4 protein sensed the stimulus in cytoplasm. After that, activated caspase-1 will process and secrete pro-inflammatory cytokines such as IL-1β and IL-18.(Martinon et al., 2009) Concomitantly, IL-1β will bind to the IL-1 receptor to activate nuclear factor kappa B (NF-κB) activity and its signaling pathway.

The encoded protein of IL-18 (IL18) was processed and secreted by caspase-1. The main function of IL18 in inflammatory response is related to the production of pro-inflammatory cytokines. Toll-like receptors (TLRs) are transmembrane proteins, which are involved in a different inflammatory pathway. TLRs recognize the pathogen-associated microbial patterns (PAMPs) and danger-associated molecular patterns (DAMPs) to activate different transcription factors for the initiation of immune response (Triantafilou et al., 2006).

59

After 6 hours of ZnO NM treatment, the upstream inflammatory genes (IL1B and NLRC4) and TLR6 were upregulated in both 2D and 3D cell models (**Figure 4.5**A). An interesting phenomena was observed in SW480 cell, high concentration of ZnO NM (1000 µM) induced a largest increase in expression of inflammatory gene in 3D SW480 cells within 6 hours treatment but the upregulation of inflammatory genes in 2D SW480 was relatively moderate as compare with 3D model and NCM460 cells. Although ZnO NM did not induce a significant increase of intracellular ROS in 3D SW480 within 6 hours treatment, quantification PCR results showed that ZnO NM trigger a severe inflammation response in the cell. This ROS-independent inflammatory response, which was found in 3D cell model, is different from the findings in 2D cell culture model from previous studies that showed signs of inflammatory response associated with upregulation of ROS (Heng et al., 2011).

When the ZnO NM treatment was extended to 24 hours (Figure 4.4B), the expression of inflammatory genes was remained high in 2D cell models especially the 2D SW480 cell. Conversely, most of the inflammatory genes expression levels in 3D cell model were reverted back to the basal level as the control groups at this timepoint. The interpretation of the reversion of the inflammatory gene expression from the high expression level during early timepoint is that the inflammatory response induced by ZnO NM to 3D cell is short term and acute type, whereas the inflammatory response observed in 2D cell model is more likely to be a long term and chronic type.
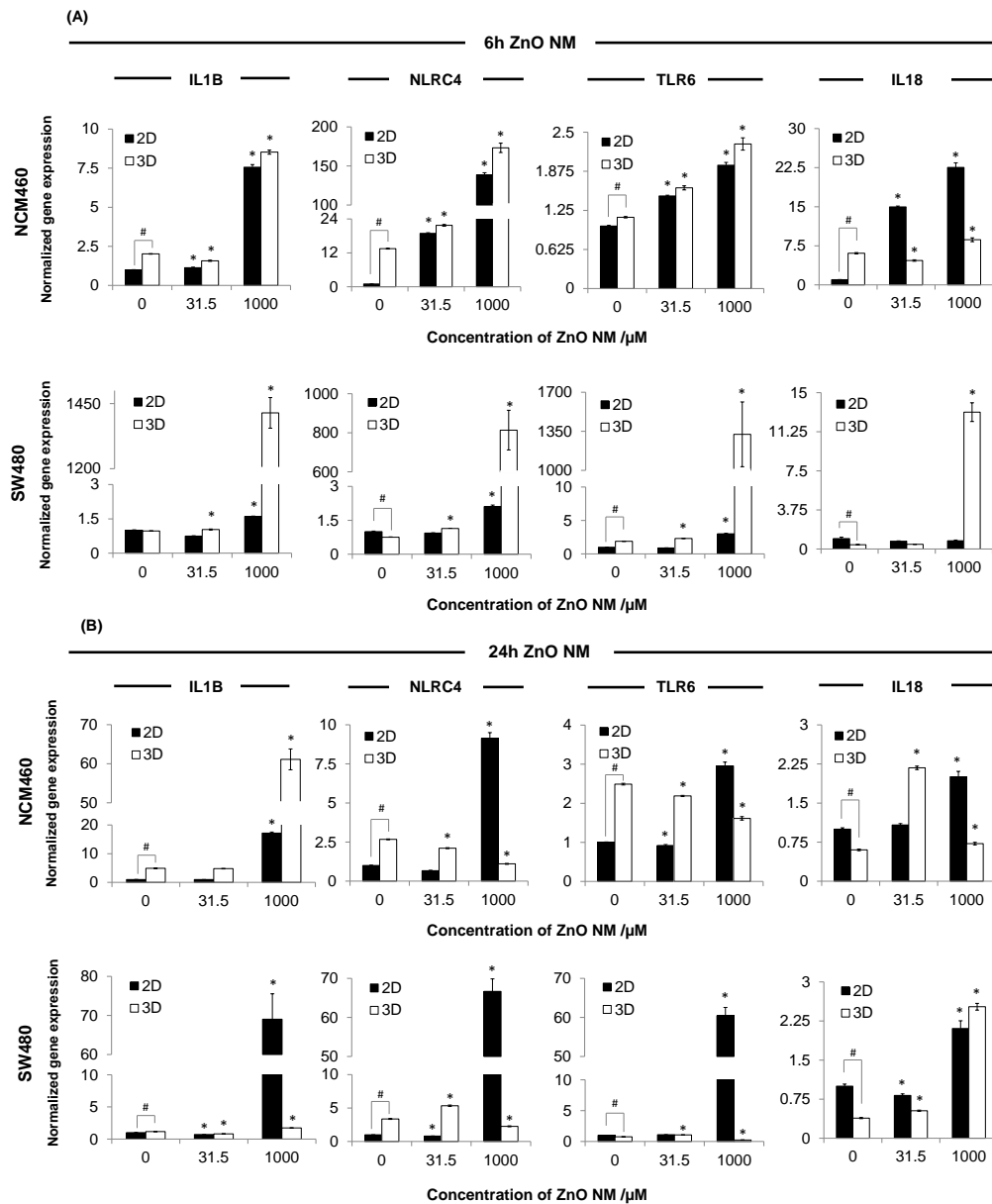
Figure 4.5: Differential expression of inflammation related genes in both 2D and 3D cell model within different timepoint. (A) The upstream inflammatory genes (IL1B and NLRC4) and TLR6 were upregulated in all cell models upon 6 hours exposure. (B) The expression of these genes in 2D cell models remained high when the treatment was extended to 24 hours but most of these genes' expression in 3D cell models was reverted back to basal level. Data represent means ± SD, *n = 3*. Student's *t*-test, *p < 0.05*, *significant different from control, #significant different between the two control groups (concentration = 0).

4.4.5 3D cells are more resistant to ZnO NM induced DNA damage

Based on above the distinct cellular responses of different cell culture models to ZnO NM, it is likely that ZnO NM also induce different downstream biological response in 2D and 3D cells. Therefore, further studies and assays related to different forms of toxicity should be performed.

We proceed with the effects of ZnO to the upmost important biomolecule in cell, deoxyribonucleic acid (DNA). Similar to other biomolecules, DNA, which located in the nucleus of eukaryotic cell, is also susceptible to spontaneous chemical reactions. As NM are known to be highly active, it is possible that ZnO NM might directly or indirectly damage the DNA. To verify whether ZnO NM induce damage to DNA, immunoblotting of pγ-H2AX was conducted. During the event of DNA damage, H2AX will be phosphorylated to recruit DNA repair proteins to the damage site. The extent of DNA damage is proportional to the phosphorylation of H2AX.

Figure 4.6 indicated the extent of DNA damage determined by the degree of pγ-H2AX. As reported in previous 2D study, ZnO NM caused nuclear fragmentation (Xia et al., 2008). Similarly, we observed the occurrence of severe DNA damage in 2D SW480 and NCM460 cells when they were treated with 12 hours with 125 and 500 μM of ZnO NM respectively. Severe DNA damage was also observed in 3D SW480 cell but there was no significant change in the level of pγ-H2AX in 3D NCM460. Overall, a general trend was observed in **Figure 4.6**, both SW480 and NCM460 cell models showed that the cells in 3D cultures were less susceptible to the toxicity of ZnO NM than the cells in 2D cultures.
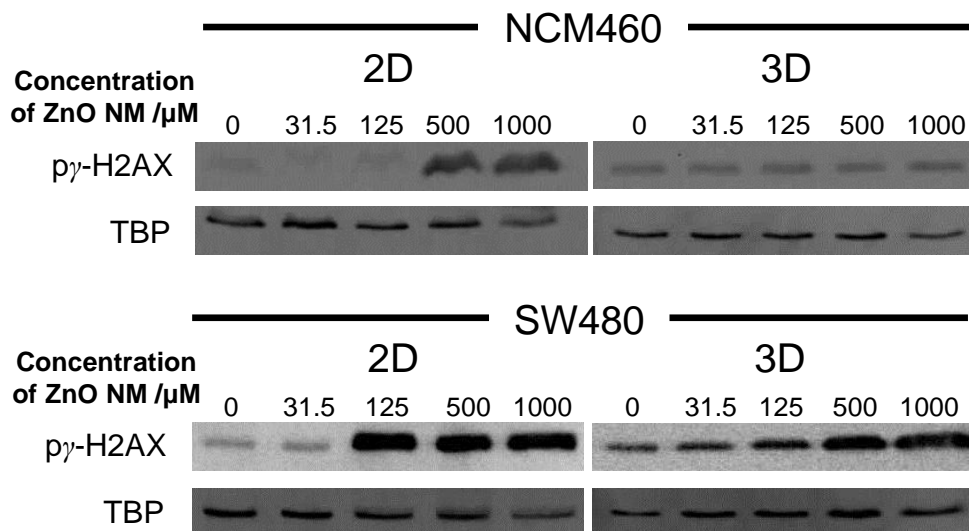
Figure 4.6: 3D cells are more resistant to ZnO NM induced DNA damage. Severe DNA damage was observed in 2D cell models at the onset of lower concentration as compared to the cells in 3D culture model within 12 hours of ZnO NM treatment. TBP denotes Tata-binding protein (housekeeping protein for loading control).

4.4.6   Different mode of cell death in 2D and 3D culture in response to the toxicity of ZnO NM

Under the circumstances of undesired events such as high oxidative stress, inflammatory response, and severe DNA damage induced by ZnO NM, the health of cell can be compromised. Based on our observation, we captured the significant change of cells morphology in 2D cell culture upon 24 hours of exposure to 500 μM ZnO NM (**Figure 4.7**). Both 2D NCM460 and SW480 cells became rounded and detached from the petri dish upon the 24 hours of 500 μM ZnO NM treatment. It was also observed that a small portion of cells in the surface of the 3D cell spheroid were disaggregated from the spheroid at the same treatment. The quantification data showed that the diameter of 3D cell spheroid reduced after the treatment, though the overall spherical shape

63

remained the same. This suggests that the disaggregation process observed in the 3D cell model occurred in a layer-by-layer manner.
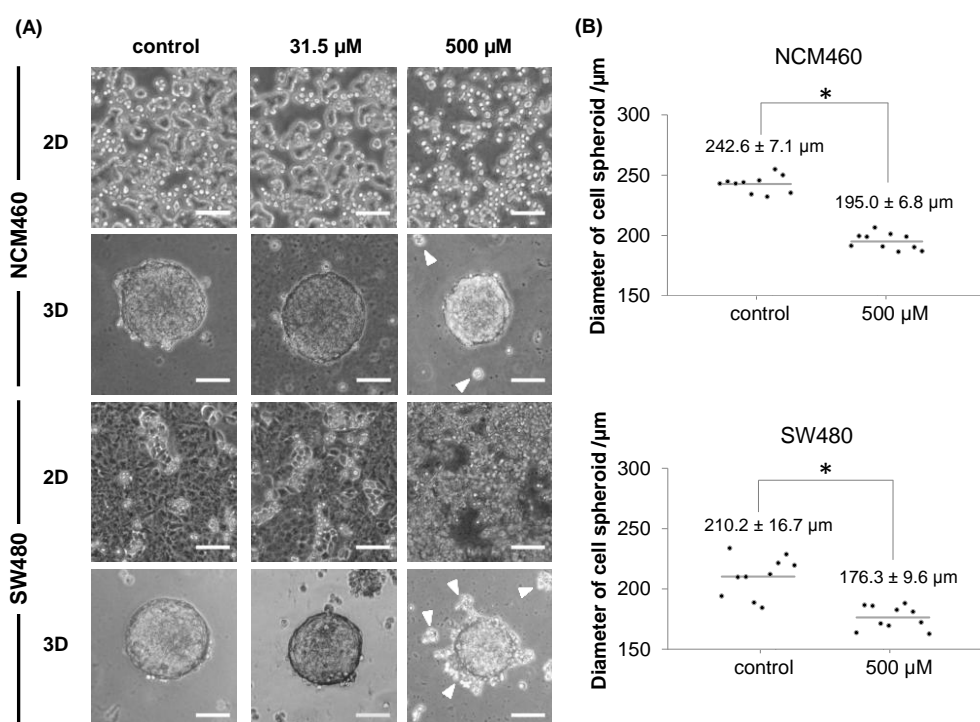
Figure 4.7: High concentration of ZnO NM compromised the cell health. (A) Both of the 2D SW480 and NCM460 cells showed a dose-dependent response to ZnO NM. Rounded and detached cells were observed after exposure to 500 µM of ZnO NM for 24 hours. Some distorted cells (indicated by the white arrow) can be found in the 3D cell models under same treatment. Scale bar: 100 µm. (B) Quantification data showed the reduction in the diameter of 3D cell spheroid after 24 hours of 500 µM ZnO NM treatment. Data represent means ± SD, *n = 10*. Student's *t*-test, *p < 0.01*, *significant different between the two groups.

The disaggregated cells in 3D cell spheroid might be the outcome of losing cell-to-cell contact. After 24 hours of 500 µM of ZnO NM treatment, about 20 % decrease in the average diameter was observed in 3D NCM460 cells spheroid (195.0 ± 6.8 µm as compared to 242.6 ± 7.1 µm for the control group, *p* < 0.01). Similarly, a reduction of 16 % in the average spheroid's diameter was found in the 3D SW480 cell model (176.3 ± 9.6 µm as compared to 210.2 ± 16.7 µm for the control group, *p* < 0.01).

To get a better understanding of the toxicity effects and mechanisms of ZnO NM to the cell heath, the mode of cell death for both 2D and 3D cell models were profiled and quantified. The annexin V/propidium iodide assay unraveled the dose-dependent response of cells to ZnO NM, with a reduced response to the toxicity of ZnO NM was observed in the 3D cell spheroids when compared to 2D culture (**Figure 4.8**). For 2D NCM460 cell model, the levels of early apoptotic, late apoptotic and necrotic cells are 3.5-, 2.5-, and 2-fold after 24 hours of ZnO NM exposure (1000 µM) as compared to the untreated control, whereas the change between 3D NCM460 cells are 1.8-, 3.2-, and 1-fold respectively. Surprisingly, a very large difference in the cell death profile was observed in the 2D and 3D SW480 cell models (4.8-, 8.5-, and 2-fold for 2D; 0-, 5.2-, and 45-fold for 3D). At high concentration of ZnO NM, there was no early apoptotic cell observed in 2D SW480, the predominant cell death was found to occur via necrosis process. In general, the main cell death mode observed in the other cell models is apoptosis. Apoptosis, or programmed cell death, is a highly regulated process occurs in cell to remove unwanted cell from a multicellular organism. Apoptosis is activated when a cell is malfunction or becomes diseased so the cell fragments can be engulfed by the phagocytic cells (Edinger and Thompson, 2004).
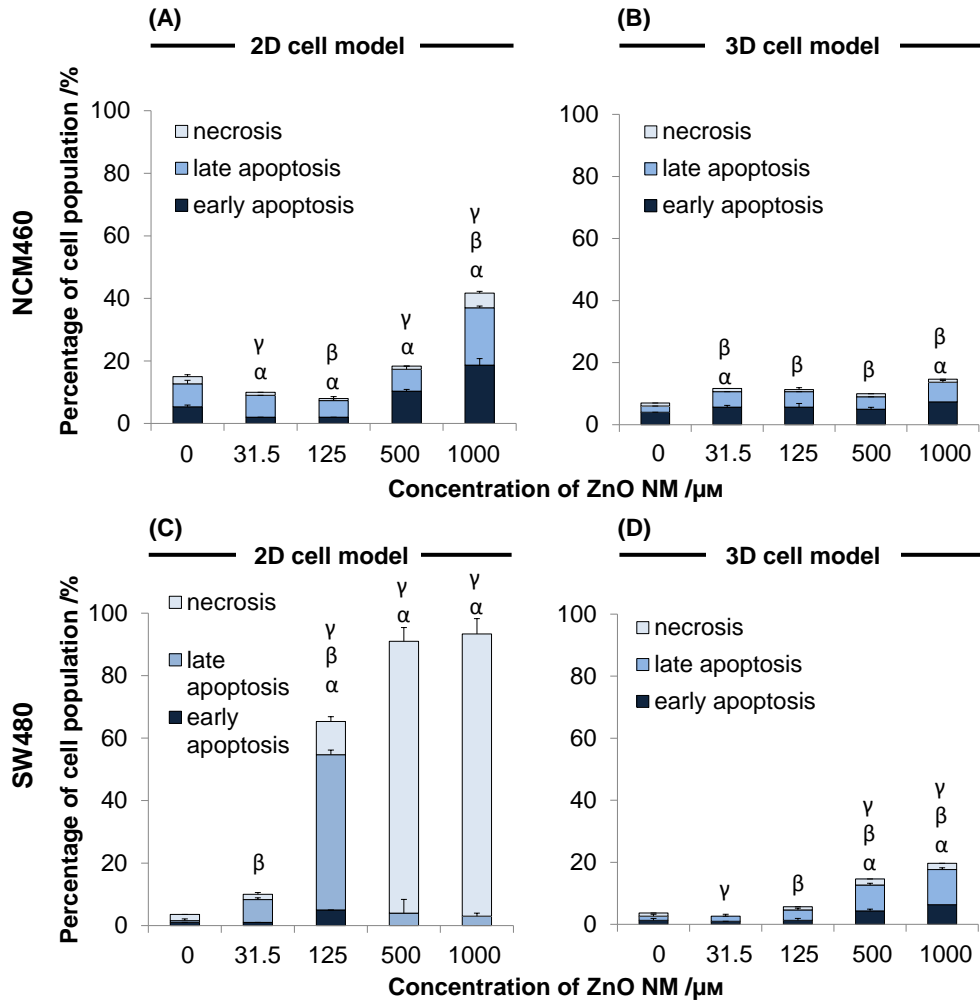
Figure 4.8: ZnO NM triggered different mode of cell death to 2D and 3D cell models. Annexin V/propidium iodide assay captures the different cell death profile in (A, B) NCM460 and (C, D) SW480. Both NCM460 and SW480 cell cultures showed that higher cell death was observed in 2D cell models as compared to 3D cell models. Data represent means $\pm$ SD, *n = 3*. Student's *t*-test, $p < 0.05$, [α]significant different with the percentage of early apoptotic cell in control group (concentration = 0), [β]significant different with the percentage of late apoptotic cell in control, [γ]significant different with the percentage of necrotic cell in control.

In contrast, necrosis is a form of traumatic cell death that is triggered by a wide range of external factors such as toxins, infection, trauma and even altered metabolism (Edinger and Thompson, 2004). The characteristics of necrosis are swelling of organelles and loss of membrane integrity. In the 2D

SW480 cell model, majority of the cells were stained positively with propidium iodine that can diffuse through the compromised membrane. At the lower concentration of ZnO NM treatment, the main mode of cell death is apoptosis. However, the cell death mode changed from apoptosis to necrosis when the concentration was increased to 500 μM. One of the possible mechanisms of this transition is the downstream events of severe DNA damage. Based on the immunoblotting of pγ-H2AX at the high concentration of ZnO NM treatment, severe DNA damage was observed in 2D SW480 cell model. DNA damage is associated with DNA repair due to the importance of genetic information in the biological organism. DNA repair is a highly energy intensive process, it can deplete the intracellular ATP store rapidly especially when the damage is severe. Low ATP state can trigger the cell to switch the mode of cell death from energy-dependent apoptosis to necrosis, a process with lower energy requirement (Leist et al., 1999).

4.4.7   Possible protective mechanism in 3D cell culture model

In summary, the toxicity of ZnO NM observed in 2D cell model is as follows; cells taken up large amounts of ZnO NM, these reactive foreign substances stimulate elevation of intracellular ROS, induce inflammatory response, trigger DNA damage and eventually cell death.

In contrast, different observations were found when the cells were cultured in 3D cell spheroid model. As mentioned in above sections, cells in 3D were found to better tolerate the toxicity of ZnO NM when compared to the cells in 2D. In order to have a better understanding of the toxicity mechanism, 3D SW480 cell spheroid was cryosectioned and immunostained

67

for NF-κB p65 protein to examine the spatiotemporal expression of NF-κB in 3D cell spheroid. NF-κB is the master transcription factor driving inflammatory responses, cell proliferation and survival (Kumar et al., 2004; Lee and Burckart, 1998).

Compared to the untreated control, intense staining of the NF-κB proteins was found around the periphery of the spheroids treated with ZnO NM (**Figure 4.9**). Interestingly, the upregulation of NF-κB proteins expression was mainly confined within the outermost 15 μm (two or three layers of cells) of the cell spheroid. This result can be attributed by the limited diffusion or transport of ZnO NM to the inner layers of the cell spheroid. In consequences, the outer cells and ECM buffered the toxic effects (elevation of oxidative stress, DNA damage and cytotoxicity) of ZnO NM to the unexposed inner cells.

However, a large upregulation of the expression of inflammatory genes upon 6 hours of ZnO NM treatment was discovered in the 3D cell model especially in the cancerous SW480 cell spheroids. This high expression of inflammatory genes might be due to the cell signaling and communications within 3D cell model (**Figure 4.5**). The arrangement of cells in 3D cell spheroids allows the cell to communicate with other cells at the side and inner layers. During the treatment of ZnO NM, the cells on the surface of the spheroid uptake NM and release inflammatory cytokines after activation of inflammatory pathways such as NF-κB signaling. As the cells were in contact with the inner cells, the inflammatory cytokines, which were secreted by the cells in outer layers, could be easily bind to the receptors on cells in the inner

layers, activate and promote systemic inflammation in the inner cells. This cascade inflammatory response might contribute to the high expression of inflammatory genes in 3D cell models.

By way of contrast, other events such as DNA damage and apoptosis did not disturb or affect the surrounding cells as the inflammatory response. Therefore, the severity of DNA damage and percentage of cell undergoing apoptosis were observed in 3D cell spheroid are low as the toxic ZnO NM were largely entrapped in the outer layers of cell spheroid. This sacrificial entrapment of toxic substances by the outer layers protected the cells in core.
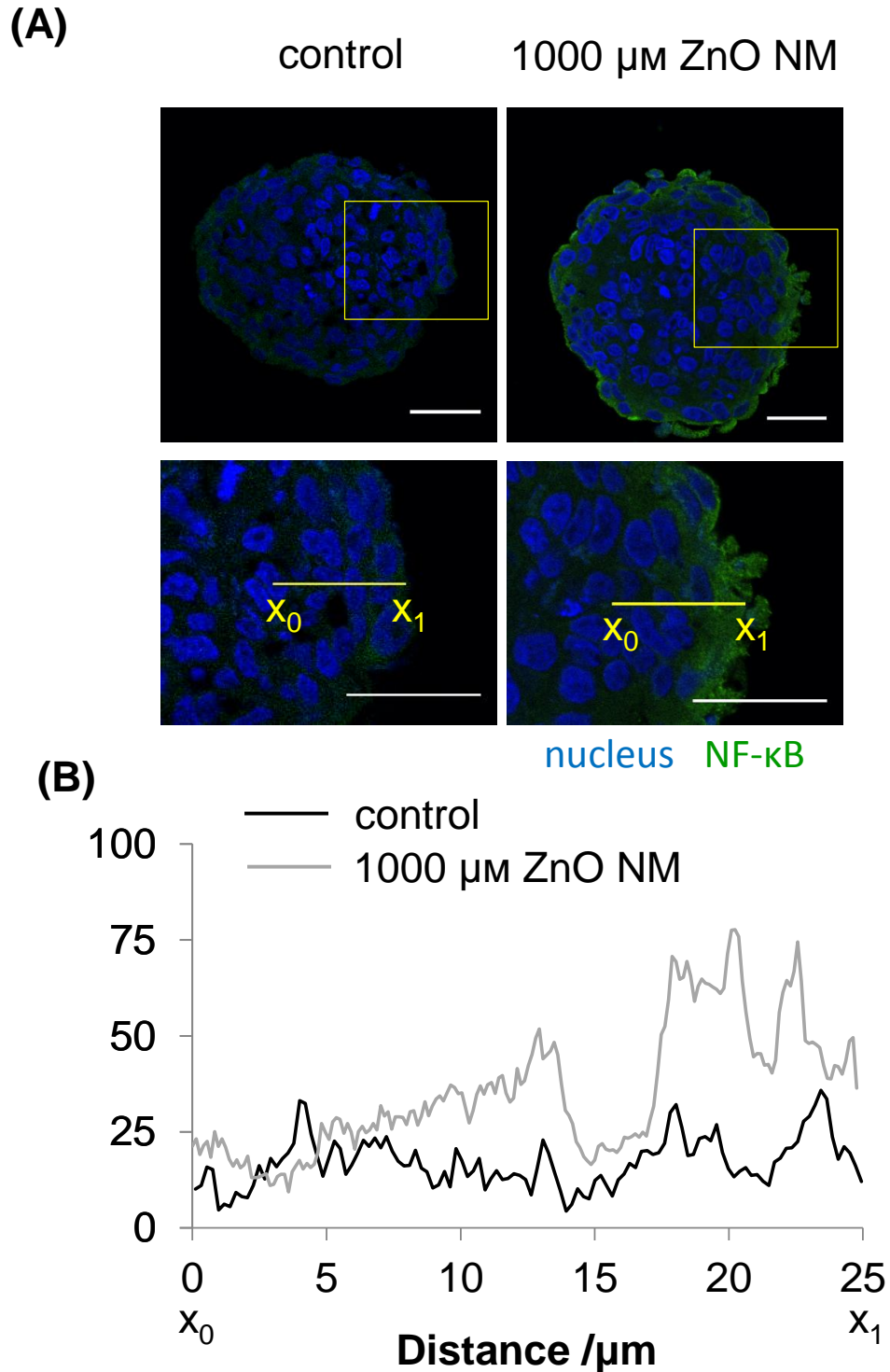
Figure 4.9: Spatiotemporal expression of inflammatory marker in 3D cell spheroids. (A) Immunofluorescence image revealed that ZnO NM induced upregulation of NF-κB in 3D cell spheroid upon 7 h treatment. NF-κB p65 were stained with Alexa Fluor® 488 (green), nuclei were stained with DAPI (blue). (B) Quantification of the NF-κB expression in the x_0x_1 line showed that the expression is largely confined in the outermost layers only. Scale bars used in (A) are 25 μm.

Taking all the findings together, we postulated some of the possible explanations for the cellular responses in the 3D cell spheroid. We hypothesized that the entrapment of ZnO NM at the outer layers of cells induced DNA damage (**Figure 4.6**), inflammatory response (**Figure 4.5**) and apoptosis (**Figure 4.8**) in these cells. The cell-to-cell communication in 3D cell model enables the transmission of inflammatory signaling from outer cells to the inner cells, resulting in a large increase in the inflammatory genes expression was observed. The apoptotic cells on the outer layers then slowly shed away from the spheroid (disaggregation of cell and reduction of spheroid's diameter in **Figure 4.7**). As most of the toxic NM were entrapped by the sacrificing outer layers, the inner cells were exposed to a less toxic environment when the outer layers shred away. Afterwards, the expression of inflammatory genes reverted back to basal level at late timepoint (24 hours treatment in **Figure 4.4B**). **Figure 4.10** summarized the proposed protective mechanism of 3D cell spheroid to toxic ZnO NM.
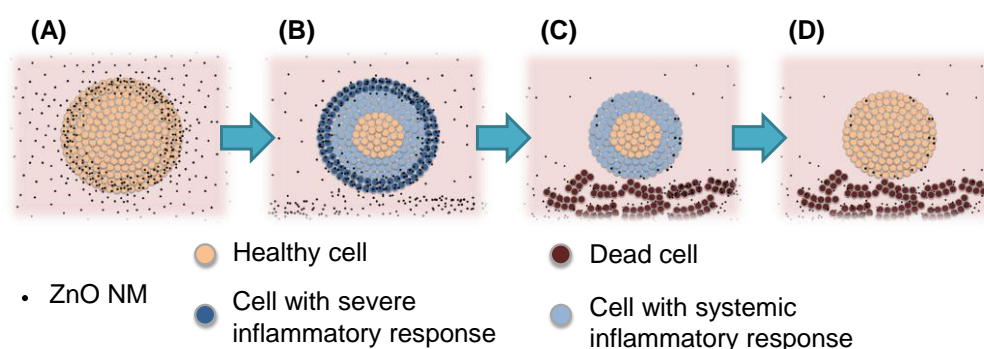
Figure 4.10: Proposed sacrificial and protective mechanism of the 3D cell spheroid. (A) Most of ZnO NM are trapped in the first few layers of the cell spheroid as physical cells and ECM limited the transport of ZnO NM to the inner layers of the cell spheroid. (B) High concentration of ZnO NM in the outer layers triggered severe inflammatory response in these cells. The inflammatory cytokines secreted by the outer cells stimulate systemic inflammatory response in the inner cells. (C) ZnO NM further induced apoptosis in the outer cells, the dead cells slowly shred away from the surface of the spheroid. (D) As the sacrificing layer entrapped most of the ZnO NM, the inner layers are exposed to a lower concentration of ZnO NM, which might be too low to induce toxic effects, so the remaining cells in the spheroid recovered from the inflammatory response at late timepoint.

4.5   Conclusion

Collectively, the results obtained by using 2D cell model showed that ZnO NM were highly toxic. However, different conclusion was obtained in 3D cell culture model. In this study, we demonstrated the differential responses of cells grown in 2D and 3D configurations to ZnO NM. Cells cultured in 3D format were more resistance to stress and the toxicity of ZnO NM. Similarly, previous studies also demonstrated that 2D cell culture model has high tendency to overestimate the toxicity of chemical entity (Cho et al., 2013b; Sauer et al., 2013). This strongly suggests that the dimensionality of cell culture system and microenvironment are important for cellular analysis as they govern the cellular response to stimuli. The tissue-ECM construct of 3D cell spheroid provides a more realistic mass transfer gradient and cell-to-cell interaction of a multilayer tissue to study the biological effects of NM. Under those circumstances, the cell communications and protective effects of outer cells on a tissue to a nanomaterial can be elucidated.

Compared to 2D cell culture model, 3D cell model takes into accounts of the effects of spatial arrangement on cell survivability and stress combating ability. In conclusion, 3D cell spheroids can recapitulate the microenvironment and characteristics of a complex tissue with all the associated interplay between cells in a 3D conformation. This *in vitro* 3D format, might be able to predict the cellular outcomes and responses of the cells in a real tissue to provide more reliable cellular interpretation of the biological interactions between NM and tissue.

Chapter 5: Bilayer Co-Culture Kidney Model

5.1 Introduction

With the prevalence of nanotechnology, the intended and unintended exposures of engineered NM have significantly increased. As a foreign entity to biological system, the information about the accumulation and clearance of NM are important for determining the biocompatibility of NM.

In vivo study showed that the clearance of NM from mammalian is dependent on the size, shape, surface charge, coatings, and other properties (Fischer et al., 2006). Liver is effective in capturing and eliminating substances with the size smaller than 20 nm. However, the coating of polymers such as polyethylene glycol (PEG) can significantly prevent the first pass extraction of NM from reticuloendothelial system (liver, spleen and bone marrow) (Choi et al., 2007). The possibility of NM circulating in blood will be significantly increased if the NM escape from the liver clearance.

Similar to liver, kidney plays an important role in detoxification to filter out waste products from blood in order to prevent accumulation of hazardous substances within human body. Kidneys filter more than one hundred liters of blood each day to effective excrete waste and reabsorb vital nutrients. Therefore, the possible nephrotoxicity of NM should be examined in detail. *In vitro* study showed that ZnO NM via oral administration can accumulate in kidney as well (Cho et al., 2013a).

In kidney, there are two types of transcellular tubular transport: tubular secretion and tubular reabsorption. The former allows the waste products remain in the blood to be transport from the blood (apical side of endothelial cell) into the filtrate (apical side of epithelial cell).

In order to resemble this apical-basal orientation of endothelial and epithelial cells in kidney proximal tubule, collagen IV coated porous transwell membrane was used as the scaffolding material to co-culture human microvascular endothelial cells (HMVEC) and human proximal tubule epithelial cells (HK-2) in order to replicate this apical-basal orientation of an opened proximal tubule (**Scheme 5.1**). This kidney proximal tubule model was then used to study transcellular transport of ZnO NM from endothelial cell barrier to epithelial cell barrier.
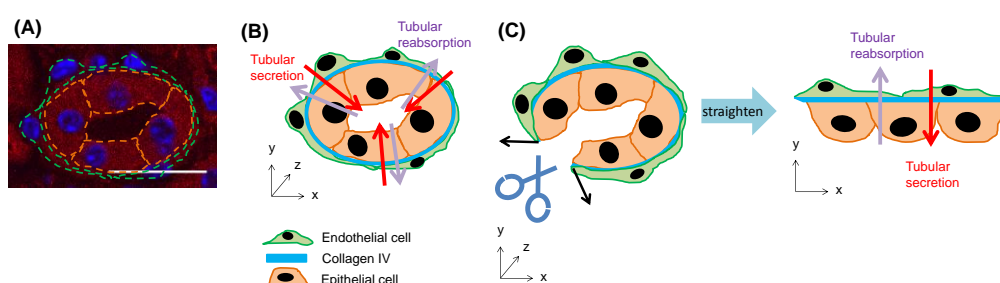
Scheme 5 Error! No text of specified style in document.**.1: Schematic presentation of kidney proximal tubule.** (A) Immunofluorescence image of the cross section of mouse's proximal tubule. Nuclei were labelled with DAPI (blue), actin filament were labelled with CF568 phalloidin (red). (B) The schematic diagram of proximal tubule. The inner layer of proximal tubule is lined by a layer of cuboidal epithelial cells; the outer layer is a layer of squamous endothelial cells (capillaries). The basal membrane, which separates the two cell types, is mainly composed of collagen IV. (C) The opened structure of proximal tubule (a cut perpendicular to the layers) can be represent as a thin layer of collagen IV sandwiched by a layer of endothelial cells and epithelial cells. Scale bar in (A) is 20 μm.

5.2   Literature review

As mentioned in **Section 5.1**, kidney could be exposed to NM. Surprisingly, the biological effects of ZnO NM to kidney tissue were scarcely investigated. In fact, kidneys are vulnerable and can develop different forms of injury due to their exposure to potential toxins on a frequent basis (Perazella,

2009). Previous studies have revealed that some of the drugs and chemicals in market are unexpectedly to be nephrotoxic, for instances, mitomycin C used in chemotherapy (Verwey et al., 1987), mannitol added in foods (Dorman et al., 1990), and cycolosporine used for immunosuppression (Morales et al., 2002). The unexpected side effects of these drugs implied that the effects of NM, which are incorporated into foods and consumable products, on kidney tissue should be determined to ensure they are not nephrotoxic agents.

Besides that, the kinetic of NM is a prerequisite for the nanotoxicity assessment. The distribution, transcellular transport, absorption, and excretion patterns of NM in human body are important parameters to determine the dosage and possible effects of NM to a particular tissue or organ (Cho et al., 2013a). However, the configuration of 2D cell culture model, which cells are adhered on culture dish to inhibit exocytosis to the basal side, cannot provide the valuable information required for assessing the biological effects of NM.

5.3 Materials and methods

5.3.1 Materials

5.3.1.1 Cell lines

Human microvascular endothelial cells (HMVEC) were obtained from American Type Cell Culture, USA. Human proximal tubule epithelial cells (HK-2) were a kind gift from Dr. Danielle Zink.

5.3.1.2   Animals

Female CB-17 Severe Combined Immunodeficiency mouse at the age of 6 − 8 week old were used, the kidney of the mouse was harvested for immunofluorescence imaging. The animal experiments were performed in compliance with protocol 097/10 approved by the Animal Use and Care Administrative Advisory Committee at the National University of Singapore.

5.3.1.3   Chemicals

ZnO NM, coomassie Brilliant blue R-250, tris, paraformaldehyde, protease and phosphatases inhibitors cocktail, Na_2HPO_4, KH_2PO_4, KCl, Triton X-100, BSA, FITC-dextran, and Tween 20 were purchased from Sigma Aldrich, Singapore. Dulbecco's Modified Eagle's Medium: Nutrient Mixture F-12 (DMEM/F12), FBS, Hoechst 33342, CellTracker Green CMFDA, and CellROX Orange Reagent were purchased from Thermo Scientific, USA. EndoGRO-MV-VEGF Complete Culture medium (EndoGRO) purchased from Merck Millipore, USA. Nitric acid (HNO_3), NaCl, and acetic acid glacial were purchased from Merck KGaA, Singapore. P/S and trypsin-EDTA were purchased from PAA Laboratories Inc., USA. Rat tail collagen IV was purchased from Corning, USA. O.C.T tissue freezing medium was purchased from Leica Microsystem, USA. NucleoSpin® RNA kit was purchased from Macherey-Nagel, USA. Methanol, glycine, SDS, and HCl were purchased from Fisher Scientific, USA. CF568 phalloidin was purchased from Biotium, USA. NucleoSpin® RNA kit was purchased from Macherey-Nagel, USA. iScript cDNA Synthesis Kit and SsoAdvanced™ SYBR® Green Supermix were purchased from Bio-rad, USA. Glycerol was purchased from QReC Chemical, Singapore.

77

5.3.1.4 Primers

The sequence of primers used in quantitative PCR is listed in **Table 5.1**.

Table 5.1: The sequence of primers used in quantitative PCR.

Gene name	Forward primer 5' to 3'	Reverse primer 5' to 3'
Glyceraldehyde 3-phosphase dehydrogenase (GAPDH)	TTC GCT CTC TGC TCC TCC T	TGA CTC CGA CCT TCA CCT TC
Interleukin-1 beta (IL1B)	TTC GAC ACA TGG GAT AAC GAG G	TTT TTG CTG TGA GTC CCG GAG
Toll-like receptor 6 (TLR6)	TTC TCC GAC GGA AAT GAA TTT GC	CAG CGG TAG GTC TTT TGG AAC
NOD-like receptor family, CARD domain containing 4 (NLRC4)	TCA GAA GGA GAC TTG GAC GAT	GGA GGC CAT TCA GGG TCA G
Interleukin 18 (IL18)	TCT TCA TTG ACC AAG GAA ATC GG	TCC GGG GTG CAT TAT CTC TAC
Interferon regulatory factor 1(IRF1)	ATG CCC ATC ACT CGG ATG C	CCC TGC TTT GTA TCG GCC TG
C-X-C motif chemokine 5 (CXCL5)	AGC TGC GTT GCG TTT GTT TAC	TGG CGA ACA CTT GCA GAT TAC

5.3.1.5 Buffers

The buffers used in this study were prepared with the following composition:

- PBS

    137 mM NaCl, 2.7 mM KCl, 10 mM Na_2HPO_4, 2 mM KH_2PO_4; pH 7.4

- Laemmli sample buffer

60 mM Tris-HCl, 2 % SDS, 10 % glycerol, 5 % β-mercaptoethanol, 0.01 %

bromophenol blue.

- Running buffer for immunoblotting

25 mM Tris, 192 mM glycine, 0.1 % SDS

- Transfer buffer for immunoblotting

25 mM Tris, 192 mM glycine, 10 % methanol, 0.05 % SDS

- Coomassie brilliant blue staining solution

50 % methanol, 10 % acetic acid, 0.1 % Coomassie Brilliant blue R-250

- Coomassie blue destaining solution

40 % methanol, 10 % acetic acid

5.3.2 Methods

5.3.2.1 Construction of kidney endo-epithelial bilayer tissue model

Scheme 5.2 illustrates the procedures of forming kidney endo-epithelial bilayer tissue model on transwell to study the transport of ZnO NM across the tissue barrier. In brief, the top and bottom side of the transwell membrane was first coated with collagen IV (13.2 μl; 100 μg ml^{-1} in 0.05 M hydrochloric acid) and air dried. The dried transwell membrane was then washed with DMEM/F12 once before the cell seeding. HK-2 cells (3.0×10^4) in DMEM/F12 (40 μl) was seeded at the bottom side of the transwell membrane. After 3 hours of culture, the transwell membrane was reverted for the seeding of HMVEC (1.5×10^4) in of EndoGRO (200 μl) at the top side.
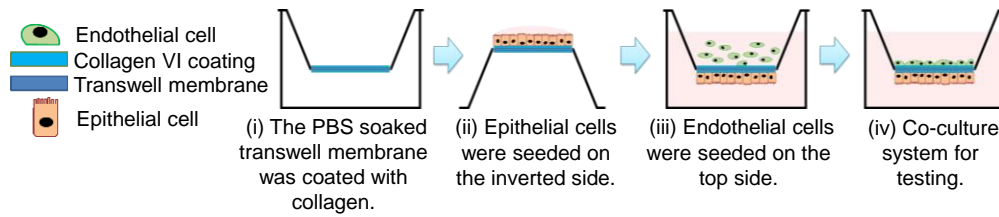
Scheme 5.2: Schematic illustrating the steps of forming kidney endo-epithelial bilayer model. HMVEC and HK-2 cells were seeded at the top and bottom side of the collagen IV coated transwell insert respectively.

5.3.2.2 Immunofluorescence imaging of mouse proximal tubule

The harvested mouse kidney was fixed with 4 % paraformaldehyde, rinsed with PBS, and dried with paper towel. The mouse kidney was then incubated in O.C.T tissue freezing medium. Frozen tissue was sectioned with a thickness of 10 μm and attached on polysine slides.

The immunofluorescence study was conducted as follows; the tissue sections on the slides were fixed again with 4 % paraformaldehyde. The fixed slides were washed with PBS thrice before immersed in 0.2 % Triton-X 100 for 15 minutes in order to permeabilized the cells. The permeabilized tissues were washed and blocked with 2 % bovine serum albumin for 1 hour. After that, the slides were incubated with CF568 phalloidin (1 : 200) and Hoechst 33342 (1 : 500) for 30 minutes to label the actin and nuclei. After staining, the slides was mounted with cover slip and imaged by Olympus FluoView FV1000 laser scanning confocal microscope (Olympus, Japan).

5.3.2.3 **Immunofluorescence imaging of kidney endo-epithelial bilayer tissue model**

HMVEC cells were pre-labelled with 0.5 µM of CellTracker Green CMFDA dye in dark for 30 minutes. The endo-epithelial bilayer model was constructed as mentioned in **Section 5.3.2.1**.

After 1 day of culture, the kidney endo-epithelial bilayer tissue model was fixed with 4 % paraformaldehyde for 30 minutes. The fixed tissue was then permeabilized with 0.2 % Triton X-100 for 15 minutes. The permeablized cells were washed with PBS and blocked with 2 % bovine serum albumin for 1h. The transwell insert was inverted for the staining of actin in HK-2, the cells were incubated with CF568 phalloidin (1 : 200) in dark for 20 minutes. After staining, the transwell membrane was washed with PBS thrice and cut out form the insert. The membrane was mounted with two cover slips for imaging by confocal.

5.3.2.4 **Quantification of cell barrier permeability**

After ZnO NM treatment, the treatment solution was removed and the cells were washed with PBS. FITC-dextran (1 mg ml^{-1}) was added into the top chamber for 5 hours. After the exposure, the solutions in the top and bottom compartment were collected. The amount of FITC-dextran across the cell barrier was determined by Synergy 2 Multi-mode reader (BioTek, USA). The excitation and emission wavelength of FITC-dextran are 492 and 518 nm respectively. The amount of FITC-dextran detected at the lower compartment was normalized to the untreated control and defined as leakiness index.

5.3.2.5 Quantification of ROS

The intracellular ROS level in the endothelial cell was determined by CellROX Orange Reagent. Five microliters of CellROX Orange Reagent was added into the treated cells 30 minutes before the end of the treatment time. At the end of the treatment, the cells were washed with PBS. The fluorescence signal from CellROX Orange Reagent, which correlated to the level of intracellular ROS, was quantified by Tali® Image Cytometry.

5.3.2.6 ICP-OES analysis of the zinc uptake and distribution

After the treatment of ZnO NM, the cells, solution at the top and bottom compartments of endo-epithelial bilayer and endothelial monolayer tissue model were collected. The collected cells and solutions were ionized by incubated with 65 % of HNO_3 overnight before diluted to 2 %. The final solution was filtered with syringe filter (0.4 µm pore size) before analyzed by inductively coupled plasma optical emission spectroscopy (ICP-OES; iCAP 6000 Series, Thermo Scientific, UK).

5.3.2.7 Isolation of RNA and quantitative PCR

Cells were grown in collagen IV coated 6-well plate. The step of RNA extraction, cDNA conversion, and quantitative PCR were stated in **Section 4.3.2.6**.

5.3.2.8 Conditional culture for cellular communication study

HMVEC (4.33×10^5) were seeded on 6-well plate coated with collagen IV. The cells were treated with 500 µM of ZnO NM for 3 hours. After treatment, the cells were washed with PBS and cultured with fresh EndoGRO for another 12 hours. The spent EndoGRO for both treated

HMVEC and untreated negative control were collected and filtered with syringe filter (0.2 μm pore size).

HK-2 (8.66×10^5) were seeded on 6-well plate coated with collagen IV. The cells were treated with the spent EndoGRO added ZnO NM or $ZnCl_2$ according to the concentration of zinc detected in filtered conditional medium for 6 hours.

5.3.2.9 Separation of protein corona

ZnO NM (1.25 mg ml^{-1}) were incubated in water, fresh EndoGRO, and spent EndoGRO respectively for 6 hours. After the incubation, the unbounded proteins were separated from the absorbed protein by centrifugation at 3000 rpm. The absorbed proteins were lysed with Laemmli sample buffer at 95 °C for 5 minutes. The proteins were separated by 12 % sodium dodecyl sulfate-polyacrylamide gel. The gel was stained with Coomassie brilliant blue staining solution for 1 hour and destained overnight. The quantification of the protein bands' intensity was done with the aid of ImageJ (Abramoff et al., 2004).

5.4 Results and discussions

5.4.1 Endo-epithelial bilayer tissue model

Confocal and fluorescence microscopy images revealed the structure of endo-epithelial bilayer model constructed in this study (**Figure 5.1**). Both HMVEC and HK-2 cells remained on their respective seeding side of transwell membrane, no cell was found to migrate across the collagen coated membrane to the opposite side. **Figure 5.1B** showed that the endothelial and

epithelial cells were able to maintain their characteristic morphology. Specifically, the flat and wide spread cell shape of HMVEC is similar to the squamous-like shape of endothelial cell in mouse's proximal tubule (**Scheme 5.1A**). In particular, the thick network of actin in HK-2 is close to the columnar-like shape of epithelial cells in mouse's proximal tubule (**Scheme 5.1A**). These morphologies justify the characteristics and functions of each cell type. The squamous-like structure of endothelial cell is favorable for fluid and liquid to flow at the apical side, the columnar-like structure of epithelial cells maximal cell-to-cell and cell-to-fluid contact for mass transfer and absorption of substances.
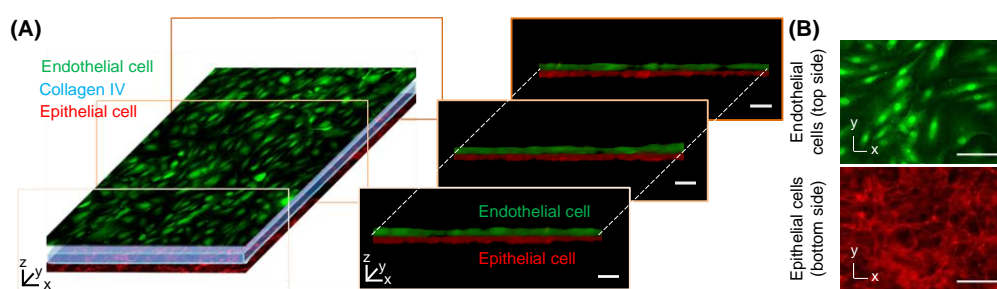
Figure 5.1: The structural conformation of endo-epithelial bilayer model. (A) The top view (x-y direction) and side view (x-z direction) of the endo-epithelial bilayer model was captured by confocal microscopy. HMVEC were pre-labelled with CellTracker Green (green), the actin of HK-2 cells were labelled with CF568 phalloidin (red). (B) The morphology of HMVEC and HK-2 cells cultured in the endo-epithelial bilayer model was determined by fluorescence imaging. The scale bar in (A) is 20 μm and in (B) is 100 μm.

5.4.2 Characterization of ZnO NM in culture medium

The physical properties such as the hydrodynamic size and zeta potential of ZnO NM were summarized in **Table 5.2**. Large aggregates were found when the ZnO NM were dispersed in serum supplemented EndoGRO medium as the hydrodynamic size was increased to 216.20 ± 2.34 nm. The

zeta potential of ZnO NM changed from positive to negative due to the formation of protein corona. Although the size of aggregates was large in EndoGRO, the system was quite stable as the magnitude of zeta potential obtained is high.

Table 5.2: The summary of the physical properties of ZnO NP in different dispersant in this study.

Dispersant	Hydrodynamic size, nm	PDI	Zeta potential, mV
Ultrapure water	75.69 ± 0.94	0.25 ± 0.02	$+ 19.30 \pm 0.53$
EndoGRO (with 5 % FBS)	216.20 ± 2.34	0.28 ± 0.03	$- 28.60 \pm 2.05$

5.4.3 Diffusion and cellular uptake of ZnO NM in endo-epithelial bilayer model

The biomimetic kidney endo-epithelial bilayer construct was used to determine the transport and uptake profile of ZnO NM. Upon 3 hours of incubation, majority of the ZnO NM was still remained at the apical side of the endothelial cell (top chamber), the diffusion of zinc across the bilayer construct was detected about 20 % (**Figure 5.2A**). There was a 6.6 % increase in the diffusion of zinc for the endothelial only monolayer. These data might be a good start for the study related to metabolism and clearance of ZnO NM by human's kidney. More importantly, the results implied the slow tubular secretion of ZnO NM and difficulty in clearance of ZnO NM. Therefore, ZnO NM, which are incorporated in consumable product, may circulate in blood stream with a long half-life once it enters human body.

The tissue digestion results (**Figure 5.2B**) revealed the occurrence of zinc accumulation in endothelial and epithelial cells after ZnO NM treatment.

ZnO NM (primary size of 24.0 nm and hydrodynamic size of about 216 nm), which have a size comparable to a lysosome (~50-500 nm) and other biological molecules, could be taken up by the cells. Despite the relatively low percentage of zinc detected in endothelial monolayer model, the accumulation of zinc in epithelial cell model was more than 5 fold higher than the endothelial cells. This difference could be attributed to the nature of epithelial cells in actively absorbing molecules.
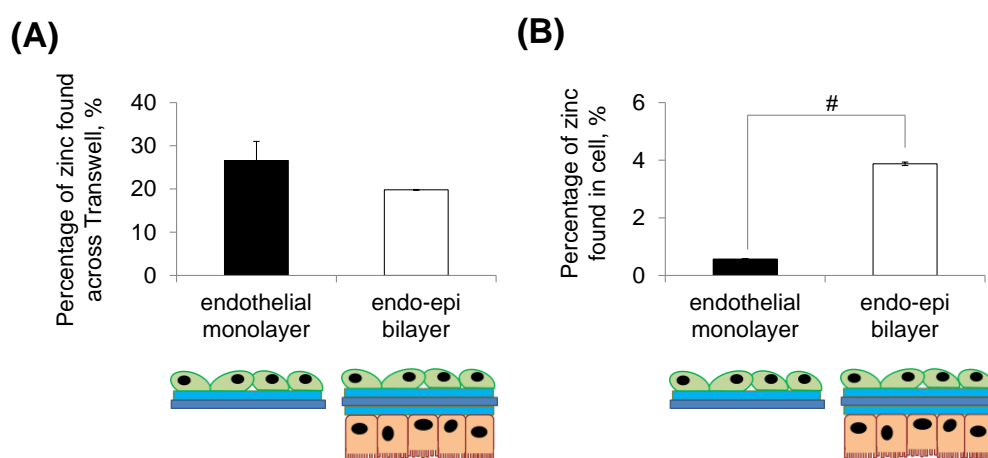
Figure 5.2: Transport and uptake of ZnO NM in the endothelial monolayer and endo-epithelial bilayer model. (A) A reduction in the diffusion of zinc was observed when the endothelial monolayer was co-cultured with epithelial cell upon 3 hours of 500 µM of ZnO NM treatment. (B) The cellular uptake of zinc in endo-epi bilayer was significantly higher than the endothelial monolayer upon 3 hours of 500 µM of ZnO NM treatment. Error bar of each value is the standard deviation of the 2 replicates. Student's *t*-test, $p < 0.01$, #significantly different between the two groups.

5.4.4 ZnO NM induced endothelial leakiness

Figure 5.3A indicate the formation of micron-sized gaps between endothelial cells upon 3 hours of ZnO NM treatment. Elevated amount of FITC-dextran, which has a hydrodynamic diameter of 4.5 nm, can pass through the endothelial cell monolayer as compared to the untreated negative control (**Figure 5.3B**). This phenomenon is similar to the nanomaterials

induced endothelial leakiness (NanoEL) observed in previous studies (Setyawati et al., 2013b). During the event of NanoEL, NM disrupted the intercellular junctions of endothelial cells and triggered actin remodeling resulting with gaps, which were observed between the endothelial cells (Setyawati et al., 2015). In fact, NanoEL not only affect the microscopic aspect such as the morphology of the cell, it also affects the function of the tissue. Blood vessel wall, which is comprised of microvascular endothelial cell, regulate the passage of materials from the blood side. Water and small solutes can easily diffuse through the endothelial cell barrier, whereas macromolecules such as proteins required transcytosis via vesicular transport to transfer from the blood side to the tissue or organ underlying the blood vessel. However, the presence of the ZnO NM induced micron-sized gap on the endothelial cell monolayer could significantly compromise the regulation of macromolecules' transport and disturb the balance of homeostasis.

The presence of epithelial cell astonishingly revoked the increased cell leakiness induced by ZnO NM. These data implied that the diffusion of macromolecules across proximal tubule was governed by both endothelial and epithelial cell layers together. The endo-epithelial bilayer was more resistant to leakiness induced by ZnO NM.
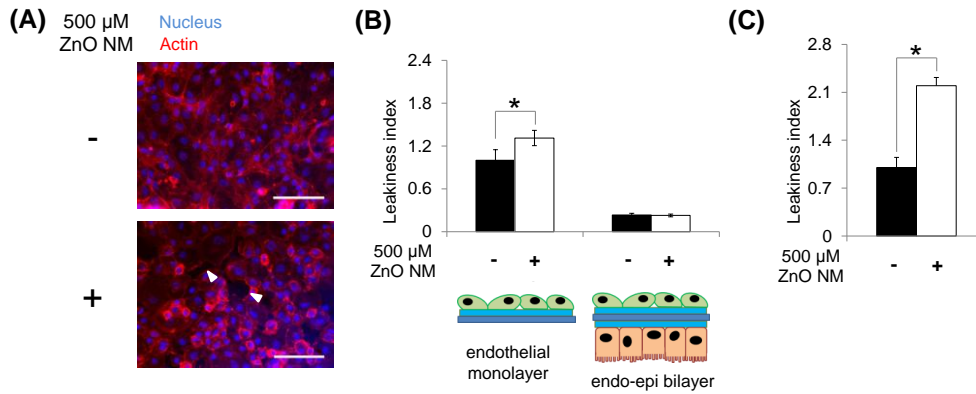
Figure 5.3: ZnO NM disrupt the integrity of endothelial cell barrier. (A) Micro sized gaps (indicated by white arrows) between endothelial cells were observed upon 3 hours of 500 μM ZnO NM exposure. The actin of cells was stained with CF568 phalloidin (red) and nuclei of cells were labelled by DAPI (blue). (B) Quantification of the cell barrier leakiness by determines the passage of FITC-dextran across the endothelial monolayer and endo-epithelial bilayer models revealed that the increase of cell barrier leakiness observed upon 3 h of 500 μM ZnO NM treatment is restricted to endothelial layer only. (C) After the 3 h of 500 μM ZnO NM treatment, the cells were washed and incubated with fresh culture medium for another 12 hours to determine the reversibility of ZnO NM's effects. The cell leakiness assay indicated that ZnO NM induced endothelial leakiness persisted and cannot be recovered within 12 hours. Scale bars in (A) are equivalent to 200 μm. Data represent means ± SD, $n > 3$. Student's t-test, $p < 0.05$, *significantly different between the two groups.

As long term cell leakiness can lead to detrimental events such as exudation, reduction in blood flow, disruption of vascular homeostasis, and excessive pro-inflammatory leukocyte extravasation (McDonald and Baluk, 2002), we further examined whether the endothelial cells are able to recover from the leaky condition back to the intact cell barrier. The quantification data in **Figure 5.3C** validates the ZnO NM induced endothelial cell barrier leakiness were sustained and persisted even after ZnO NM treatment solution had been removed.

5.4.5 Cells lose ability to maintain intracellular oxidative homeostasis when accumulation of zinc exceed the tolerate level

It is important not to neglect the effects of ZnO NM to the intracellular oxidative stress balance due to most studies on ZnO NM concluded that ZnO NM elevate intracellular ROS and consequently induce other undesired biological effects in the cell (Tee et al., 2015). Similarly, an elevation of intracellular oxidative stress in HMVEC was observed after 3 h of ZnO NM treatment but not at the early timepoint (**Figure 5.4A**). From **Figure 5.4B**, it is obvious that HMVEC has been taken in ZnO NM upon 1 hour of ZnO NM exposure. Therefore, we ruled out the possibility that the ZnO NM have not been internalized by the cell. In fact, the late occurrence of ROS upregulation may be due to the cells were able to restore their oxidative homeostasis before the accumulation of zinc exceeds the tolerable level. At the same time, previous study showed that fibroblasts were able to maintain the intracellular ROS balance at low concentration of ZnO NM treatment (Setyawati et al., 2013c).
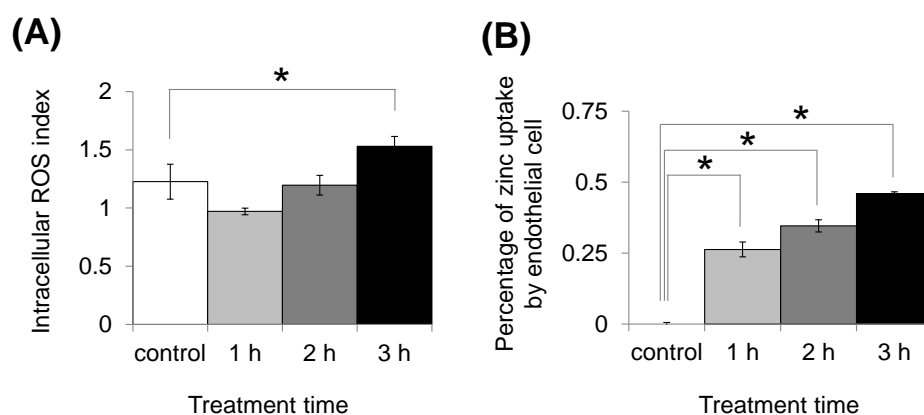
Figure 5.4: Disruption of oxidative balance associated with accumulation of zinc. (A) Elevation of intracellular oxidative stress in HMVEC within 3 h of 500 µM of ZnO NM treatment. Intracellular ROS index was defined by the normalized cell number with high level of intracellular ROS. (B) Gradual increase of zinc accumulation in endothelial cell upon 3 h of 500 µM ZnO NM treatment. Data represent means ± SD, $n = 3$. Student's *t*-test, $p < 0.05$, *significantly different between the two groups.

5.4.6 ZnO NM stimulated inflammatory response in endothelial cell

ZnO NM, which are foreign entity to the cell, have been known to stimulate inflammatory response in cell system. To verify the effects of ZnO NM to the cell, we used quantitative PCR to compare the expression of inflammatory genes between ZnO NM treated endothelial cells and the negative control.

Figure 5.5 showed that the expression of NLRC4, IL1B, and IRF1 genes were significantly upregulated after 3 hours of ZnO NM exposure (500 µM). As opposed to these genes, the expression of IL18, CXCL5, and TLR6 genes were downregulated at the same timepoint. One possible inference of the data was that the inflammatory status of endothelial cells upon 3 hours of ZnO NM treatment was still at the early stage. Therefore, the former 3 genes, which are involved in the early stage of inflammation, were upregulated. In contrast, the IL18 and CXCL5, which are the downstream inflammatory

90

markers, as such a slight suppression of these genes were observed. The encoded proteins of NLRC4 (NLRC4 protein), IL1B (IL-1β), and IRF1 (IRF-1 protein) genes are important in the early stages of inflammation. NLRC4 protein senses the stimulus in cell cytosol to form NLRC4 inflammasome complex in order to promote activation of caspase-1. Activated caspase-1 secretes pro-inflammatory cytokines, IL-1β and IL-18. Concomitantly, IL-1β binds to IL-1 receptor to mediate inflammatory signaling pathway and activate activity of NF-κB. Activated NF-κB will translocate into cell nucleus to stimulate expression of IRF1 (Wang et al., 2009). IRF-1 protein can activate interferons α and β transcription to regulate immune response.
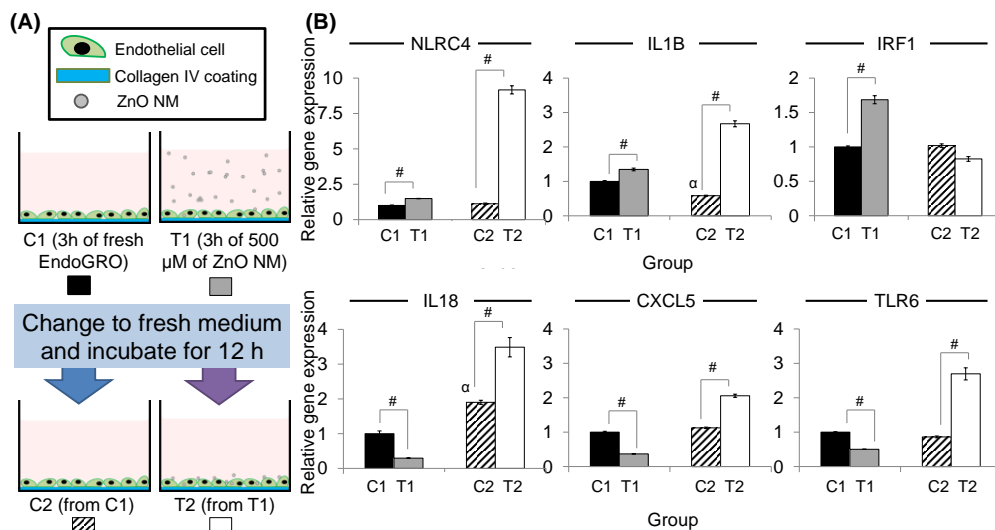
Figure 5.5: Persistent inflammatory response in endothelial cell. (A) Schematic illustrates the procedures of examined the tendency of ZnO NM to induce inflammatory responses in endothelial cell culture. (B) 3 hours of 500 µM ZnO NM treatment upregulated expressions of inflammatory genes and the effects persisted even after ZnO NM was removed for 12 hours. Data represent means ± SD, $n = 3$. Student's t-test, $p < 0.01,$ [#]significantly different between the two groups, [α]significantly different between the two control groups (C1 and C2).

IL18, which is secreted by activated caspase-1, is related to the production of pro-inflammatory cytokines. Cytokines such as IL-1β stimulate

the expression of CXCL5. Chemokine CXCL5 is important for regulating the sequestration of other chemokines and recruiting neutrophils to the site of inflammation. TLRs are transmembrane proteins that recognize PAMPs and DAMPs to activate innate immune response. The suppression of TLR6 gene expression in endothelial cells might be explained by the fact that ZnO NM is neither a pathogen nor endogenous molecules released by injured cells.

As there is blood and fluid flow in real situation and substances will be carried away by fluid, the ZnO NM treatment solution was removed and the culture was replenished with fresh culture medium for additional 12 hours of culture in order to further study the influence of ZnO NM to endothelial cell. Although the NM were removed, the endothelial cell still had high expression of inflammatory genes except IRF1 in the extended study. Together with the continuous leakiness effects were observed in previous section, this response also suggested that endothelial cells are incapable to recover from the damage induced by ZnO NM in a short term and ZnO NM can be considered as a persistent causative agent of inflammatory responses to endothelial cells.

5.4.7 The direct and indirect effects of ZnO NM to epithelial cell

After determining the effects of ZnO NM to endothelial cell, we also questioned about the effects of ZnO NM to the underlying epithelial cells. By using the diffusion data obtained from the endo-epithelial bilayer model (**Figure 5.2**) and conditional medium from the treated endothelial cell, the dose of ZnO NM diffused across the cell layers to epithelial cell layer can be used to determine the direct and indirect effects of ZnO NM to the epithelial cells.

92

The data obtained from endo-epithelial bilayer model showed that about 20 % of ZnO NM, which is equivalent to 100 μM of ZnO NM for a starting treatment of 500 μM, could pass through the bilayer. The data obtained from endothelial monolayer was 26.6 % (which is equivalent to 133 μM of ZnO NM for a starting treatment of 500 μM). Although the concentration difference was relatively small, significant differences in the expression of inflammatory genes was observed between these two concentrations (**Figure 5.6**). This observation highlighted the importance of accurate dosage in toxicity study in order to prevent overestimation of the toxicity of substance.

ZnO NM treatment induced the upregulation of NLRC4, IL1B, IRF1, IL18, and TLR6 genes expression in epithelial cell. These data suggest that ZnO NM also trigger the inflammatory response in epithelial cell, which was also observed in endothelial cell.
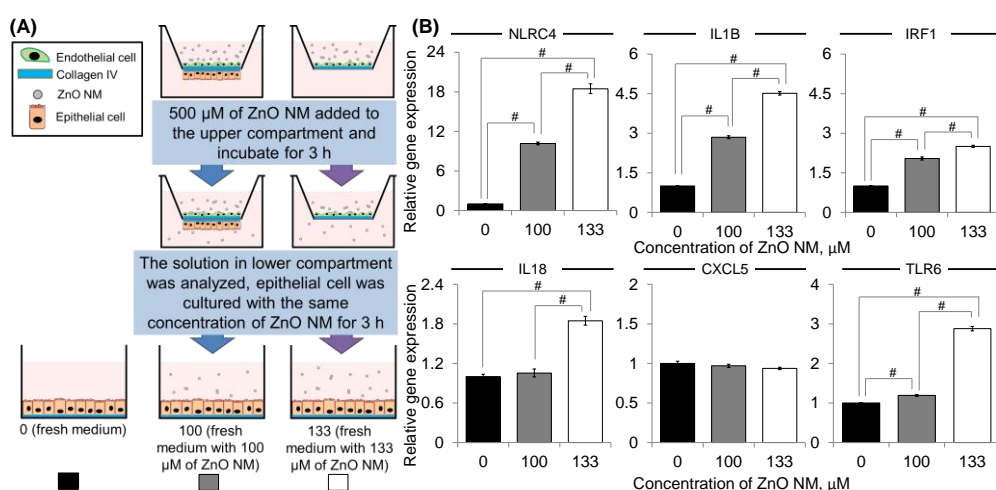
Figure 5.6: Direct effect of ZnO NM to the epithelial cell. (A) Schematic summarized the procedures of determine the dosage of treatment for direct effect study. (B) Epithelial cell showed a concentration dependent response to ZnO NM. Data represent means ± SD, $n = 3$. Student's t-test, $p < 0.01$, [#]significantly different between the two groups.

To determine the indirect effects of ZnO NM on epithelial cell, conditional culture of monolayer epithelial cells was conducted. In the conditional medium, a low concentration of zinc was detected (5 μM detected by ICP-OES, **Figure 5.7**). To address the issue of ZnO NM might dissolve in the conditional medium to form Zn^{2+} that might exert its toxic effects, the two extreme conditions of 5 μM ZnO NM and 5 μM Zn^{2+} (by adding $ZnCl_2$) were included in this analysis. In **Figure 5.8**, the responses of epithelial cells treated with the conditional medium were significantly different as compared to the two extreme conditions. Therefore, the possibility of the observed upregulation of the inflammatory genes expression in conditional culture group (M group) was solely due to the low concentration of ZnO NM or Zn^{2+} can be omitted. Based on the data, we can speculate that there was some subtle interaction from the ZnO NM treated endothelial cell to the epithelial cells. Besides IRF1, the expression of other 5 studied genes were upregulated more than 25 % as compared to the control. The upregulation of IL1B, IL18, CXCL5, and TLR6 genes can be attributed to endogenous molecules, cytokines and chemokines released by the injured endothelial cells (Chen et al., 2014). Endothelial cells are known to be cells that actively participating and regulating inflammatory process, they sequester cytokines and chemokines to recruit leukocyte and memory T cells to the inflammatory site. The cytokines and chemokines released by the endothelial cells can induce systemic effects on other cells and alter the gene expression pattern in the cells which received the signaling molecules (Szente, 2003).

94
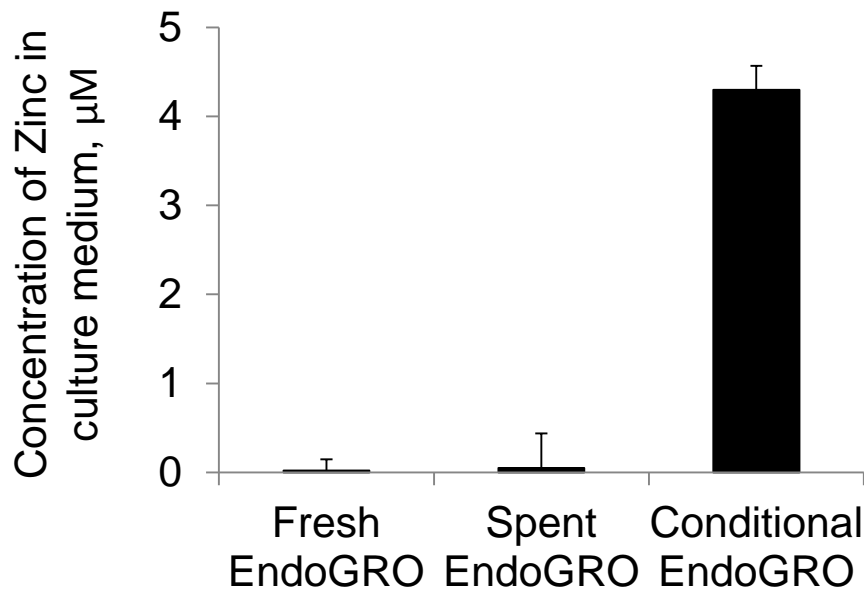
Figure 5.7: Low concentration of zinc was found in the filtered conditional medium. ICP-OES analysis found a low concentration of zinc in the conditional medium used for conditional culture of HK-2 cells. Data represent means ± SD, *n = 3*.
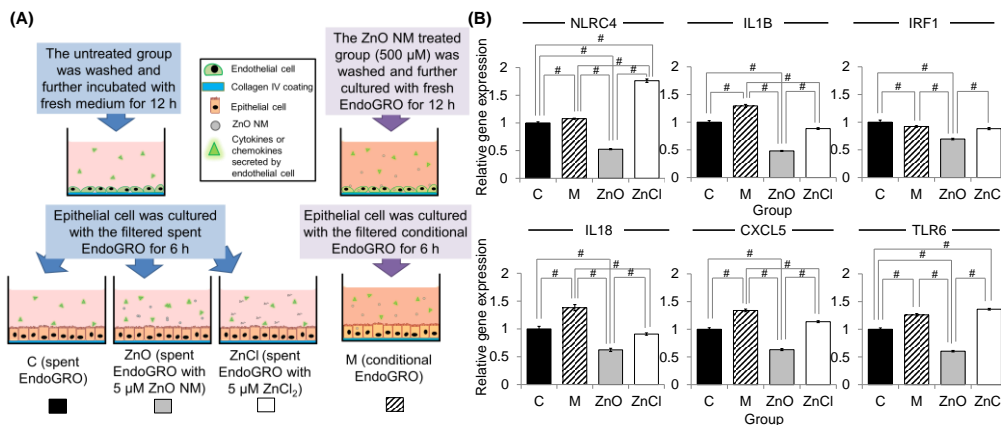
Figure 5.8: Indirect effect of ZnO NM to the epithelial cell. (A) Schematic summarized the procedures of determine the dosage of treatment for indirect effect study (conditional culture of epithelial cells with the medium obtained from endothelial cell culture). (B) The M group, which treated with conditional medium from injured endothelial cell, showed different inflammatory response as compared to the groups treated with equal amount of ZnO NM or Zn^{2+}. Data represent means ± SD, *n = 3*. Student's *t*-test, *p < 0.01*, [#]significantly different between the two groups.

It is interesting to see that the addition of 5 µM ZnO NM astonishingly suppressed the expression of all the six inflammatory related genes in this study. This unexpected anti-inflammatory effect may be attributed by the disturbed chemokines and cytokines gradient in conditional medium after the addition of low concentration of ZnO NM. The high surface area to volume ratio of NM gives it a highly reactive surface; as a result, molecules can be easily absorbed on the surface of NM. It is possible that the chemokines and cytokines released by the endothelial cells were absorbed on the surface of ZnO NM; in turn, the effective concentration of the chemokines and cytokines in the spent EndoGRO with 5 µM ZnO NM was lower than the negative control. The protein corona assay (**Figure 5.9**) provides some evidences that certain proteins have high adsorption affinity to ZnO NM.
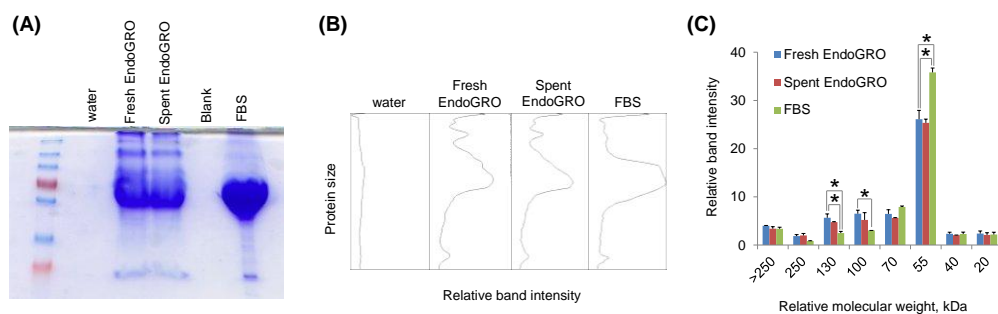
Figure 5.9: Protein corona formation on the ZnO NM. (A) The proteins absorbed on the surface of ZnO NM were separated by sodium dodecyl sulfate/polyacrylamide gel. (B) The intensity of the protein bar was quantified by imageJ. (C) ZnO NM have strong affinity to proteins with the size of 100 and 130 kDa, the proteins were intensified by ZnO NM. Data represent means ± SD, n = 3. Student's *t*-test, *p < 0.05,* *significantly different between the two groups.

5.5   Conclusion

In this study, kidney endo-epithelial bilayer tissue construct was established. This bilayer model is suitable for diffusion, nanotoxicity and

nano-bio interaction assessment. Based on the results and data in this study, the roles of different cell types in a tissue system and the importance of cell-type interactions (endothelial cells and epithelial cells) in cellular responses were elicited.

By using the endo-epithelial bilayer tissue model and the monolayer cultures, the direct and indirect effects of the ZnO NM to kidney tissue can be separated and studied. The data showed that ZnO NM can induce cell barrier leakiness, trigger oxidative stress and prompt chronic inflammatory response in endothelial cells. The cytokines and chemokines released by injured endothelial cells can induce a systemic effect on epithelial cells. Nevertheless, this model is also applicable to other tissue type that has a similar endo-epithelial configuration. In conclusion, this kidney endo-epithelial bilayer tissue construct was shown as an easy-to-establish and representative *in vitro* model to take account of the cell-to-cell interactions and diffusion pattern of NM for the analysis of nano-bio interactions.

Chapter 6: ZnO NMs, Safer by Design: Attenuating its Toxicity with Silica coating

6.1   Introduction

ZnO NM is also well known for their antimicrobial properties that can be utilized in food packaging and food preservation (Espitia et al., 2012). However, the perceived high toxicity of ZnO NM to mammalian cells in 2D cell culture model has limited their potential biological applications. Surface modification of ZnO NM with a suitable chemical might be a potential solution to reduce the toxicity while maintain the antimicrobial property.

Surface modification on NM is a commonly used technique to tailor the physical, chemical, and biological properties of NM to achieve desired applications. Many different methods for NM surface modification have evolved. In general, surface modification of NM can be achieved by physico-chemical (Huczko, 2000), mechanical (Requicha et al., 2009), and biological methods (Wang et al., 2012).

ZnO NM tend to aggregate in aqueous solution due to the formation of Zn-O-Zn bonds among the hydroxyl groups of ZnO molecules (Hong et al., 2006). This poor stability of ZnO NM in water greatly restricted the biological applications of ZnO NM. Many attempts were made on surface modification of ZnO NM to improve its stability and dispersibility in aqueous solution. However, the formation of hydroxyl groups after water adsorption also imparts the formation of covalent bond with other organic molecules without the need of surface functionalization with the presence of water (Noei et al., 2008).

Although many methods have been shown to effectively reduce the toxicity of ZnO NM by reducing the dissolution (Sotiriou et al., 2014; Xia et

al., 2011), not all the method is suitable to be applied on the ZnO NM used for biological applications. The basic criteria of surface modification on ZnO NM, which are going to be applied in biological applications, are listed as follows (Gao and Xu, 2009):

- Good dispersibility in water.

- Good stability for long term storage.

- Retain the functionalities of ZnO NM (antimicrobial activity for food packaging).

- Good biocompatibility (at least before the ZnO NM interact with the targeted subjects).

One of the problems associated with most of the NM is the poor stability in solution, small but highly reactive NM tend to form aggregates in solution. This property largely affects the performances of the NM and limits the shelf life. Capping agents, stabilizing agents, and surfactants are commonly added during or after the synthesis of NM to reduce the agglomeration (Gutiérrez-Wing et al., 2012; Singh et al., 2009). However, the physical adsorption of these molecules on NM can be disturbed by the change of environment. Therefore, chemical modification on the surface might be more stable. Silica particles, which possess high hydrophilicity property, can be used as a potential candidate for chemical modification to improve dispersibility (He et al., 2008).

6.2   Literature review

As a popular NM with unique electrical and chemical properties for various applications, there are a large number of studies on the surface modification of ZnO NM in order to enhance the desired properties and remove the shortfalls.

One of the examples of surface modification on ZnO NM is grafting polystyrene on the surface of ZnO NM. Polystyrene coating effectively improve the dispersion of particle but the coating also demonstrated a significant reduction on the photocatalytic activity of ZnO NM (Hong et al., 2009). More examples of surface modification on ZnO NM are summarized in **Table 6.1**.

Table 6.1: Summary of different surface modification and their effects on ZnO NM.

Surface modification	Change in the properties	Applications	Reference
Depositing of palladium	• Improve photocatalytic activity.	Photocatalyst for oxidation of gas phase alkenes.	(Liqiang et al., 2004)
Poly(methacrylic acid)	• Enhance dispersibility of ZnO NM in water.	Water-based coating, ceramic and texture finishing agent.	(Tang et al., 2006)
Silica coating	• Improve dispersity. • Reduce photocatalytic activity.	Photocatalyst in water suspension.	(Hong et al., 2006)
Silver	• Enhance photocatalytic activity to form active oxygen species. • Improve photostability.	Photocatalyst in water suspension.	(Xie et al., 2010b)
Aminopropyltriethoxysilane	• Increase photostability.	Sunblock.	(Grasset et al., 2003)

Poly(vinylpyrrolidone)	• Improve monodispersity.	Optical devices and displays.	(Guo et al., 2000)
	• Reduce aggregation.		
	• Increase stability.		
	• Enhance near-band-edge UV photoluminescence.		
	• Reduce defect-induced green emission.		

The summary in **Table 6.1** showed that surface modification can effectively improve certain properties of ZnO NM; however, trade-off for certain properties such as reactivity were also observed in some of the techniques. Therefore, selection and optimization of the modification are crucial to enhance the desired properties without compromise other necessary properties of ZnO NM for a particular application.

Although most of the *in vitro* studies take account of the exposure route of ZnO NM in the selection of targeted cell lines for toxicity study, we rarely pay attention to the possible form of the ZnO NM before it reach the targeted cells. Different exposure routes can lead to different outcomes and form of NM. The ingested NM will encounter digestive juices secreted by the organs in digestive system. Each of these juices has different chemical compositions, enzymes and pH that could dissolve or change the properties of the NM. One of the crucial parameters that will affect dissolution of ZnO NM is the pH of the solution. If the toxicity of ZnO NM is due to the dissolution to Zn^{2+} ion, the surface modification of ZnO NM, which is going to be used in food and biological applications, need to be able to effectively prevent dissolution of ZnO NM in different digestive juices.

To more accurately replicate the outcomes of ingested NM in human body, we utilized synthetic gastrointestinal fluids to determine the dissolution of the ZnO NM and justify the effectiveness of the surface modification on reducing dissolution of ZnO NM.

Enlightened by the stability and inert property of silica dioxide (Yang et al., 2009), we choose silica coating as the potential surface modification to reduce the toxicity of ZnO NM.

6.3 Materials and methods

6.3.1 Materials

6.3.1.1 Cell lines

SW480, human colorectal adenocarcinoma epithelial cell (DLD-1), *Escherichia coli* (*E. coli*) bacteria and *Staphylococcus aureus* (*S. aureus*) bacteria were purchased from American Type Cell Culture, USA.

6.3.1.2 Chemicals

ZnO nanopowder, zinc chloride ($ZnCl_2$), ammonium hydroxide (NH_4OH), lysozyme, α-amylase, DMEM, pectin, pepsin, xylan, glucose, citric acid, peptone, porcine mucin, cysteine, Magnesium Sulfate heptahydrate ($MgSO_4 \cdot 7H_2O$), magnesium chloride ($MgCl_2$), potassium phosphate dibasic (K_2HPO_4), starch, potassium bromide (KBr), KCl, KH_2PO_4, Na_2HPO_4, potassium bicarbonate ($KHCO_3$), Tetraethyl orthosilicate (TEOS), and Tween 80 were purchased from Sigma Aldrich, Singapore. Yeast extract and agarose were purchased from First Base, Singapore. Calcium chloride dehydrate ($CaCl_2 \cdot 2H_2O$), Sodium hydrogen carbonate ($NaHCO_3$), and NaCl were purchased from Merck KGaA, Singapore. P/S and trypsin-EDTA were purchased from PAA Laboratories Inc., USA. Annexin V/propidium iodide kit, and FBS were purchased from Thermo Scientific, USA. Ethanol and

isopropanol were purchased from Fisher Scientific, USA. Luria-Bertani (LB) broth powder was purchased from BD Biosciences, Singapore.

6.3.1.3 Buffers

The buffers used in this study were prepared with the following composition:

- PBS

  137 mM NaCl, 2.7 mM KCl, 10 mM Na_2HPO_4, 2 mM KH_2PO_4; pH 7.4

- Synthetic saliva (Naim et al., 2004)

  2.5 mM K_2HPO_4, 2.4 mM Na_2HPO_4, 157 mM $KHCO_3$, 10 mM NaCl, 0.15 mM $MgCl_2$, 0.15 mM citric acid, 1.5 mM $CaCl_2$, 1 mg ml^{-1} α-amylase, 0.1 mg ml^{-1} lysozyme from chicken egg white; pH 6.7

- Synthetic gastric juice (Naim et al., 2004)

  0.4 mg ml^{-1} glucose, 3.0 mg ml^{-1} yeast extract, 1.0 mg ml^{-1} peptone, 4.0 mg ml^{-1} porcine mucin, 0.5 mg ml^{-1} cysteine, 0.08 mg ml^{-1} NaCl, 0.4 mg ml^{-1} $NaHCO_3$, 0.04 mg ml^{-1} K_2HPO_4, 0.04 mg ml^{-1} KH_2PO_4, 0.008 mg ml^{-1} $CaCl_2$-$2H_2O$, 0.008 mg ml^{-1} $MgSO_4 \cdot 7H_2O$, 1.0 mg ml^{-1} xylan, 3.0 mg ml^{-1} soluble starch, 0.002 USP ml^{-1} pectin, 0.1 % Tween 80, 3.0 mg ml^{-1} pepsin; pH 2.0.

6.3.2 Methods

6.3.2.1 2D cell culture

SW480 and DLD-1 were grown in DMEM supplemented with 10% FBS and 1% P/S and maintained in a standard cell culture condition of 37 °C

with 5 % CO_2. For the treatment, cells were seeded in density of 1.2×10^5 cells for each well.

6.3.2.2   3D cell culture

The 3D cell spheroids were constructed as Section 4.3.2.2. The cell seeding used for SW480 and DLD-1were 1.2×10^5 cells for each agarose hydrogel.

6.3.2.3   Synthesis of silica coated ZnO NM

ZnO nanopowders (26 mg) were dispersed in isopropanol (20 ml) and ethanol (40 ml) mixture. Water (5 ml) and NH_4OH (1.34 ml, 28 % NH_3) was added into the mixture. The solution was sonicated in water bath for 30 minutes at room temperature. TEOS (400 µl) was added dropwise into the stirred mixture. The reaction was allowed to proceed at room temperature for 8 h with continuous stirring. The silica coated ZnO NM were collected by centrifugation at 6000 rpm and washed with water thrice to remove the supernatants (Leng et al., 2007).

6.3.2.4   Characterization of NM

The surface elements of NM were determined by energy-dispersive X-ray spectroscopy (EDX). All the samples were coated with carbon inside a vacuum chamber before the EDX analysis. The surface elements of NM were further confirmed by X-ray photoelectron spectroscopy (XPS).

The functional groups of the NM were characterized by fourier transform infrared spectroscopy (FTIR; FTIR 8400S, Shimadzu). Samples (2

mg) were throughout mixed with KBr (198 mg) to form uniform sample pellet before analysis.

6.3.2.5 Dissolution of ZnO NM in synthetic gastrointestinal fluid

ZnO NM (1250 mM) were incubated in synthetic saliva at 37 °C water bath shaker for 30 minutes. The synthetic saliva treated pellet was obtained by centrifugation at 6000 rpm for 10 minutes. Synthetic gastric juice (40 ml) was added into the pellet for an incubation of 2 hours at 37 °C water bath shaker. The supernatant and synthetic gastric juice treated pellet was separated by centrifugation at 6000 rpm for 10 minutes. The synthetic saliva and synthetic gastric juice treated pellets were re-dispersed in water. The composition of zinc was determined by inductively coupled plasma optical emission spectrometry (ICP-OES) with acid digestion step outlined in Section 5.3.2.7.

6.3.2.6 Antimicrobial testing

E. coli and *S. aureus* were maintained in LB broth of 37 °C with shaking of 250 rpm. The sonicated NM solution (1 ml) was added into the bacteria solution (4 ml, $OD_{600} = 0.01$) and cultured at 37 °C for 3 and 21 hours. The OD_{600} value of the bacteria at the beginning and the end of the experiment were determined by Synergy 2 Multi-mode reader. Ampicillin (50 $\mu g\ ml^{-1}$) was used as the positive control to inhibit the growth of bacteria.

6.3.2.7 Annexin V/propidium iodide assay

The procedures of annexin V/propidium iodide assay were outlined in Section 4.3.2.8. In brief, SW480 and DLD-1 cells were treated with NM and Zn^{2+} (prepared from $ZnCl_2$ solution) mixture (the concentration of $ZnCl_2$ and NM were based on the dissolution data determined from ICP-OES analysis)

on 24-well plate for 12 hours. All the dead and alive cells were collected and incubated with the dyes as manufacturer's instruction. The apoptotic and necrotic cells were assayed by Tali® Image cytometer.

6.3.2.8 Statistical analysis

Data reported are means ± SD. Statistical analysis was ascertained with paired sample Student's *t*-test comparison. Comparison was considered as statistically significant with *p*-value of < 0.05.

6.4 Results and discussions

6.4.1 Confirmation of silica coating on ZnO NM

TEOS is one of the commonly used silicate esters precursor of silicon dioxide that can be crosslinked (Abbott et al., 1961). The hydroxyl groups of ZnO nanopowder allows hydrolyzed TEOS to condense on the surface of ZnO to form Zn-O-Si linkage in the presence of ammonia catalyst. The chemical reaction of this surface coating can be described by the following equation:

$$ZnO(s) + Si(OC_2H_5)_4(aq) + 2H_2O(aq) \xrightarrow{NH_3} ZnO - SiO_2(s) + 4C_2H_5OH(aq)$$
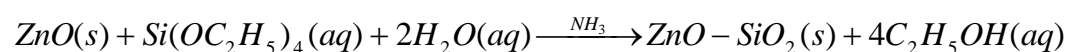
The polymerization via siloxane bond results in the formation of silica network as a shell on the ZnO NM core. After the reaction, silica coated ZnO NM were obtained. The reaction was described in **Scheme 6.1**.
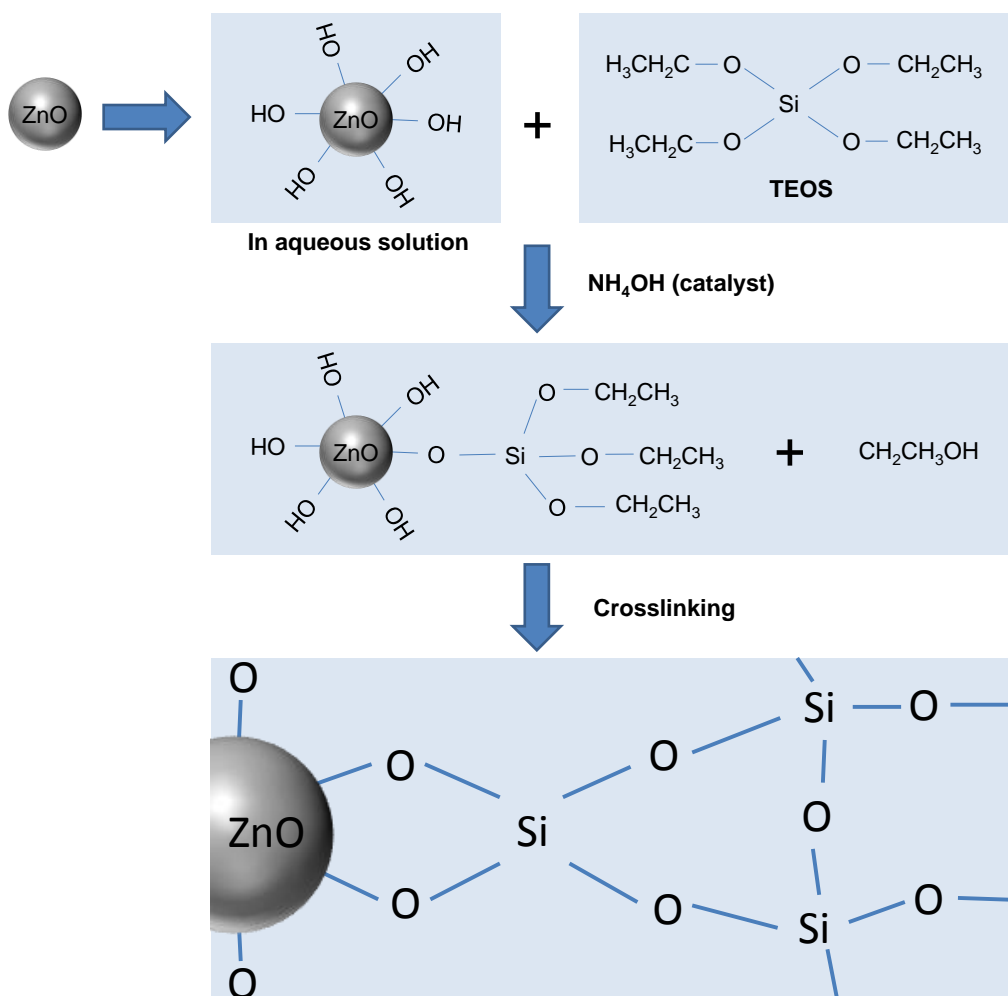
Scheme 6.1: Reactions pertinent to the formation of Silica coated ZnO NM. Ammonia catalysed the condensation of TEOS on the surface of hydrolysed ZnO NM. Further crosslink or polymerization of TEOS resulted in a silica shell on the ZnO core (not to scale).

Characterization of ZnO NM and silica coated ZnO NM in **Figure 6.1** confirmed the silica coating on the ZnO NM. Compared to the TEM images of rod-shaped ZnO NM in **Figure 6.1A**, there was an additional layer on the ZnO NM in **Figure 6.1B**. The identity of this coating was verified by FTIR and XPS analysis. The 950-1200 cm^{-1} broad band observed in FTIR spectrum can be attributed to the asymmetric stretching vibration of Si-O-Si (siloxane bonds due to the silica polymerization) (Karakassides et al., 1999; Siddiquey et al.,

2008). The results of surface elemental composition analysis by XPS agreed with the FTIR spectra for the presence of silica on the surface of ZnO NM. Besides the presence of Si 2p peak in the silica coated ZnO NM sample, another major change in the XPS spectra was the missing of Zn 2p peak in XPS spectra of silica coated ZnO NM. The missing of zinc characteristic peak might be caused by the thick and intact silicon dioxide on the surface that prevented the penetration of X-rays into the ZnO NM core.
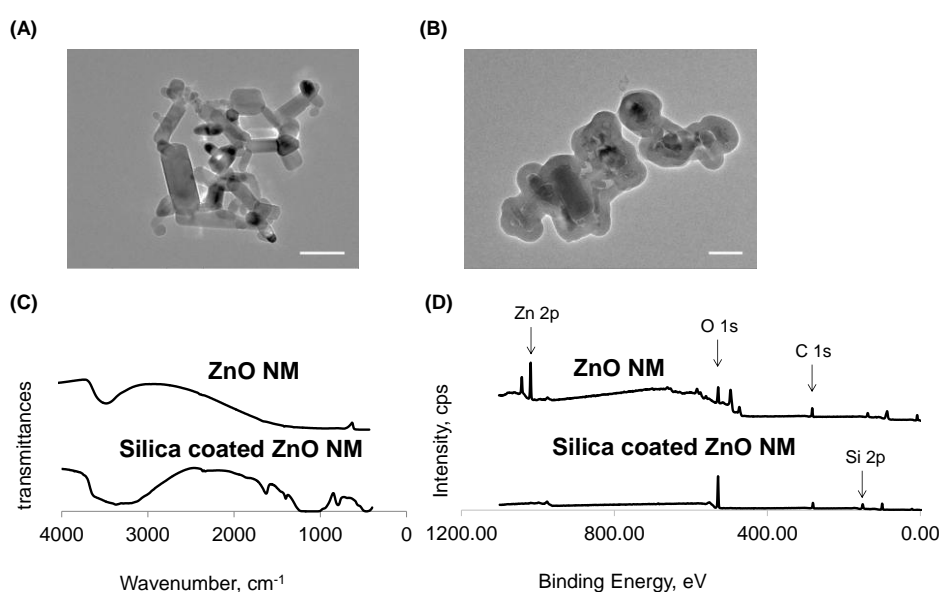
Figure 6.1: Characterization of silica coated ZnO NM. TEM images of (A) ZnO nanopodwer and (B) silica coated ZnO NM revealed the shape and size of the NM. (C) FTIR spectra of the non-coated and silica coated ZnO NM shows the functional groups on each NM. (D) Surface elements of the non-coated and silica coated ZnO NM were determined by XPS spectra. Scale bar used in (A) and (B) are 100 nm.

The physical properties of non-coated and silica coated ZnO NM were summarized in **Table 6.2**. After the silica coating, the hydrodynamic size of the ZnO NM increased. Based on **Figure 6.1**, some of the aggregated NM was coated together in a cluster rather than individual coated. This may explained

the large hydrodynamic size and polydisperse characteristic of silica coated ZnO NM. The larger magnitude of silica coated sample as compared to the uncoated ZnO NM suggests that silica coated sample was more stable than uncoated ZnO NM. Further improvements can be devoted on the coating procedures to precisely coat the individual ZnO NM to reduce the size of the products.

Table 6.2: The summary of the physical properties of non-coated and silica coated ZnO NM in water.

NM	Hydrodynamic size, nm	PDI	Zeta potential, mV
ZnO NM	258.2 ± 8.4	0.37 ± 0.02	+ 17.2 ± 0.8
Silica coated ZnO NM	623.8 ± 23.7	0.53 ± 0.05	- 21.2 ± 0.5

All data are means ± standard deviation of three independent measurements.

6.4.2   Silica coating retains the anti-microbial properties of ZnO NM

After the confirmation of successful coating, we determine the effect of silica coating on the properties of ZnO NM. As the intended application of ZnO NM is antimicrobial agent in food related products, the antimicrobial activity of the non-coated and silica coated ZnO NM to the gram negative *E. coli* and gram positive *S. aureus* bacteria was determined. The results in **Figure 6.2** showed that silica coating on ZnO NM is able to retain the antimicrobial capability of ZnO NM as the silica coated ZnO NM exhibit comparable growth inhibition as the non-coated ZnO NM to both *E. coli* and *S. aureus*.
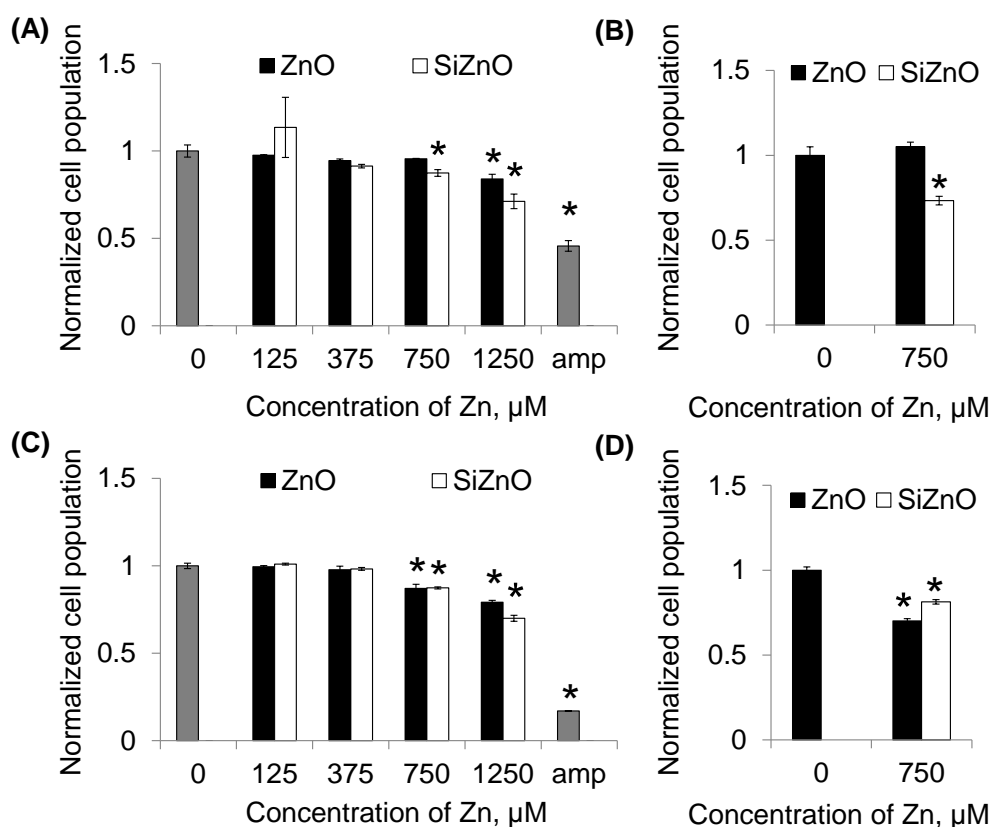
Figure 6.2: Silica coated ZnO NM have comparable antimicrobial properties as non-coated ZnO NM. The growth of *E. coli* was inhibited upon (A) 3 hours and (B) 21 hours of non-coated and silica coated ZnO NM exposure. Both non-coated and silica coated ZnO NM reduce the growth of *S. aureus* upon (C) 3 hours and (D) 21 hours treatment. amp denoted 50 µg ml^{-1} of ampicillin. Data represent means ± SD, *n = 3*. Student's *t*-test, *p < 0.05*, *significantly different between the group and untreated negative control (concentration = 0).

6.4.3 Silica coating is stable in both neutral and acidic environment

To determine the main objective of this study, we tested the effectiveness of silica coating to prevent dissolution of ZnO NM in both synthetic saliva and synthetic gastric juice. **Figure 6.3** shows that majority of ZnO NM (about 98 %) remained as ZnO with or without coating when dispersed in synthetic saliva, whereas almost all of the non-coated ZnO NM (about 98 %) were dissolved to Zn^{2+} in the synthetic gastric juice. As expected, the dissolution of ZnO NM was low in neutral environment but high in acidic

environment. On the other hand, the presence of silica shell effectively reduced the dissolution of ZnO NM in acidic condition. More than 80 % of reduction in the dissolution of the ZnO NM, this agrees that ZnO NM was protected by the silica coating. During most of the cell culture assays, NM was found to be able to absorb proteins in the cell culture medium to form a protein corona, which might protect the NM from dissolution, on the surface. The presence of enzymes such as pepsin in gastric juice can effectively degrade the proteins into peptide and expose the NM to the acidic fluids.
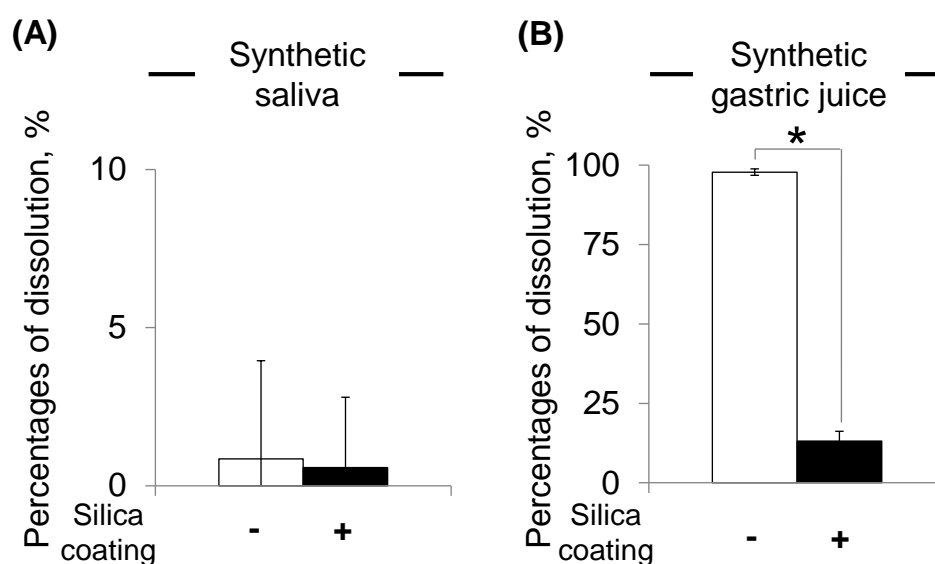
Figure 6.3: Silica coating effectively reduce the dissolution of ZnO NM in the acidity environment. (A) The dissolution of ZnO NM is low in synthetic saliva. (B) High dissolution of ZnO NM was significantly reduced by the silica coating. Data represent means ± SD, $n = 3$. Student's t-test, $p < 0.05$, *significantly different between the two groups.

6.4.4 Differential cytotoxicity of NM in 2D and 3D cell culture model

We have verified that silica coating was effective to reduce dissolution and yet maintain the antimicrobial properties of ZnO NM, we then proceed to the toxicity testing on mammalian gastrointestinal cell lines to determine

whether silica coating can also reduce the potential harmful effects of ZnO NM. With the dissolution data of NM in synthetic gastric juice, we treated the colorectal epithelial cells, SW480 and DLD-1 with the Zn^{2+} and NM equivalent to the concentration after incubation in gastric juice to replicate the condition after stomach digestion.

In **Figure 6.4** and **6.5**, high cytotoxicity was observed in 2D cell culture model treated with ZnO NM and dissolved Zn^{2+} ions upon 12 hours timepoint as previously reported (Yang et al., 2009). Silica coating was effective to reduce the toxicity of ZnO NM to both 2D SW480 and DLD-1 cells. In general, many studies concluded that ZnO NM are more toxic as compared to SiO_2 NM (Yang et al., 2009; Zhou et al., 2014).

Interestingly, an opposite trend was observed when the same treatment was conducted in 3D colorectal organoids. Both 3D SW480 and DLD-1 cells showed low cytotoxicity to the non-coated ZnO NM and Zn^{2+} ions treatment, whereas silica coated ZnO NM was found to have higher toxicity to the 3D cells as compared to uncoated ZnO NM. The opposite results in 2D and 3D cell culture model suggest further experiment and evaluation is needed to determine the toxicity and the biological mechanism of NM to the intestinal cells.

In fact, *in vivo* studies showed that silica NM can accumulate and retard in the tissue for long period (Xie et al., 2010a; Yamashita et al., 2011). Besides that, silica NM were not inert to biological system, they could induce structural abnormalities to placenta of mice (Yamashita et al., 2011).

Although the use of silica coating could effectively reduce dissolution of ZnO NM, whether silica coating is a good solution to reduce the toxicity of ZnO NM or not still remained to be determined.
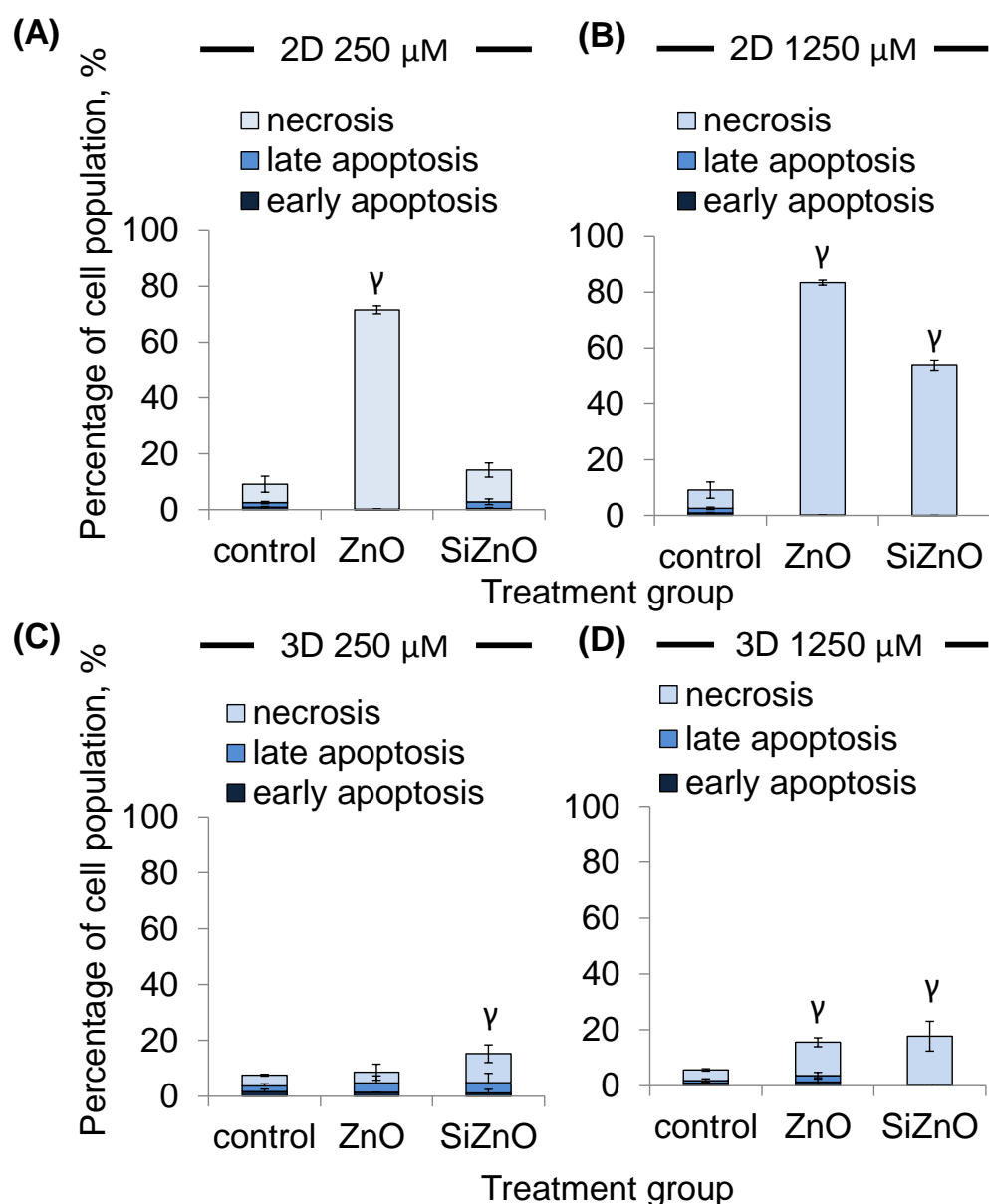
Figure 6.4: Cell dimensionality affects the toxicity of non-coated and silica coated ZnO NM to SW480 cells. ZnO NM and dissolved Zn^{2+} induce high cytotoxicity to SW480 in 2D cell culture upon 12 hours of (A) 250 μM and (B) 1250 μM. Silica coated ZnO NM are less cytotoxic as compared to non-coated ZnO NM, whereas higher toxicity was observed in 3D cell culture model for the silica coated ZnO NM treated groups for both (C) 250 μM and (D) 1250 μM treatment as compared to non-coated ZnO NM. ZnO denoted ZnO NM, SiZnO denoted silica coated ZnO NM. Data represent means ± SD, $n = 3$. Student's t-test, $p < 0.05$, [α]significant different with the percentage of early apoptotic cell in control group (concentration = 0), [β]significant different with the percentage of late apoptotic cell in control, [γ]significant different with the percentage of necrotic cell in control.

117
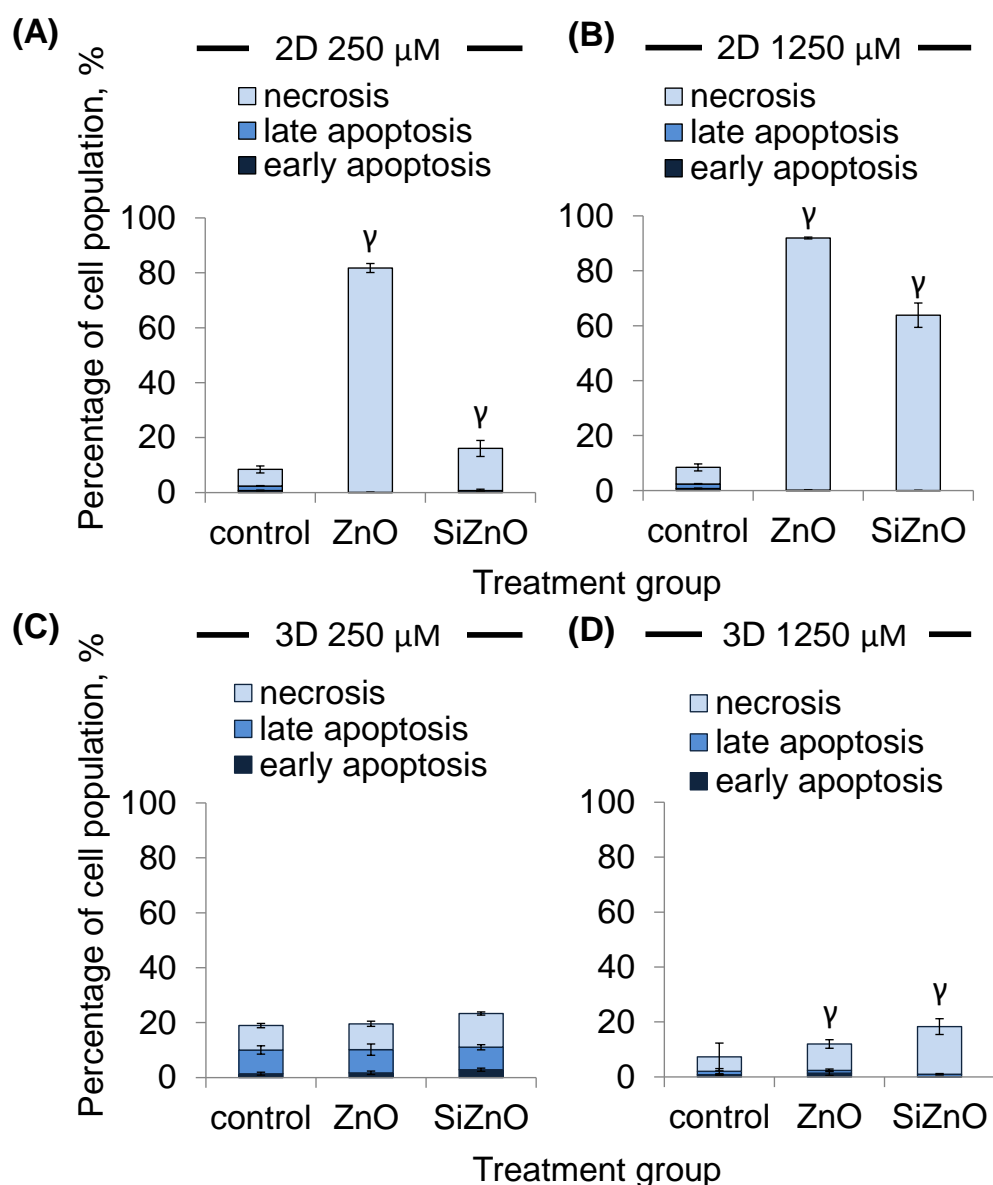
Figure 6.5: Cell dimensionality affects the toxicity of non-coated and silica coated ZnO NM to DLD-1 cells. ZnO NM and dissolved Zn^{2+} induce high cytotoxicity to SW480 in 2D cell culture upon 12 hours of (A) 250 μM and (B) 1250 μM. Silica coated ZnO NM are less cytotoxic as compared to non-coated ZnO NM, whereas higher toxicity was observed in 3D cell culture model for the silica coated ZnO NM treated groups for both (C) 250 μM and (D) 1250 μM as compared to non-coated ZnO NM. ZnO denoted ZnO NM, SiZnO denoted silica coated ZnO NM. Data represent means ± SD, $n = 3$. Student's t-test, $p < 0.05$, [α]significant different with the percentage of early apoptotic cell in control group (concentration = 0), [β]significant different with the percentage of late apoptotic cell in control, [γ]significant different with the percentage of necrotic cell in control.

6.5   Conclusion

We showed that synthetic gastrointestinal fluids are useful to determine the chemical form of ingested NM for more detailed nanotoxicity study. Silica coating, which formed by TEOS precursor, is stable in both neutral and acidity conditions. Silica coating effectively reduces the dissolution of ZnO NM and is able to maintain the antimicrobial activity of ZnO NM. However, higher toxicity was observed in silica coated ZnO NM than uncoated ZnO NM when the treatment was conducted in 3D cells.

These differential results between 2D and 3D cell culture models highlighted the importance of cell dimensionality for toxicity assessment. 3D cell spheroid, which provides a more *in vivo*-like microenvironment of colorectal cells, could more readily resemble the tissue response to the effects of NM. The simplification of tissue, which make up of multilayer of cells, into 2D cell culture might reduce the capability of cell-to-cell and cell-to-matrix communication; as a result, compromise the ability of 2D cell culture to accurately predict the tissue response.

Chapter 7: Conclusion

7.1   Promise of 3D cell cultures in nanotoxicity assessment

Nanotoxicity study is important to ensure the safe use of NM. In order to match the rapid growing of nanotechnology and not to hold back the development of nanotechnology, representative and reliable models should be used to effectively and efficiently determine the toxicity and biological interactions of NM.

In vitro model is still a good start for scientific research. However, the important characteristics of a tissue should not be oversimplified. Some of the parameters such as the cell-to-cell, cell-to-ECM interaction, and mass transfer pattern should be included in the model in order to maintain the reliability and quality of the *in vitro* model.

This study shows the tremendous flexibility of 3D cell culture model in offering great opportunity to uncover the biological interactions and toxicity mechanisms of NM that would remain undiscovered in the monolayer model. We demonstrated the ability of 3D cell culture models to replicate the characteristics of cells in tissue. Besides that, different cellular responses to NM can be determined in 3D cell culture models, for example, the cytotoxicity, inflammatory responses, gene expression, and protein expression.

3D cell spheroid model is suitable for mimicking multilayered tissue type. The toxicity results obtained from 3D cell spheroid model showed that the cellular responses of cells cultured in 3D format are significantly different with the cells cultured in 2D format as our hypothesis. These results suggest the importance of cell dimensionality, cell-to-cell interactions and cell-to-matrix interactions in affecting the downstream cellular responses to stimulus.

The presence of cell layer and ECM significantly reduce the mass transfer of ZnO NM to the inner layers of cells, in turn, lower toxicity (cytotoxicity, inflammatory response, DNA damage, oxidative stress) was observed in the 3D cell culture model. However, the cell-to-cell interactions can result in a systemic inflammatory response in the neighbouring cells.

Co-culture transwell model is convenient for the study of diffusion and transcellular transport of NM across tissue barrier. Both endothelial and epithelial cells are involved in the regulation of NM transport. Besides that, we also determine the active role of endothelial cells in inflammatory response. The upregulation of intracellular ROS in endothelial cells was found to occur when the accumulation of zinc in cells exceed a tolerable level.

In this study, we showed two different 3D cell culture models and their potential applications in mimicking different tissue types in human body. Nevertheless, more efforts can be devoted to further improve the current 3D cell culture models in order to achieve better predictive efficiency of *in vitro* model. For example, the cell spheroid can be improved by introducing more than one cell type to allow the cells to self-sort and self-orientate to a multicellular spheroid or microtissues. Multi-cellular microtissues are useful for cell-to-cell contact study, targeting analysis and understanding the interaction of NM with surface receptor. For the bilayer tissue model, improvement such as curvature of membrane can be introduced to the system. Most of the tissues are formed on a curved surface to ensure maximum contact surface. The curved surface stretches the cells and might enhance cell adhesion (Hu et al., 2014).

7.2   Other potential applications of 3D cell culture model

We demonstrated the advantages and flexibility of 3D cell culture models in nanotoxicity study. Similarly, 3D cell culture model can outperform the 2D cell culture model for nanomedicine study to determine the therapeutic effects of chemical entity under controlled environment in the early stage of development (Kunz-Schughart et al., 2004). Screening study of anticancer drug library found that 2D monolayer cell culture model tends to overestimate the effect of active compounds and gives artifact. This is partly due to the inability of 2D cell culture model to replicate the important characteristics of real tissue and the cellular responses.

3D cell spheroid provides a physiological relevant structure as tumour; more specifically, 3D cell spheroid can replicate the nature morphology of tumour as cell aggregate. Furthermore, the presence of physical cell barrier and ECM in the cell spheroid model is more suitable to predict the mass transfer and efficacy of anti-cancer drugs in cancer therapy to inhibit the growth of cancerous cell and killing effects of the drugs. Besides that, the cell spheroid model can be improved by embedding the cell spheroid in 3D matrix or scaffolds in order to study cancerous cell migration and invasion (Sodek et al., 2008). The presence of ECM provides a more realistic microenvironment to determine the efficacy of nanodrugs to inhibit metastatic cells for releasing metalloproteinase which digests and reconstitutes ECM (Kanekura et al., 2002; Poincloux et al., 2011).

Besides that, 3D cell culture model is easier to be established and used as compared to tumour xenograft in animal for cancer study. The structure of 3D cell spheroid is similar to tumour mass with a necrotic core due to limited mass transfer into the centre. Overall, 3D cell spheroid can serve as a good model to predict the biological interactions of nanodrugs to tumour.

Endo-epithelial bilayer model can also be used as a model to determine mass transfer of nanodrugs from the bloodstream to the targeted tissue or organ. By changing the cell types on the bilayer model, different tissue constructed by dual cell types can be formed. The transwell configuration provides a good system to determine the diffusion of nanodrugs from one compartment to another and the cellular uptake of nanodrugs by each cell type.

REFERENCES

Abbott, A.D., Wright, J.R., Goldschmidt, A., Stewart, W.T., and Bolt, R.O. (1961). Silicate esters and related compounds. J Chem Eng Data *6*, 437-442.

Abramoff, M.D., Magelhaes, P.J., and Ram, S.J. (2004). Image processing with ImageJ. Biophotonics Int *11*, 36-42.

Achilli, T-M., Meyer, J., and Morgan J. R. (2012) Advances in the formation, use and understanding of multicellular spheroids. Expert Opin Biol Ther *12*, 1347-1360.

Ahmed, D., Eide, P.W., Eilertsen, I.A., Danielsen, S.A., Eknas, M., Hektoen, M., Lind, G.E., and Lothe, R.A. (2013). Epigenetic and genetic features of 24 colon cancer cell lines. Oncogenesis *2*, e71.

Andrea, G., Guo, B., Rama, S.K., John, C.R., Kennedy, I.M., and Abdul, I.B. (2007). Induction of inflammation in vascular endothelial cells by metal oxide nanoparticles: Effect of particle composition. Environ Health Perspect *115*, 403-409.

Arora, S., Rajwade, J.M., and Paknikar, K.M. (2012). Nanotoxicology and in vitro studies: the need of the hour. Toxicol Appl Pharmacol *258*, 151-165.

AshaRani, P., Low, K. M. G., Hande, M. P., Valiyaveettil, S. (2008). Cytotoxicity and genotoxicity of silver nanoparticles in human cells. ACS Nano *3*, 279-290.

Ashkenas, J., Muschler, J., and Bissell, M.J. (1996). The extracellular matrix in epithelial biology: Shared molecules and common themes in distant phyla. Dev Biol *180*, 433-444.

Barford, J.P. (1995). Fundamental and applied aspects of animal cell cultivation (Singapore University Press, National University of Singapore).

Barrila, J., Radtke, A.L., Crabbe, A., Sarker, S.F., Herbst-Kralovetz, M.M., Ott, C.M., and Nickerson, C.A. (2010). Organotypic 3D cell culture models: using the rotating wall vessel to study host-pathogen interactions. Nat Rev Microbiol *8*, 791-801.

Becheri, A., Dürr, M., Lo Nostro, P., and Baglioni, P. (2008). Synthesis and characterization of zinc oxide nanoparticles: application to textiles as UV-absorbers. J Nanopart Res *10*, 679-689.

Bissell, M.J., Rizki, A., and Mian, I.S. (2003). Tissue architecture: the ultimate regulator of breast epithelial function. Curr Opin Cell Biol *15*, 753-762.

Brinkmann, V., Foroutan, H., Sachs, M., Weidner, K.M., and Birchmeier, W. (1995). Hepatocyte growth factor/scatter factor induces a variety of tissue-specific morphogenic programs in epithelial cells. J Cell Biol *131*, 1573-1586.

Cairns, R.A., Harris, I.S., and Mak, T.W. (2011). Regulation of cancer cell metabolism. Nat Rev Cancer *11*, 85-95.

Castro-Poças F. M., Dinis-Ribeiro M., Araújo T. P., Pedroto I. (2015). Echoendoscopic characterization of the human colon. Rev Esp Enferm Dig *107*, 469-475.

Cedervall, T., Lynch, I., Lindman, S., Berggård, T., Thulin, E., Nilsson, H., Dawson, K.A., and Linse, S. (2007). Understanding the nanoparticle–protein corona using methods to quantify exchange rates and affinities of proteins for nanoparticles. Proc Natl Acad Sci U S A *104*, 2050-2055.

Chang, T.T., and Hughes-Fulford, M. (2009). Monolayer and spheroid culture of human liver hepatocellular carcinoma cell line cells demonstrate distinct global gene expression patterns and functional phenotypes. Tissue Eng Part A *15*, 559-567.

Checco, A., Rahman, A., and Black, C.T. (2014). Robust superhydrophobicity in large-area nanostructured surfaces defined by block-copolymer self assembly. Adv Mater *26*, 886-891.

Chen, Z., Liu, Y., Sun, B., Li, H., Dong, J., Zhang, L., Wang, L., Wang, P., Zhao, Y., and Chen, C. (2014). Polyhydroxylated metallofullerenols stimulate IL-1β secretion of macrophage through TLRs/MyD88/NF-κB pathway and NLRP3 inflammasome activation. Small *10*, 2362-2372.

Chia, S.L., Tay, C.Y., Setyawati, M.I., and Leong, D.T. (2015). Decoupling the direct and indirect biological effects of ZnO nanoparticles using a communicative dual cell type tissue construct. Small DOI: 10.1002/smll.201502306.

Cho, W.-S., Kang, B.-C., Lee, J.K., Jeong, J., Che, J.-H., and Seok, S.H. (2013a). Comparative absorption, distribution, and excretion of titanium dioxide and zinc oxide nanoparticles after repeated oral administration. Particle and fibre toxicology *10*, 1-9.

Cho, W.S., Duffin, R., Bradley, M., Megson, I.L., MacNee, W., Lee, J.K., Jeong, J., and Donaldson, K. (2013b). Predictive value of in vitro assays depends on the mechanism of toxicity of metal oxide nanoparticles. Part Fibre Toxicol *10*, 55.

Choi, H.S., Liu, W., Misra, P., Tanaka, E., Zimmer, J.P., Itty Ipe, B., Bawendi, M.G., and Frangioni, J.V. (2007). Renal clearance of quantum dots. Nat Biotech *25*, 1165-1170.

Cohen, Y., Rallo, R., Liu, R., and Liu, H.H. (2013). In silico analysis of nanomaterials hazard and risk. Acc Chem Res *46*, 802-812.

Cong, Y., Pang, C., Dai, L., Banta, G.T., Selck, H., and Forbes, V.E. (2011). Importance of characterizing nanoparticles before conducting toxicity tests. Integr Environ Assess Manag *7*, 502-503.

Danielsen, P.H., Cao, Y., Roursgaard, M., Møller, P., and Loft, S. (2015). Endothelial cell activation, oxidative stress and inflammation induced by a panel of metal-based nanomaterials. Nanotoxicology *9*, 813-824.

Domansky, K., Inman, W., Serdy, J., Dash, A., Lim, M.H.M., and Griffith, L.G. (2010). Perfused multiwell plate for 3D liver tissue engineering. Lab Chip *10*, 51-58.

Dorman, H.R., Sondheimer, J.H., and Cadnapaphornchai, P. (1990). Mannitol-induced acute renal failure. Medicine *69*, 153-159.

Du, Y., Lo, E., Ali, S., and Khademhosseini, A. (2008). Directed assembly of cell-laden microgels for fabrication of 3D tissue constructs. Proc Natl Acad Sci U S A *105*, 9522-9527.

Edinger, A.L., and Thompson, C.B. (2004). Death by design: apoptosis, necrosis and autophagy. Curr Opin Cell Biol *16*, 663-669.

El-Shabouri, M.H. (2002). Positively charged nanoparticles for improving the oral bioavailability of cyclosporin-A. Int J Pharm *249*, 101-108.

Ema, M., Kobayashi, N., Naya, M., Hanai, S., and Nakanishi, J. (2010). Reproductive and developmental toxicity studies of manufactured nanomaterials. Reprod Toxicol *30*, 343-352.

Esmaeillou, M., Moharamnejad, M., Hsankhani, R., Tehrani, A.A., and Maadi, H. (2013). Toxicity of ZnO nanoparticles in healthy adult mice. Environ Toxicol Pharmacol *35*, 67-71.

Espitia, P., Soares, N.d., Coimbra, J.d., de Andrade, N., Cruz, R., and Medeiros, E. (2012). Zinc oxide nanoparticles: synthesis, antimicrobial activity and food packaging applications. Food Bioproc Tech *5*, 1447-1464.

Faddah, L.M., Baky, N.A.A., Al-Rasheed, N.M., Al-Rasheed, N.M., Fatani, A.J., and Atteya, M. (2012). Role of quercetin and arginine in ameliorating nano zinc oxide-induced nephrotoxicity in rats. BMC Complement Altern Med *12*, 1-14.

Fadeel, B., and Garcia-Bennett, A.E. (2010). Better safe than sorry: understanding the toxicological properties of inorganic nanoparticles manufactured for biomedical applications. Adv Drug Deliv Rev *62*, 362-374.

Ferdowsian, H.R., and Beck, N. (2011). Ethical and scientific considerations regarding animal testing and research. PLoS One *6*, e24059.

Fernández-Checa, J.C., García-Ruiz, C., Colell, A., Morales, A., Marí, M., Miranda, M., and Ardite, E. (1998). Oxidative stress: role of mitochondria and protection by glutathione. Biofactors *8*, 7-11.

Filipe, P., Silva, J.N., Silva, R., Cirne de Castro, J.L., Marques Gomes, M., Alves, L.C., Santus, R., and Pinheiro, T. (2009). Stratum corneum is an effective barrier to TiO2 and ZnO nanoparticle percutaneous absorption. Skin Pharmacol Physiol *22*, 266-275.

Fischer, H.C., and Chan, W.C.W. (2007). Nanotoxicity: The growing need for in vivo study. Curr Opin Biotechnol *18*, 565-571.

Fischer, H.C., Liu, L., Pang, K.S., and Chan, W.C.W. (2006). Pharmacokinetics of nanoscale quantum dots: in vivo distribution, sequestration, and clearance in the rat. Adv Funct Mater *16*, 1299-1305.

Gaiser, B., Fernandes, T., Jepson, M., Lead, J., Tyler, C., and Stone, V. (2009). Assessing exposure, uptake and toxicity of silver and cerium dioxide nanoparticles from contaminated environments. Environ Health *8*, 1-4.

Gao, J., and Xu, B. (2009). Applications of nanomaterials inside cells. Nano Today *4*, 37-51.

Garnett, M.C., and Kallinteri, P. (2006). Nanomedicines and nanotoxicology: some physiological principles. Occup Med (Lond) *56*, 307-311.

George, S., Xia, T., Rallo, R., Zhao, Y., Ji, Z., Lin, S., Wang, X., Zhang, H., France, B., Schoenfeld, D., *et al.* (2011). Use of a high-throughput screening approach coupled with in vivo zebrafish embryo screening to develop hazard ranking for engineered nanomaterials. ACS Nano *5*, 1805-1817.

Glicklis, R., Merchuk, J.C., and Cohen, S. (2004). Modeling mass transfer in hepatocyte spheroids via cell viability, spheroid size, and hepatocellular functions. Biotechnol Bioeng *86*, 672-680.

Godugu, C., Patel, A.R., Desai, U., Andey, T., Sams, A., and Singh, M. (2013). AlgiMatrix™ based 3D cell culture system as an in-vitro tumor model for anticancer studies. PLoS One *8*, e53708.

Grasset, F., Saito, N., Li, D., Park, D., Sakaguchi, I., Ohashi, N., Haneda, H., Roisnel, T., Mornet, S., and Duguet, E. (2003). Surface modification of zinc oxide nanoparticles by aminopropyltriethoxysilane. J Alloys Compd *360*, 298-311.

Guo, L., Yang, S., Yang, C., Yu, P., Wang, J., Ge, W., and Wong, G.K.L. (2000). Synthesis and characterization of poly(vinylpyrrolidone)-modified zinc oxide nanoparticles. Chem Mater *12*, 2268-2274.

Gutiérrez-Wing, C., Velázquez-Salazar, J.J., and José-Yacamán, M. (2012). Procedures for the synthesis and capping of metal nanoparticles. In Nanoparticles in Biology and Medicine, M. Soloviev, ed. (Humana Press), pp. 3-19.

Hagens, W.I., Oomen, A.G., de Jong, W.H., Cassee, F.R., and Sips, A.J.A.M. (2007). What do we (need to) know about the kinetic properties of nanoparticles in the body? Regul Toxicol Pharmacol *49*, 217-229.

Hailing, Y. (2007). Half way to the trillion dollar market? A critical review of the diffusion of nanotechnologies (London, UK: Cientifica), pp. 10.

Haisler, W.L., Timm, D.M., Gage, J.A., Tseng, H., Killian, T.C., and Souza, G.R. (2013). Three-dimensional cell culturing by magnetic levitation. Nat Protoc *8*, 1940-1949.

Hariharan, S., Bhardwaj, V., Bala, I., Sitterberg, J., Bakowsky, U., and Ravi Kumar, M.N.V. (2006). Design of estradiol loaded PLGA nanoparticulate formulations: A potential oral delivery system for hormone therapy. Pharm Res *23*, 184-195.

Haycock, J. (2011). 3D cell culture: a review of current approaches and techniques. Methods Mol Biol *695*, 1 - 15.

He, X., Nie, H., Wang, K., Tan, W., Wu, X., and Zhang, P. (2008). In vivo study of biodistribution and urinary excretion of surface-modified silica nanoparticles. Anal Chem *80*, 9597-9603.

Heng, B., Zhao, X., Tan, E., Khamis, N., Assodani, A., Xiong, S., Ruedl, C., Ng, K., and Loo, J.-C. (2011). Evaluation of the cytotoxic and inflammatory potential of differentially shaped zinc oxide nanoparticles. Arch Toxicol *85*, 1517-1528.

Hillegass, J.M., Shukla, A., Lathrop, S.A., MacPherson, M.B., Fukagawa, N.K., and Mossman, B.T. (2010). Assessing nanotoxicity in cells in vitro. Wiley Interdiscip Rev Nanomed Nanobiotechnol *2*, 219-231.

Hong, R., Pan, T., Qian, J., and Li, H. (2006). Synthesis and surface modification of ZnO nanoparticles. Chem Eng J *119*, 71-81.

Hong, R.Y., Li, J.H., Chen, L.L., Liu, D.Q., Li, H.Z., Zheng, Y., and Ding, J. (2009). Synthesis, surface modification and photocatalytic property of ZnO nanoparticles. Powder Technol *189*, 426-432.

Hong, T. K., Tripathy, N., Son, H. J., Ha, K. T., Jeong, H. S., and Hahn, Y. B. (2013). A comprehensive in vitro and in vivo study of ZnO nanoparticles toxicity. J Mater Chem B Mater Biol Med *1*, 2985-2992.

Huang, C. C., Aronstam, R.S., Chen, D. R., and Huang, Y. W. (2010). Oxidative stress, calcium homeostasis, and altered gene expression in human lung epithelial cells exposed to ZnO nanoparticles. Toxicology in vitro : an international journal published in association with BIBRA *24*, 45-55.

Huang, J., Bu, L., Xie, J., Chen, K., Cheng, Z., Li, X., Chen, X. (2010). Effects of nanoparticle size on cellular uptake and liver MRI with polyvinylpyrrolidone-coated iron oxide nanoparticles. ACS Nano *4*, 7151-7160.

Huczko, A. (2000). Template-based synthesis of nanomaterials. Appl Phys A Mater Sci Process *70*, 365-376.

Hutchinson, L., and Kirk, R. (2011). High drug attrition rates--where are we going wrong? Nat Rev Clin Oncol *8*, 189 - 190.

Ishiwata, R., Yokoyama, U., Matsusaki, M., Asano, Y., Kadowaki, K., Ichikawa, Y., Umemura, M., Fujita, T., Minamisawa, S., Shimoda, H.*, et al.* (2014). Three-dimensional multilayers of smooth muscle cells as a new experimental model for vascular elastic fiber formation studies. Atherosclerosis *233*, 590-600.

Jiang, W., Mashayekhi, H., and Xing, B. (2009). Bacterial toxicity comparison between nano- and micro-scaled oxide particles. Environ Pollut *157*, 1619-1625.

Jones, C.F., and Grainger, D.W. (2009). In vitro assessments of nanomaterial toxicity. Adv Drug Deliv Rev *61*, 438-456.

Joris, F., Manshian, B.B., Peynshaert, K., De Smedt, S.C., Braeckmans, K., and Soenen, S.J. (2013). Assessing nanoparticle toxicity in cell-based assays: influence of cell culture parameters and optimized models for bridging the in vitro-in vivo gap. Chem Soc Rev *42*, 8339-8359.

Joshi, A.W., Raybagkar, V.H., Vijayshri, Desa, K.V., Mahamuni, R., and Bendre, B.S. (2009). Emerging Physics (India: Pearson Education), pp. 184.

Justice, B.A., Badr, N.A., and Felder, R.A. (2009). 3D cell culture opens new dimensions in cell-based assays. Drug discovery today *14*, 102-107.

Kanekura, T., Chen, X., and Kanzaki, T. (2002). Basigin (cd147) is expressed on melanoma cells and induces tumor cell invasion by stimulating production of matrix metalloproteinases by fibroblasts. Int J Cancer *99*, 520-528.

Kao, Y.-Y., Chen, Y.-C., Cheng, T.-J., Chiung, Y.-M., and Liu, P.-S. (2012). Zinc Oxide nanoparticles interfere with zinc ion homeostasis to cause cytotoxicity. Toxicol Sci *125*, 462-472.

Karakassides, M.A., Gournis, D., and Petridis, D. (1999). An infrared reflectance study of SiO vibrations in thermally treated alkali-saturated montmorillonites. Clay Miner *34*, 429-429.

Kathawala, M.H., Xiong, S., Richards, M., Ng, K.W., George, S., and Loo, S.C.J. (2013). Emerging in vitro models for safety screening of high-volume production nanomaterials under environmentally relevant exposure conditions. Small *9*, 1504-1520.

Ke, J., Wu, X., He, X., Lian, L., Zou, Y., Wang, H., Luo, Y., Wang, L., and Lan, P. (2012). A subpopulation of CD24^{+} cells in colon cancer cell lines possess stem cell characteristics. Neoplasma *59*, 282-288.

Kelm, J.M., Timmins, N.E., Brown, C.J., Fussenegger, M., and Nielsen, L.K. (2003). Method for generation of homogeneous multicellular tumor spheroids applicable to a wide variety of cell types. Biotechnol Bioeng *83*, 173-180.

Khan, M.A. (1984). Minipig: Advantages and disadvantages as a model in toxicity testing. Int J Toxicol *3*, 337-342.

Kim, J.B. (2005). Three-dimensional tissue culture models in cancer biology. Semin Cancer Biol *15*, 365-377.

Kim, J.S., Yoon, T.-J., Yu, K.N., Kim, B.G., Park, S.J., Kim, H.W., Lee, K.H., Park, S.B., Lee, J.-K., and Cho, M.H. (2006). Toxicity and tissue distribution of magnetic nanoparticles in mice. Toxicol Sci *89*, 338-347.

Knight, E., and Przyborski, S. (2015). Advances in 3D cell culture technologies enabling tissue-like structures to be created in vitro. J Anat *227*, 746-756.

Kumar, A., Takada, Y., Boriek, A., and Aggarwal, B. (2004). Nuclear factor-κB: Its role in health and disease. J Mol Med *82*, 434-448.

Kunz-Schughart, L.A., Freyer, J.P., Hofstaedter, F., and Ebner, R. (2004). The use of 3-D cultures for high-throughput screening: the multicellular spheroid model. J Biomol Screen *9*, 273-285.

Lam, H.F., Conner, M.W., Rogers, A.E., Fitzgerald, S., and Amdur, M.O. (1985). Functional and morphologic changes in the lungs of guinea pigs exposed to freshly generated ultrafine zinc oxide. Toxicol Appl Pharmacol *78*, 29-38.

Le Belle, J.E., Orozco, N.M., Paucar, A.A., Saxe, J.P., Mottahedeh, J., Pyle, A.D., Wu, H., and Kornblum, H.I. (2011). Proliferative neural stem cells have high endogenous ROS levels that regulate self-renewal and neurogenesis in a PI3K/Akt-dependant manner. Cell Stem Cell *8*, 59-71.

Lee, J.-I., and Burckart, G.J. (1998). Nuclear factor kappa B: important transcription factor and therapeutic target. J Clin Pharmacol *38*, 981-993.

Leist, M., Single, B., Naumann, H., Fava, E., Simon, B., Kühnle, S., and Nicotera, P. (1999). Inhibition of mitochondrial ATP generation by nitric oxide switches apoptosis to necrosis. Exp Cell Res *249*, 396-403.

Leng, N., Lizeng, G., Xiyun, Y., and Taihong, W. (2007). Functionalized tetrapod-like ZnO nanostructures for plasmid DNA purification, polymerase chain reaction and delivery. Nanotechnology *18*, 015101.

Li, X., Valadez, A.V., Zuo, P., and Nie, Z. (2012). Microfluidic 3D cell culture: potential application for tissue-based bioassays. Bioanalysis *4*, 1509-1525.

Li, Y., Zhang, W., Niu, J., Chen, Y. (2012). Mechanism of photogenerated reactive oxygen species and correlation with the antibacterial properties of engineered metal-oxide nanoparticles. ACS Nano *6*, 5164-5173.

Li, Y., Sun, X., LaMont, J.T., Pardee, A.B., and Li, C.J. (2003). Selective killing of cancer cells by β-lapachone: Direct checkpoint activation as a strategy against cancer. Proc Natl Acad Sci U S A *100*, 2674-2678.

Limbach, L. K., Li, Y., Grass, R. N., Brunner, T. J., Hintermann, M. A., Muller, M., Gunther D., Stark, W. J. (2005). Oxide Nanoparticle Uptake in

Human Lung Fibroblasts: Effects of Particle Size, Agglomeration, and Diffusion at Low Concentrations. Environ Sci Technol *39*, 9370–9376.

Lin, W., Xu, Y., Huang, C.-C., Ma, Y., Shannon, K., Chen, D.-R., and Huang, Y.-W. (2009). Toxicity of nano- and micro-sized ZnO particles in human lung epithelial cells. J Nanopart Res *11*, 25-39.

Liqiang, J., Baiqi, W., Baifu, X., Shudan, L., Keying, S., Weimin, C., and Honggang, F. (2004). Investigations on the surface modification of ZnO nanoparticle photocatalyst by depositing Pd. J Solid State Chem *177*, 4221-4227.

Liu, H., Ma, L., Liu, J., Zhao, J., Yan, J., and Hong, F. (2010). Toxicity of nano-anatase TiO2 to mice: Liver injury, oxidative stress. Toxicol Environ Chem *92*, 175-186.

Loessner, D., Stok, K.S., Lutolf, M.P., Hutmacher, D.W., Clements, J.A., and Rizzi, S.C. (2010). Bioengineered 3D platform to explore cell-ECM interactions and drug resistance of epithelial ovarian cancer cells. Biomaterials *31*, 8494-8506.

Love, S.A., Maurer-Jones, M.A., Thompson, J.W., Lin, Y.-S., and Haynes, C.L. (2012). Assessing nanoparticle toxicity. Annu Rev Anal Chem *5*, 181-205.

Mak, I.W., Evaniew, N., and Ghert, M. (2014). Lost in translation: animal models and clinical trials in cancer treatment. Am J Transl Res *6*, 114-118.

Martignoni, M., Groothuis, G.M.M., and de Kanter, R. (2006). Species differences between mouse, rat, dog, monkey and human CYP-mediated drug metabolism, inhibition and induction. Expert Opin Drug Metab Toxicol *2*, 875-894.

Martinon, F., Mayor, A., and Tschopp, J. (2009). The inflammasomes: guardians of the body. Annu Rev Immunol *27*, 229-265.

Mazzoleni, G., Di Lorenzo, D., and Steimberg, N. (2009). Modelling tissues in 3D: the next future of pharmaco-toxicology and food research? Genes Nutr *4*, 13-22.

McDonald, D.M., and Baluk, P. (2002). Significance of blood vessel leakiness in cancer. Cancer Res *62*, 5381-5385.

Mitsudome, T., and Kaneda, K. (2013). Gold nanoparticle catalysts for selective hydrogenations. Green Chem *15*, 2636-2654.

Moon, S., Hasan, S.K., Song, Y.S., Xu, F., Keles, H.O., Manzur, F., Mikkilineni, S., Hong, J.W., Nagatomi, J., Haeggstrom, E*., et al.* (2010). Layer by layer three-dimensional tissue epitaxy by cell-laden hydrogel droplets. Tissue Eng Part C Methods *16*, 157-166.

Moos, P.J., Chung, K., Woessner, D., Honeggar, M., Cutler, N.S., and Veranth, J.M. (2010). ZnO particulate matter requires cell contact for toxicity in human colon cancer cells. Chem Res Toxicol *23*, 733-739.

Morabito, K., Shapley, N.C., Steeley, K.G., and Tripathi, A. (2011). Review of sunscreen and the emergence of non-conventional absorbers and their applications in ultraviolet protection. Int J Cosmet Sci *33*, 385-390.

Morales, J.M., Wramner, L., Kreis, H., Durand, D., Campistol, J.M., Andres, A., Arenas, J., Nègre, E., Burke, J.T., Groth, C.G.*, et al.* (2002). Sirolimus does not exhibit nephrotoxicity compared to cyclosporine in renal transplant recipients. Am J Transplant *2*, 436-442.

Myungjin Lee, J., Mhawech-Fauceglia, P., Lee, N., Cristina Parsanian, L., Gail Lin, Y., Andrew Gayther, S., and Lawrenson, K. (2013). A three-dimensional microenvironment alters protein expression and chemosensitivity of epithelial ovarian cancer cells in vitro. Lab Invest *93*, 528-542.

Naim, F., Messier, S., Saucier, L., and Piette, G. (2004). Postprocessing in vitro digestion challenge to evaluate survival of escherichia coli O157:H7 in fermented dry sausages. Appl Environ Microbiol *70*, 6637-6642.

Netzlaff, F., Lehr, C.M., Wertz, P.W., and Schaefer, U.F. (2005). The human epidermis models EpiSkin®, SkinEthic® and EpiDerm®: An evaluation of morphology and their suitability for testing phototoxicity, irritancy, corrosivity, and substance transport. Eur J Pharm Biopharm *60*, 167-178.

Ng, K.W., Khoo, S.P.K., Heng, B.C., Setyawati, M.I., Tan, E.C., Zhao, X., Xiong, S., Fang, W., Leong, D.T., and Loo, J.S.C. (2011). The role of the tumor suppressor p53 pathway in the cellular DNA damage response to zinc oxide nanoparticles. Biomaterials *32*, 8218-8225.

Nichol, J.W., Koshy, S.T., Bae, H., Hwang, C.M., Yamanlar, S., and Khademhosseini, A. (2010). Cell-laden microengineered gelatin methacrylate hydrogels. Biomaterials *31*, 5536-5544.

Nickerson, C., Richter, E., and Ott, C.M. (2007). Studying host–pathogen interactions in 3-D: organotypic models for infectious disease and drug development. J Neuroimmune Pharmacol *2*, 26-31.

Noei, H., Qiu, H., Wang, Y., Loffler, E., Woll, C., and Muhler, M. (2008). The identification of hydroxyl groups on ZnO nanoparticles by infrared spectroscopy. Phys Chem Chem Phys *10*, 7092-7097.

Oberdörster, G., Maynard, A., Donaldson, K., Castranova, V., Fitzpatrick, J., Ausman, K., Carter, J., Karn, B., Kreyling, W., Lai, D.*, et al.* (2005). Principles for characterizing the potential human health effects from exposure to nanomaterials: elements of a screening strategy. Part Fibre Toxicol *2* 8.

Ohmori, T., Yang, J.-L., Price, J.O., and Arteaga, C.L. (1998). Blockade of tumor cell transforming growth factor-βs enhances cell cycle progression and

sensitizes human breast carcinoma cells to cytotoxic chemotherapy. Exp Cell Res *245*, 350-359.

Olaf, H.D. (2013). Drug screening: strategy and methods. In Forensic Drug Analysis (Future Science Ltd), pp. 48-58.

Pelaz, B., Charron, G., Pfeiffer, C., Zhao, Y., de la Fuente, J.M., Liang, X.-J., Parak, W.J., and del Pino, P. (2013). Interfacing engineered nanoparticles with biological systems: anticipating adverse nano–bio interactions. Small *9*, 1573-1584.

Perazella, M.A. (2009). Renal vulnerability to drug toxicity. Clin J Am Soc Nephrol *4*, 1275-1283.

Perel, P., Roberts, I., Sena, E., Wheble, P., Briscoe, C., Sandercock, P., Macleod, M., Mignini, L.E., Jayaram, P., and Khan, K.S. (2007). Comparison of treatment effects between animal experiments and clinical trials: systematic review. BMJ *334*, 197.

Petersen, C.M., Christensen, E.I., Andresen, B.S., and Moller, B.K. (1992). Internalization, lysosomal degradation and new synthesis of surface membrane CD4 in phorbol ester-activated T-lymphocytes and U-937 cells. Exp Cell Res *201*, 160-173.

Piccinno, F., Gottschalk, F., Seeger, S., and Nowack, B. (2012). Industrial production quantities and uses of ten engineered nanomaterials in Europe and the world. J Nanopart Res *14*, 1-11.

Plunkett, Jack, W., Plunkett, M.B., Steinberg, J.S., Faualk, J., and Snider, I. (2015). Nanotechnology & MEMS Industry Market Research (Plunkett Research Ltd).

Poincloux, R., Collin, O., Lizárraga, F., Romao, M., Debray, M., Piel, M., and Chavrier, P. (2011). Contractility of the cell rear drives invasion of breast tumor cells in 3D Matrigel. Proc Natl Acad Sci U S A *108*, 1943-1948.

Rangarajan, A., Hong, S.J., Gifford, A., and Weinberg, R.A. (2004). Species- and cell type-specific requirements for cellular transformation. Cancer cell *6*, 171-183.

Rao, A.S. (1997). Viruses. In Introduction to microbiology, A.K. Ghosh, ed. (New Delhi: Prentice-Hall of India Learning).

Rasmussen, J.W., Martinez, E., Louka, P., and Wingett, D.G. (2010). Zinc oxide nanoparticles for selective destruction of tumor cells and potential for drug delivery applications. Expert Opin Drug Deliv *7*, 1063-1077.

Raspopov, R.V., Trushina, E.N., Mustafina, O.K., Tananova, O.N., Gmoshinskii, I.V., and Khotimchenko, S.A. (2011). Efficacy of using zinc oxide nanoparticles in nutrition. Experiments on the laboratory animal. Vopr Pitan *80*, 39-44.

Ray, P.D., Huang, B.-W., and Tsuji, Y. (2012). Reactive oxygen species (ROS) homeostasis and redox regulation in cellular signaling. Cell Signal *24*, 981-990.

Requicha, A.A.G., Arbuckle, D.J., Mokaberi, B., and Yun, J. (2009). Algorithms and software for nanomanipulation with atomic force microscopes. Int J Rob Res *28*, 512-522.

BBC Research. (2014). Nanotechnology: a realistic market assessment (United States: BBC Research), http://www.bccresearch.com/market-research/nanotechnology/nanotechnology-realistic-market-assessment-nan031d.html

Roduner, E. (2006). Size matters: why nanomaterials are different. Chem Soc Rev *35*, 583-592.

Romano, A.D., Serviddio, G., de Matthaeis, A., Bellanti, F., and Vendemiale, G. (2010). Oxidative stress and aging. J Nephrol *23*, S29-36.

Sadauskas, E., Danscher, G., Stoltenberg, M., Vogel, U., Larsen, A., and Wallin, H. (2009). Protracted elimination of gold nanoparticles from mouse liver. Nanomedicine *5*, 162-169.

Sakaki, H. (1996). Recent progress in quantum structure materials, physics and devices. Curr Opin Solid State Mater Sci *1*, 17-20.

Saliani, M., Jalal, R., Goharshadi, E. K. (2016). Mechanism of oxidative stress involved in the toxicity of ZnO nanoparticles against eukaryotic cells. Nanomed J *3*, 1-14.

Santos, E., Hernández, R.M., Pedraz, J.L., and Orive, G. (2012). Novel advances in the design of three-dimensional bio-scaffolds to control cell fate: Translation from 2D to 3D. Trends Biotechnol *30*, 331-341.

Sauer, U.G., Vogel, S., Hess, A., Kolle, S.N., Ma-Hock, L., van Ravenzwaay, B., and Landsiedel, R. (2013). In vivo–in vitro comparison of acute respiratory tract toxicity using human 3D airway epithelial models and human A549 and murine 3T3 monolayer cell systems. Toxicology in vitro : an international journal published in association with BIBRA *27*, 174-190.

Sawai, J., Shoji, S., Igarashi, H., Hashimoto, A., Kokugan, T., Shimizu, M., and Kojima, H. (1998). Hydrogen peroxide as an antibacterial factor in zinc oxide powder slurry. J Ferment Bioeng *86*, 521-522.

Schleh, C., Semmler-Behnke, M., Lipka, J., Wenk, A., Hirn, S., Schäffler, M., Schmid, G., Simon, U., and Kreyling, W.G. (2012). Size and surface charge of gold nanoparticles determine absorption across intestinal barriers and accumulation in secondary target organs after oral administration. Nanotoxicology *6*, 36-46.

Schulte, P., Geraci, C., Zumwalde, R., Hoover, M., and Kuempel, E. (2008). Occupational risk management of engineered nanoparticles. J Occup Environ Hyg *5*, 239-249.

Setyawati, M.I., Fang, W., Chia, S.L., and Leong, D.T. (2013a). Nanotoxicology of common metal oxide based nanomaterials: their ROS-y and non-ROS-y consequences. Asia-Pac J Chem Eng *8*, 205-217.

Setyawati, M.I., Tay, C.Y., Chia, S.L., Goh, S.L., Fang, W., Neo, M.J., Chong, H.C., Tan, S.M., Loo, S.C., Ng, K.W.*, et al.* (2013b). Titanium dioxide nanomaterials cause endothelial cell leakiness by disrupting the homophilic interaction of VE-cadherin. Nature communications *4*, 1673.

Setyawati, M.I., Tay, C.Y., Docter, D., Stauber, R.H., and Leong, D.T. (2015). Understanding and exploiting nanoparticles' intimacy with the blood vessel and blood. Chem Soc Rev *44*, 8174-8199.

Setyawati, M.I., Tay, C.Y., and Leong, D.T. (2013c). Effect of zinc oxide nanomaterials-induced oxidative stress on the p53 pathway. Biomaterials *34*, 10133-10142.

Seunarine, K., Gadegaard, N., Tonnen, M., Meredith, D.O., Riehle, M.O., and Wilkinson, C.D.W. (2006). 3D polymer scaffolds for tissue engineering. Nanomedicine *1*, 281-296.

Sharma, V., Singh, P., Pandey, A.K., and Dhawan, A. (2012). Induction of oxidative stress, DNA damage and apoptosis in mouse liver after sub-acute oral exposure to zinc oxide nanoparticles. Mutat Res Genet Toxicol Environ Mutagen *745*, 84-91.

Siddiquey, I.A., Furusawa, T., Sato, M., and Suzuki, N. (2008). Microwave-assisted silica coating and photocatalytic activities of ZnO nanoparticles. Mater Res Bull *43*, 3416-3424.

Singh, A.K., Viswanath, V., and Janu, V.C. (2009). Synthesis, effect of capping agents, structural, optical and photoluminescence properties of ZnO nanoparticles. J Lumin *129*, 874-878.

Singh, P., and Nanda, A. (2014). Enhanced sun protection of nano-sized metal oxide particles over conventional metal oxide particles: an in vitro comparative study. Int J Cosmet Sci *36*, 273-283.

Sodek, K., Brown, T., and Ringuette, M. (2008). Collagen I but not Matrigel matrices provide an MMP-dependent barrier to ovarian cancer cell penetration. BMC Cancer *8*, 1-11.

Soenen, S.J., Rivera-Gil, P., Montenegro, J.-M., Parak, W.J., De Smedt, S.C., and Braeckmans, K. (2011). Cellular toxicity of inorganic nanoparticles: Common aspects and guidelines for improved nanotoxicity evaluation. Nano Today *6*, 446-465.

Song, W., Zhang, J., Guo, J., Zhang, J., Ding, F., Li, L., and Sun, Z. (2010). Role of the dissolved zinc ion and reactive oxygen species in cytotoxicity of ZnO nanoparticles. Toxicol Lett *199*, 389-397.

Sotiriou, G.A., Watson, C., Murdaugh, K.M., Darrah, T.H., Pyrgiotakis, G., Elder, A., Brain, J.D., and Demokritou, P. (2014). Engineering safer-by-design

silica-coated ZnO nanorods with reduced DNA damage potential. Environ Sci Nano *1*, 144-153.

Source, P.O. (2015). Zinc oxide In The Project on Emerging Nanotechnologies, P.O. Source, http://www.nanotechproject.org/cpi/browse/nanomaterials/zinc-oxide/

Stefanidou, M., Maravelias, C., Dona, A., and Spiliopoulou, C. (2006). Zinc: a multipurpose trace element. Arch Toxicol *80*, 1-9.

Sun, T., Jackson, S., Haycock, J.W., and MacNeil, S. (2006). Culture of skin cells in 3D rather than 2D improves their ability to survive exposure to cytotoxic agents. J Biotechnol *122*, 372-381.

Sun, T.Y., Gottschalk, F., Hungerbühler, K., and Nowack, B. (2014). Comprehensive probabilistic modelling of environmental emissions of engineered nanomaterials. Environ Pollut *185*, 69-76.

Sundqvist, A., Zieba, A., Vasilaki, E., Herrera Hidalgo, C., Soderberg, O., Koinuma, D., Miyazono, K., Heldin, C.H., Landegren, U., Ten Dijke, P., *et al.* (2013). Specific interactions between Smad proteins and AP-1 components determine TGFbeta-induced breast cancer cell invasion. Oncogene *32*, 3606-3615.

Szente, B.E. (2003). Cytokine signaling. In The Cytokine Handbook, A.W. Thomson, and M.T. Lotze, eds. (San Diego: Elsevier Science), pp. 85-102.

Tang, E., Cheng, G., Ma, X., Pang, X., and Zhao, Q. (2006). Surface modification of zinc oxide nanoparticle by PMAA and its dispersion in aqueous system. Appl Surf Sci *252*, 5227-5232.

Tay, C.Y., Pal, M., Yu, H., Leong, W.S., Tan, N.S., Ng, K.W., Venkatraman, S., Boey, F., Leong, D.T., and Tan, L.P. (2011). Bio-inspired micropatterned platform to steer stem cell differentiation. Small *7*, 1416-1421.

Tay, C.Y., Yu, H., Pal, M., Leong, W.S., Tan, N.S., Ng, K.W., Leong, D.T., and Tan, L.P. (2010). Micropatterned matrix directs differentiation of human mesenchymal stem cells towards myocardial lineage. Exp Cell Res *316*, 1159-1168.

Tee, J.K., Ong, C.N., Bay, B.H., Ho, H.K., and Leong, D.T. (2015). Oxidative stress by inorganic nanoparticles. Wiley Interdiscip Rev Nanomed Nanobiotechnol, n/a-n/a.

Thomas, S.P., and Mathew, E.J. (2013). Micro and nano zinc oxide filled NR composites. In Natural Rubber Materials: Volume 2: Composites and Nanocomposites, S. Thomas, C.H. Chan, L.A. Pothen, J. Joy, and H. Maria, eds. (Cambridge, UK: The Royal Society of Chemistry).

Tibbitt, M.W., and Anseth, K.S. (2012). Dynamic microenvironments: the fourth dimension. Sci Transl Med *4*, 160ps124.

Timm, D.M., Chen, J., Sing, D., Gage, J.A., Haisler, W.L., Neeley, S.K., Raphael, R.M., Dehghani, M., Rosenblatt, K.P., Killian, T.C*., et al.* (2013). A high-throughput three-dimensional cell migration assay for toxicity screening with mobile device-based macroscopic image analysis. Sci Rep *3*, 3000.

Trachootham, D., Alexandre, J., and Huang, P. (2009). Targeting cancer cells by ROS-mediated mechanisms: a radical therapeutic approach? Nat Rev Drug Discov *8*, 579-591.

Triantafilou, M., Gamper, F.G., Haston, R.M., Mouratis, M.A., Morath, S., Hartung, T., and Triantafilou, K. (2006). Membrane sorting of toll-like receptor (TLR)-2/6 and TLR2/1 heterodimers at the cell surface determines heterotypic associations with CD36 and intracellular targeting. J Biol Chem *281*, 31002-31011.

Trumbo, P., Yates, A.A., Schlicker, S., and Poos, M. (2001). Dietary reference intakes: vitamin A, vitamin K, arsenic, boron, chromium, copper, iodine, iron, manganese, molybdenum, nickel, silicon, vanadium, and zinc. J Am Diet Assoc *101*, 294-301.

Turturici, G., Tinnirello, R., Sconzo, G., and Geraci, F. (2014). Extracellular membrane vesicles as a mechanism of cell-to-cell communication: advantages and disadvantages. Am J Physiol Cell Physiol *306*, C621-C633.

van der Burg, B., Wedebye, E.B., Dietrich, D.R., Jaworska, J., Mangelsdorf, I., Paune, E., Schwarz, M., Piersma, A.H., and Kroese, E.D. (2015). The ChemScreen project to design a pragmatic alternative approach to predict reproductive toxicity of chemicals. Reprod Toxicol *55*, 114-123.

Vandebriel, R.J., and De Jong, W.H. (2012). A review of mammalian toxicity of ZnO nanoparticles. Nanotechnol Sci Appl *5*, 61-71.

Vergani, L., Grattarola, M., and Nicolini, C. (2004). Modifications of chromatin structure and gene expression following induced alterations of cellular shape. Int J Biochem Cell Biol *36*, 1447-1461.

Verwey, J., De Vries, J., and Pinedo, H.M. (1987). Mitomycin C-induced renal toxicity, a dose-dependent side effect? Eur J Cancer Clin Oncol *23*, 195-199.

Volkmer, E., Drosse, I., Otto, S., Stangelmayer, A., Stengele, M., Kallukalam, B.C., Mutschler, W., and Schieker, M. (2008). Hypoxia in static and dynamic 3D culture systems for tissue engineering of bone. Tissue Eng Part A *14*, 1331-1340.

Von Recum, A.F., and Van Kooten, T.G. (1996). The influence of micro-topography on cellular response and the implications for silicone implants. J Biomater Sci Polym Ed *7*, 181-198.

Wang, B., Feng, W., Wang, M., Wang, T., Gu, Y., Zhu, M., Ouyang, H., Shi, J., Zhang, F., Zhao, Y*., et al.* (2008). Acute toxicological impact of nano- and

submicro-scaled zinc oxide powder on healthy adult mice. J Nanopart Res *10*, 263-276.

Wang, J., Zhou, G., Chen, C., Yu, H., Wang, T., Ma, Y., Jia, G., Gao, Y., Li, B., Sun, J.*, et al.* (2007a). Acute toxicity and biodistribution of different sized titanium dioxide particles in mice after oral administration. Toxicol Lett *168*, 176-185.

Wang, Q., Li, S., Liu, P., and Min, X. (2012). Bio-templated CdSe quantum dots green synthesis in the functional protein, lysozyme, and biological activity investigation. Mater Chem Phys *137*, 580-585.

Wang, X., Lu, H., Urvalek, A.M., Li, T., Yu, L., Lamar, J., DiPersio, C.M., Feustel, P.J., and Zhao, J. (2011). KLF8 promotes human breast cancer cell invasion and metastasis by transcriptional activation of MMP9. Oncogene *30*, 1901-1911.

Wang, X., Song, J., and Wang, Z.L. (2007b). Nanowire and nanobelt arrays of zinc oxide from synthesis to properties and to novel devices. J Mater Chem *17*, 711-720.

Wang, Y., John, R., Chen, J., Richardson, J.A., Shelton, J.M., Bennett, M., Zhou, X.J., Nagami, G.T., Zhang, Y., Wu, Q.Q.*, et al.* (2009). IRF-1 promotes inflammation early after ischemic acute kidney injury. J Am Soc Nephrol *20*, 1544-1555.

Wang, Y., Song, S., Liu, J., Liu, D., and Zhang, H. (2015). ZnO-functionalized upconverting nanotheranostic agent: multi-modality imaging-guided chemotherapy with on-demand drug release triggered by pH. Angew Chem Int Ed Engl *54*, 536-540.

Weigelt, B., Lo, A., Park, C., Gray, J., and Bissell, M. (2010). HER2 signaling pathway activation and response of breast cancer cells to HER2-targeting agents is dependent strongly on the 3D microenvironment. Breast Cancer Res Treat *122*, 35-43.

Williams, E.S., Panko, J., and Paustenbach, D.J. (2009). The European Union's REACH regulation: a review of its history and requirements. Crit Rev Toxicol *39*, 553-575.

Wu, J., Liu, W., Xue, C., Zhou, S., Lan, F., Bi, L., Xu, H., Yang, X., and Zeng, F.-D. (2009). Toxicity and penetration of TiO2 nanoparticles in hairless mice and porcine skin after subchronic dermal exposure. Toxicol Lett *191*, 1-8.

Wu, X., Peters-Hall, J.R., Bose, S., Peña, M.T., and Rose, M.C. (2011). Human bronchial epithelial cells differentiate to 3D glandular acini on basement membrane matrix. Am J Respir Cell Mol Biol *44*, 914-921.

Xia, T., Kovochich, M., Liong, M., Mädler, L., Gilbert, B., Shi, H., Yeh, J.I., Zink, J.I., and Nel, A.E. (2008). Comparison of the mechanism of toxicity of zinc oxide and cerium oxide nanoparticles based on dissolution and oxidative stress properties. ACS Nano *2*, 2121-2134.

Xia, T., Li, N., and Nel, A.E. (2009). Potential health impact of nanoparticles. Annu Rev Public Health *30*, 137-150.

Xia, T., Zhao, Y., Sager, T., George, S., Pokhrel, S., Li, N., Schoenfeld, D., Meng, H., Lin, S., Wang, X.*, et al.* (2011). Decreased dissolution of ZnO by iron doping yields nanoparticles with reduced toxicity in the rodent lung and zebrafish embryos. ACS Nano *5*, 1223-1235.

Xie, G., Sun, J., Zhong, G., Shi, L., and Zhang, D. (2010a). Biodistribution and toxicity of intravenously administered silica nanoparticles in mice. Arch Toxicol *84*, 183-190.

Xie, W., Li, Y., Sun, W., Huang, J., Xie, H., and Zhao, X. (2010b). Surface modification of ZnO with Ag improves its photocatalytic efficiency and photostability. J Photochem Photobiol A Chem *216*, 149-155.

Yamada, K.M., and Cukierman, E. (2007). Modeling tissue morphogenesis and cancer in 3D. Cell *130*, 601-610.

Yamashita, K., Yoshioka, Y., Higashisaka, K., Mimura, K., Morishita, Y., Nozaki, M., Yoshida, T., Ogura, T., Nabeshi, H., Nagano, K.*, et al.* (2011). Silica and titanium dioxide nanoparticles cause pregnancy complications in mice. Nat Nanotechnol *6*, 321-328.

Yan, Y., Wang, X., Pan, Y., Liu, H., Cheng, J., Xiong, Z., Lin, F., Wu, R., Zhang, R., and Lu, Q. (2005). Fabrication of viable tissue-engineered constructs with 3D cell-assembly technique. Biomaterials *26*, 5864-5871.

Yang, H., Liu, C., Yang, D., Zhang, H., and Xi, Z. (2009). Comparative study of cytotoxicity, oxidative stress and genotoxicity induced by four typical nanomaterials: the role of particle size, shape and composition. J Appl Toxicol *29*, 69-78.

Yang, K., Park, H.-J., Han, S., Lee, J., Ko, E., Kim, J., Lee, J.S., Yu, J.H., Song, K.Y., Cheong, E.*, et al.* (2015). Recapitulation of in vivo-like paracrine signals of human mesenchymal stem cells for functional neuronal differentiation of human neural stem cells in a 3D microfluidic system. Biomaterials *63*, 177-188.

Yong, K.-T., Law, W.-C., Hu, R., Ye, L., Liu, L., Swihart, M.T., and Prasad, P.N. (2013). Nanotoxicity assessment of quantum dots: from cellular to primate studies. Chem Soc Rev *42*, 1236-1250.

Yoon, M., Campbell, J.L., Andersen, M.E., and Clewell, H.J. (2012). Quantitative in vitro to in vivo extrapolation of cell-based toxicity assay results. Crit Rev Toxicol *42*, 633-652.

Zhang, S., Gelain, F., and Zhao, X. (2005). Designer self-assembling peptide nanofiber scaffolds for 3D tissue cell cultures. Semin Cancer Biol *15*, 413-420.

Zhi-Peng, S., Lang, L., Li, Z., and Dian-Zeng, J. (2006). Rapid synthesis of ZnO nano-rods by one-step, room-temperature, solid-state reaction and their gas-sensing properties. Nanotechnology *17*, 2266-2270.

Zhou, E.H., Watson, C., Pizzo, R., Cohen, J., Dang, Q., Ferreira de Barros, P.M., Park, C.Y., Chen, C., Brain, J.D., Butler, J.P.*, et al.* (2014). Assessing the impact of engineered nanoparticles on wound healing using a novel in vitro bioassay. Nanomedicine *9*, 2803-2815.

Zoroddu, M.A., Medici, S., Ledda, A., Nurchi, V.M., Lachowicz, J.I., and Peana, M. (2014). Toxicity of nanoparticles. Curr Med Chem *21*, 3837-3853.

Zumdahl, S.S., and DeCoste, D.J. (2012). Atoms, molecules, and ions, Vol 7th Ed (United States of America: Mary Finch).

APPENDIX A: LISTS OF PUBLICATION

First authored peer-reviewed journal publications:

1. **Chia, S.L.**, Tay, C.Y., Setyawati, M.I., and Leong, D.T. (2016). Biomimicry 3D gastrointestinal spheroid platform for the assessment of toxicity and inflammatory effects of zinc oxide nanoparticles. Small *11*, 702-712.

2. **Chia, S.L.**, Tay, C.Y., Setyawati, M.I., and Leong, D.T. (2015). Decoupling the direct and indirect biological effects of ZnO nanoparticles using a communicative dual cell type tissue construct. Small, *12*, 647-657.

Co-authored peer-reviewed journal publications:

3. Setyawati, M.I., Fang, W., **Chia, S.L**., and Leong, D.T. (2013). Nanotoxicology of common metal oxide based nanomaterials: their ROS-y and non-ROS-y consequences. Asia-Pac J Chem Eng *8*, 205-217.

4. Setyawati, M.I., Tay, C.Y., **Chia, S.L.**, Goh, S.L., Fang, W., Neo, M.J., Chong, H.C., Tan, S.M., Loo, S.C., Ng, K.W.*, et al.* (2013). Titanium dioxide nanomaterials cause endothelial cell leakiness by disrupting the homophilic interaction of VE-cadherin. Nat Commun *4*, 1673.

5. Tay, C.Y., Fang, W., Setyawati, M.I., **Chia, S.L.**, Tan, K.S., Hong, C.H.L., and Leong, D.T. (2014). Nano-hydroxyapatite and Nano-titanium dioxide exhibit different subcellular distribution and apoptotic profile in human oral epithelium. ACS Appl Mater Interfaces *6*, 6248-6256.

6. Kutty, R.V., **Chia, S.L.**, Setyawati, M.I., Muthu, M.S., Feng, S.S., Leong, D.T. (2015). In vivo and ex vivo proofs of concept that cetuximab conjugated vitamin E TPGS micelles increases efficacy of

delivered docetaxel against triple negative breast cancer. Biomaterials *63*, 58-69.

7. Tay, C.Y., Muthu, M.S., Chia, S.L., Nguyen, K.T., Feng, S.S., Leong, D.T. (2016) Reality check for nanomaterials-mediated therapy with 3D biomimetic culture systems. Adv Funct Mater (Just accepted).

APPENDIX B: COPYRIGHTS

JOHN WILEY AND SONS LICENSE
TERMS AND CONDITIONS

Dec 16, 2015

This Agreement between Sing Ling Chia ("You") and John Wiley and Sons ("John Wiley and Sons") consists of your license details and the terms and conditions provided by John Wiley and Sons and Copyright Clearance Center.

License Number	3770580711400
License date	Dec 16, 2015
Licensed Content Publisher	John Wiley and Sons
Licensed Content Publication	Small
Licensed Content Title	Nanotoxicity: Biomimicry 3D Gastrointestinal Spheroid Platform for the Assessment of Toxicity and Inflammatory Effects of Zinc Oxide Nanoparticles (Small 6/2015)
Licensed Content Author	Sing Ling Chia, Chor Yong Tay, Magdiel I. Setyawati, David T. Leong
Licensed Content Date	Feb 6, 2015
Pages	1
Type of use	Dissertation/Thesis
Requestor type	Author of this Wiley article
Format	Print and electronic
Portion	Figure/table
Number of figures/tables	10

Original Wiley figure/table number(s)	Figure 1 Figure 2 Figure 3 Figure 4 Figure 5 Figure 6 Figure 7 Figure 8 Supplementary Figure 1 Supplementary Figure 2
Will you be translating?	No
Title of your thesis / dissertation	Investigating biological effects of nanoparticles with 3-dimensional cell models
Expected completion date	Jan 2016
Expected size (number of pages)	120
Requestor Location	Sing Ling Chia 4 Engineering Drive 4 Singapore, Singapore 117585 Attn: Sing Ling Chia
Billing Type	Invoice
Billing Address	Sing Ling Chia 4 Engineering Drive 4 Singapore, Singapore 117585 Attn: Sing Ling Chia
Total	0.00 USD

JOHN WILEY AND SONS LICENSE
TERMS AND CONDITIONS

Dec 16, 2015

This Agreement between Sing Ling Chia ("You") and John Wiley and Sons ("John Wiley and Sons") consists of your license details and the terms and conditions provided by John Wiley and Sons and Copyright Clearance Center.

License Number	3770590052976
License date	Dec 16, 2015
Licensed Content Publisher	John Wiley and Sons
Licensed Content Publication	Small
Licensed Content Title	Decoupling the Direct and Indirect Biological Effects of ZnO Nanoparticles Using a Communicative Dual Cell-Type Tissue Construct
Licensed Content Author	Sing Ling Chia, Chor Yong Tay, Magdiel I. Setyawati, David T. Leong
Licensed Content Date	Dec 15, 2015
Pages	1
Type of use	Dissertation/Thesis
Requestor type	Author of this Wiley article
Format	Print and electronic
Portion	Figure/table
Number of figures/tables	11
Original Wiley figure/table number(s)	Figure 1 Figure 2 Figure 3 Figure 4 Figure 5 Figure 6 Figure 7 Figure 8 Figure S1 Figure S2 Figure S4
Will you be translating?	No

Title of your thesis / dissertation	Investigating biological effects of nanoparticles with 3-dimensional cell models
Expected completion date	Jan 2016
Expected size (number of pages)	120
Requestor Location	Sing Ling Chia 4 Engineering Drive 4 Singapore, Singapore 117585 Attn: Sing Ling Chia
Billing Type	Invoice
Billing Address	Sing Ling Chia 4 Engineering Drive 4 Singapore, Singapore 117585 Attn: Sing Ling Chia
Total	0.00 USD